POLARISATION AND ANGULAR CORRELATION STUDIES OF THE $6^3P_1 - 6^1S_0$ INTERCOMBINATION LINE OF MERCURY BY ELECTRON IMPACT

BY

AKHLAQUE ABBAS ZAIDI

Thesis submitted to the University of Stirling
for the degree of Doctor of Philosophy

Institute of Atomic Physics
University of Stirling
STIRLING FK9 4LA

January 1980

"Polarisation and Angular Correlation Studies of the $6^3P_1 - 6^1S_0$ Intercombination Line of Mercury by Electron Impact".

Ph.D Thesis, January 1980 by A.A. Zaidi

University of Stirling, Scotland

ERRATA

Page 112

(1) Table 1 to be changed to Table 3.

(2) The normalised Stokes parameters in this table (table 3 now) have been incorrectly quoted. Each value of P_1, P_2 and P_3 should be given the opposite sign i.e; Table 3(a), P_1, P_2 and P_3 are now -0.31 ± 0.05, $+0.21 \pm 0.06$ and $+0.14 \pm 0.05$, respectively. Similarly in Table 3(b).

Page 116

last line: Values of 0.42 and 0.26 to be changed to -0.42 and -0.26.

Page 117

second line: Value of 0.13 to be changed to -0.13.

ABSTRACT

A crossed-beam apparatus was used to measure the polarisation of the $6^3P_1 - 6^1S_0$ intercombination line (λ = 253.7 nm) of mercury, excited by electron impact, in the energy range from threshold at 4.89 eV to 7.5 eV. An isotope cell was used to absorb selectively the radiation emitted from odd isotopes with non-zero nuclear spins and, hence, eliminate the effect of hyperfine structure on the polarisation. These results are compared with the polarisation of the radiation when the effect of hyperfine structure was present. The degree of polarisation is found to increase after the elimination of the hyperfine effect.

A delayed coincidence technique was utilised to measure the electron-photon coincidence rates for the excitation/de-excitation process, $6^1S_0 \rightarrow 6^3P_1 \rightarrow 6^1S_0$, in mercury by electron impact. The electrons, inelastically scattered with an energy loss of 4.89 eV, were detected in coincidence with photons emitted from the subsequent decay of the 6^3P_1 state. These observations were made for fixed electron energies of 5.5 eV and 6.5 eV at electron scattering angles of 50° and 70°. The vector polarisation and coherence parameters of the coincident photon radiation are evaluated in terms of the Stokes parameters to determine the coherent nature of the excitation process. Although the coherence of the above excitation/de-excitation process increased after the elimination of the hyperfine effect, the process is still partially coherent.

ACKNOWLEDGEMENTS

I am deeply indebted to Professor H Kleinpoppen, my principal supervisor, whose enthusiastic dedication, keen interest and invaluable encouragement throughout the course of this research has been a source of immense inspiration.

I wish to express my profound gratitude to my supervisor, Dr I McGregor, for his major contribution to all phases of this work. His knowledge of experimental details coupled with unfailing co-operation made it possible to overcome various difficulties associated with this experiment.

I am grateful to Dr M C Standage for his help in the construction of the isotope cell.

My thanks go to Drs D Hils, J Beyer and in particular to Dr A J Duncan, who kindly read the manuscript, for their cooperation and assistance. I would like to thank Messrs S M Khalid and N A Malik for useful discussions.

I am grateful to Mr R R Harrison of Shared Technical Services for his excellent drawing of the figures.

I wish to thank our capable technicians Messrs A J Duncan and A D Sherman for their readily available technical assistance.

I would like to express my sincere thanks to Mrs H Queen for typing the thesis in spite of great pressure of other work.

I acknowledge a studentship for two years (September 1975 - September 1977) from the University of Stirling and financial

assistance towards tuition fees by the British Council and the University of Stirling.

Finally I am indebted to my wife for her co-operation, tolerance and hard work to financially support the family.

CONTENTS

1. INTRODUCTION

1.1. Historical Background

The polarisation of atomic line radiation by electron impact has been studied for a wide range of atoms. Such studies are important in order to test the predictions of the general theory for the polarisation of atomic radiation. Polarisation measurements of electron impact atomic line radiation date back to the 1920's when several experiments were conducted. The work of Skinner and Appleyard (1928) on mercury is of particular interest since they measured the polarisation of the radiation as a function of the incident electron energy whereas all other earlier measurements were performed at a fixed electron energy. They found the polarisation to vary with the incident electron energy and obtained for the 253.7 nm line of mercury a maximum of -0.30 at 6.7 eV. Like all other experiments their measured polarisation was almost zero at the threshold of excitation. The theory of the polarisation of line radiation by Oppenheimer (1927,28) and Penney (1932) made it clear that there was a serious discrepancy between the experimental observations and the theoretical threshold polarisations. This discrepancy gave rise to a growing interest in the polarisation studies of atomic line radiation by electron impact, especially near threshold energy.

A renewed interest was stimulated by the new theoretical approach to the problem by Percival and Seaton (1958). They revised the older theories, which failed to give unambiguous results when the fine structure or hyperfine structure separations are comparable

with the radiative line width, by taking into account the finite level width of the excited fine and hyperfine structure states. In the same year, Baranger and Gerjouy (1958) developed a theory in which they associated the disagreement between experimental results and theoretical predictions for threshold polarisation with the formation of atomic compound states. However, the most important applications of their atomic compound model were related to angular distribution and polarisation of line radiation following excitation through atomic compound states.

The discrepancy between theoretical predictions and experimental data can in part be attributed to the energy spread normally present in an electron beam. No electron beam can have a precisely defined energy and the measured polarisation will be at best some average over the electron energy spread. Since the earlier observations were in accord with a polarisation which fell to a low value within a small energy range above threshold, it was necessary to examine the behaviour of polarisation in the vicinity of the excitation threshold with improved energy resolution. More refined experiments on the polarisation of the $4^1D_2 - 2^1P_1$ (492.2 nm) line of helium by McFarland (1964), Heddle and Keesing (1967), Heideman et al (1969) and Heddle et al (1974) have shown a reasonable agreement between them in indicating a value consistent with the theoretical threshold polarisation of 0.60, but the polarisation in each case was found to be varying rapidly in a narrow energy range above threshold. Similarly the work of Fedorov and Mezentsev (1965) and Heideman et al (1969) on the polarisation of the $7^1D_2 - 6^1P_1$ (434.7 nm), $7^3S_1 - 6^3P_1$ (435.8 nm) and $6^3D_2 - 6^1P_1$ (577.0 nm) lines of mercury exhibited sharp changes near threshold. Ottley and Kleinpoppen (1975) carried out

polarisation studies of the $6^3P_1 - 6^1S_0$ (253.7 nm) line of mercury and their work also showed a considerable structure in the polarisation close to threshold. All of these measurements with improved energy resolution clearly demonstrate that the earlier experiments, which seemed to indicate that the polarisation tends to zero when the incident electron energy is lowered to the threshold value, lacked sufficient energy resolution to reveal detailed structure in the polarisation near threshold.

One common feature of the above mentioned polarisation measurements of helium and mercury lines is the anomalous behaviour of the polarisation as a function of electron energy in the neighbourhood of threshold. The polarisation, however, may not always vary rapidly in the region of threshold as found by Hafner and Kleinpoppen (1967) and Enemark and Gallagher (1972) for the lithium and sodium lines. The polarisation for these alkali resonance lines was found to increase monotonically when the incident electron energy was lowered from higher values to the excitation threshold. The observed anomaly in the polarisation of helium and mercury lines has been associated with the existence of negative-ion states, which are not confined to the neighbourhood of a threshold. Two possible mechanisms for the excitation of an atom are:

$$\text{(a)} \quad e + A \rightarrow A^* + e$$

$$\text{(b)} \quad e + A \rightarrow A^{-*} \rightarrow A^* + e$$
$$\qquad\qquad\qquad\qquad\qquad\qquad\qquad\qquad \downarrow \longrightarrow A + h\nu$$

(a) is the direct excitation process where A^* is an excited state of the atom, and

(b) is the process where the final excited state results

from an intermediate state. This intermediate state is a negative-ion state with a lifetime of $\sim 10^{-14}$s.

Recently Heideman et al (1979) have suggested an additional mechanism that may cause a polarisation anomaly in a limited energy range around the ionisation threshold. This mechanism concerns the influence of electron correlation effects as a result of which the incident and atomic electrons may acquire significant orbital angular momenta even if their velocities are very small. Consequently the excitation of magnetic substates with $M_L \geq 1$ may become quite likely and the polarisation of the emitted radiation may deviate appreciably from the value at threshold, where only $M_L = 0$ excitation is possible. This mechanism is, however, applicable to transitions from an excited state whose excitation threshold is close to the ionisation threshold.

The recent success of a new type of experiment, which is different in its approach to the traditional experiment, has considerably changed the state of investigation of atomic collision physics. The introduction of coincidence techniques for the study of electron impact excitation processes has opened a wide range of new aspects. The traditional work in electron-atom collisions has usually involved averages over fundamental collision parameters with the result that important detail is lost in the averaging process. For example, measurements of the line polarisation involve an average over all electron scattering angles since the analysis of the radiation takes place without regard to the electrons. New information on the details of the collision process can be obtained by an experiment which allows an analysis of only that radiation emitted from atoms which are excited to a

given state by electrons scattered in a particular direction. The method of detecting inelastically scattered electrons in delayed coincidence with photons emitted in a given direction provides a technique for precisely this kind of measurement. In electron-atom scattering experiments, the scattering plane is defined by the incoming beam of electrons and the direction in which the scattered electrons are detected (axis of the detector). Any electron having excited an atom and scattered in a given direction is characterised by the scattering angle and the amount of energy it has lost, implying that all those electrons scattered in a particular direction and detected in coincidence with photons emitted from excited atoms in a given state have experienced the same scattering process. Although the delayed coincidence technique has been widely used in nuclear physics, the use of this method is rather new to atomic physics.

Besides the electron-photon coincidence method, outlined above and used in the present experiment, two other commonly used delayed coincidence techniques are, photon-photon coincidence and electron-electron coincidence methods. The photon-photon coincidence method was first used by Brannen et al (1955) to obtain the value of 11.2 ± 0.2 ns for the lifetime of the 7^3S_1 state of mercury. It has since been used by many workers for the lifetime measurements of atoms and molecules (for example, Kaul 1966, Popp et al 1970, Holt and Pipkin 1974, King et al 1975b and 76). The electron-electron coincidence method was first reported by Ehrhardt et al (1969) where the correlations between the outgoing electrons from the ionisation of helium were measured. This technique of detecting the scattered and ejected electrons in coincidence for the measurements of the ionisation of atoms by electron impact has been used by various

groups (for example, Weigold et al 1973, Ehrhardt et al 1974, Backx et al 1975, Jung et al 1975).

The electron-photon coincidence method was first adopted by Imhof and Read (1969) to determine the lifetime of the 4^1S state of helium. The main advantage of this method is the complete elimination of the effects of unwanted cascading from higher states. This technique has since been used by Imhof and Read (1971a, b, c) and other workers (for example Smith et al 1973 and 75, Shaw et al 1975) to measure lifetimes in atoms and molecules, both neutral and ionic. King and Adams (1974) used electron-photon delayed coincidence method to determine the lifetime of the 6^3P_1 state in mercury and found it to be 120.0 ± 0.7 ns with an accuracy of approximately 0.5%. Their work was extended by King et al (1975a) to the lifetime measurements of five other levels of mercury. A detailed review of the measurement of lifetimes in atoms, molecules and ions using coincidence techniques has been given by Imhof and Read (1977). King et al (1972) have shown in a coincidence experiment that threshold polarisations can be determined in electron-atom excitations at energies well above threshold. They studied the polarisation of $3^1P - 2^1S$ (501.6 nm) transition in helium by detecting only those photons which were in coincidence with electrons inelastically scattered in the forward direction.

The pioneer work in electron-photon angular correlation measurements was carried out by Eminyan et al (1973) for the 2^1P and 3^1P states of helium. From the angular correlation in each case, they deduced the parameters λ and $|\chi|$, where λ is the ratio of the partial differential cross section σ_0 for exciting the M = 0 substate to the total differential cross section σ and χ is the relative phase between the excitation amplitudes a_0 and a_1 for exciting the magnetic substates M = 0 and M = ± 1 of the n^1p states. This development led to series of measurements on helium by Eminyan et al (1974 and 75), Tan et al (1977), Ugbabe et al (1977),

Sutcliffe et al (1978), Fon et al (1979) and Hollywood et al (1979). This technique has been applied to the 2P state of atomic hydrogen by Williams (1975), Dixon et al (1978) and Hood et al (1979). The electron-photon angular correlation measurements have also been used on neon by Ugbabe et al (1977) and on argon by Arriola et al (1975). This technique has been used by Malcolm and McConkey (1979) to study the λ and $|\chi|$ parameters as well as threshold polarisations for the resolved 104.8 and 106.7 nm lines of argon. Kleinpoppen and McGregor (1979) studied the angular correlations for the 116.5 and 123.6 nm lines of krypton and determined the collision parameters λ and χ. Standage and Kleinpoppen (1976) reported linear and circular polarisation measurements of the $3^1P - 2^1S$ (501.6 nm) photons detected in delayed coincidence with the electrons inelastically scattered from the 3^1P level of helium. Zehnle et al (1978) applied this method for the vector polarisation analysis of the $K(4^2P - 4^2S)$ photons for K - He collisions. Andersen et al (1979) performed similar measurements of the Stokes parameters for the $Mg(3^2P - 3^2S)$ photons in a coincidence experiment involving Mg^+ - He, Ne and Ar collisions.

1.2. The Present Work

The work presented in this thesis was carried out in two stages. In the first stage an experiment was performed to observe the influence of the hyperfine structure on the polarisation of the $6^3P_1 - 6^1S_0$ intercombination line of mercury excited by electron impact. The polarisation of electron impact line radiation depends on many parameters: apart from the electron energy, the atom density and the excited state configuration, the polarisation is also affected

by the level width and the fine and hyperfine structure separations. An important result of the theory (Percival and Seaton, 1958) is the dependence of the polarisation on the ratio of the fine and hyperfine structure separations of the excited state. Hafner and Kleinpoppen (1967) measured the polarisation of the first resonance lines of Li^6, Li^7 and Na^{23} and demonstrated that the polarisation was very sensitive to the natural level width and to the fine and hyperfine structure separations of the excited states. Their experimental results are in good agreement with the theoretical calculations (Flower and Seaton, 1967) of the threshold polarisation of these lines. Unlike Hafner and Kleinpoppen who used isotopically pure atoms, an isotope cell was used to eliminate the effect of the hyperfine structure in the observed photon radiation originating from the natural isotopic composition of mercury.

For the first stage, an existing crossed-beam apparatus was used in which the target was in the form of an atomic beam of the natural isotopic mixture of mercury. The atomic beam was intersected by an electron beam from a directly heated tungsten hairpin cathode. The use of a 127^o cylindrical monochromator resulted in an electron energy resolution of $\sim$100 meV. The radiation from the $6^3P_1 - 6^1S_0$ transition was observed perpendicular to the direction of the electron beam and the polarisation was measured as a function of the incident electron energy in the range from threshold to 7.5 eV. The comparison of the polarisation measurements with and without the isotope cell present was made to determine the effect of the hyperfine structure.

In the second stage, an experiment was conducted using the electron-photon coincidence technique to measure linear and circular

polarisations of the $6^3P_1 - 6^1S_0$ line of mercury in order to determine the coherent nature of the excitation process.

In this case some modifications to the crossed-beam apparatus were necessary to accommodate changes which were required for the electron-photon coincidence experiment. For example, in order to obtain higher currents in the interaction region, the use of a monochromator was abandoned and a three stage electron gun was built which produced an electron beam with an energy width of 400 meV. This electron beam was intersected with the mercury beam and the resulting electron-photon delayed coincidence rates were measured by detecting inelastically scattered electrons in the scattering plane and the subsequent decay photons perpendicular to the scattering plane. These measurements were taken for a fixed incident electron energy of 5.5 eV at an electron scattering angle of 50^o. The observations were then made at incident electron energies of 5.5 and 6.5 eV with electron scattering angles of 50^o and 70^o, after the elimination of the effect of the hyperfine structure in the photon radiation by the use of the isotope cell as in the first stage. With these measurements it was possible to make a complete polarisation analysis of the coincident photon radiation by the determination of the Stokes parameters.

Some theoretical aspects regarding the polarisation of atomic line radiation, electron-photon angular correlations and the Stokes parameters are discussed in Chapter II. Chapter III describes the apparatus for the first stage of the experiment and gives a detailed account of the changes made for the second stage. Results of the measurements for the two parts of the experiment are discussed in Chapter IV. Chapter V contains the conclusions of the present work and suggestions for future work.

2. THEORY

2.1. Polarisation of Atomic Line Radiation by Electron Impact

The radiation emitted in the decay of atoms after excitation by an electron beam is, in general, polarised and shows an anisotropic angular distribution. Referring to figure 1, an atom at O, initially in the ground state, is excited by an incident electron moving along the ZO direction. The excited atom decays spontaneously by emitting a photon. The radiating atom can be characterised by an oscillating dipole orientated in an arbitrary direction in space which can be visualised as the resultant of three orthogonal component dipoles placed along the OZ, OX and OY directions. The radiation may be considered as resulting from an incoherent superposition of the radiation from these three electric dipoles.

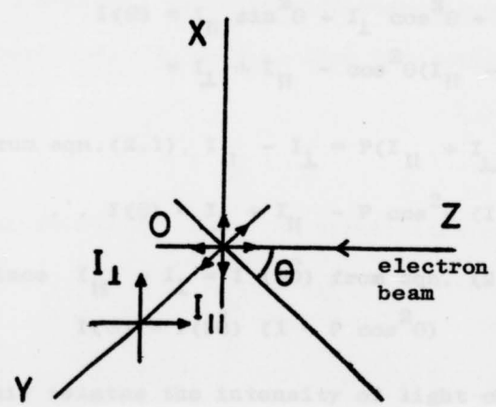

Fig.1. Atom as an electric dipole radiator

If the intensities of radiation of the three dipoles along OZ, OX and OY directions are denoted, respectively, by $I_\parallel$, $I_\perp$ and $I_\perp$, assuming cylindrical symmetry about the OZ axis, then the degree of polarisation P of the line radiation is defined as

$$P = \frac{I_{\parallel} - I_{\perp}}{I_{\parallel} + I_{\perp}} \qquad (2.1)$$

The total intensity of radiation perpendicular to OZ in OY direction (see fig.1) is given by

$$I(90^{\circ}) = I_{\parallel} + I_{\perp} \qquad (2.2)$$

The intensity of light for a single dipole in a direction making an angle Θ with the dipole axis is given by,

$$I(\Theta) = I_o \sin^2\Theta$$

where I_o is the intensity of the dipole in a direction at right angles to its axis.

The combined radiation intensity of the three dipoles at a point located in YZ plane and making an angle Θ with the Z-direction (see fig.1) is thus,

$$I(\Theta) = I_{\parallel} \sin^2\Theta + I_{\perp} \cos^2\Theta + I_{\perp}$$
$$= I_{\perp} + I_{\parallel} - \cos^2\Theta(I_{\parallel} - I_{\perp})$$

From eqn.(2.1), $I_{\parallel} - I_{\perp} = P(I_{\parallel} + I_{\perp})$

$$\therefore I(\Theta) = I_{\perp} + I_{\parallel} - P \cos^2\Theta \, (I_{\parallel} + I_{\perp})$$

Since $I_{\parallel} + I_{\perp} = I(90^{\circ})$ from eqn. (2.2), therefore,

$$I(\Theta) = I(90^{\circ}) \, (1 - P \cos^2\Theta) \qquad (2.3)$$

This relates the intensity of light observed at an angle Θ to that observed at 90° with respect to the electron beam direction.

The polarisation P can therefore be determined by measuring $I_{\parallel}$ and $I_{\perp}$ and using eqn.(2.1) or by obtaining the angular intensity distribution and using relation (2.3).

The atomic line radiation is polarised due to a non-uniform distribution of magnetic substates of the excited state. The polarisation depends on the transition probabilities for π and σ transitions between magnetic substates of the emitting state and the state into which the atom decays. The π-radiation arises when the electric vector of the radiation is parallel to the electron beam direction whereas the σ-radiation has its electric vector perpendicular to the beam. The intensities produced by these radiations are referred to as $I_{\parallel}$ and $I_{\perp}$, respectively, being polarised parallel and perpendicular to the beam direction. $I_{\parallel}$ is associated with transitions for which $\Delta M_J = 0$ and $I_{\perp}$ with transitions for which $\Delta M_J = \pm 1$.

If A_M^{π} and A_M^{σ} are transition probabilities for π and σ transitions, respectively, of a magnetic substate with magnetic quantum number M (which could represent M_L, M_J or M_F), then the total transition probability is

$$A = A_M^{\pi} + A_M^{\sigma}$$

The branching ratios for π and σ transitions are, respectively,

$$\frac{A_M^{\pi}}{A} \text{ and } \frac{A_M^{\sigma}}{A}$$

The intensity components related to π and σ radiations are given by,

$$I_{\parallel} \propto \Sigma_M \frac{A_M^{\pi}}{A} Q_M \text{ and } I_{\perp} \propto \Sigma_M \frac{1}{2} \frac{A_M^{\sigma}}{A} Q_M$$

where Q_M is the cross section for a magnetic substate with magnetic quantum number M.

The polarisation given by,

$$P = \frac{I_{\parallel} - I_{\perp}}{I_{\parallel} + I_{\perp}}, \text{ becomes}$$

$$P = \frac{\frac{1}{A} \Sigma_M A_M^{\pi} Q_M - \frac{1}{A} \Sigma_M \frac{1}{2} A_M^{\sigma} Q_M}{\frac{1}{A} \Sigma_M A_M^{\pi} + \frac{1}{A} \Sigma_M \frac{1}{2} A_M^{\sigma} Q_M}$$

$$\text{with } \frac{1}{2} A_M^{\sigma} = \frac{1}{2} (A - A_M^{\pi}),$$

$$P = \frac{\frac{3}{2} \frac{1}{A} \Sigma_M A_M^{\pi} Q_M - \frac{1}{2} \Sigma_M Q_M}{\frac{1}{2} \frac{1}{A} \Sigma_M A_M^{\pi} Q_M + \frac{1}{2} \Sigma_M Q_M}$$

The rate coefficients K^{π} and K for completely linearly polarised and totally unpolarised light intensities, respectively, are proportional to the respective line intensities and are given by,

$$K^{\pi} \propto \frac{1}{A} \Sigma_M A_M^{\pi} Q_M \text{ and } K \propto \Sigma_M Q_M \propto Q$$

$$\therefore P = \frac{3K^{\pi} - K}{K^{\pi} + K} \qquad (2.4)$$

Considering the excitation/de-excitation process, $1_S \rightarrow 1_P \rightarrow 1_S$, the total excitation cross section is given by,

$$Q = Q_0 + Q_{+1} + Q_{-1}$$

where Q_0 is the cross section for π-radiation with M = 0 and Q_{+1}, Q_{-1} are cross sections for σ-radiations corresponding to M = ±1.

Owing to symmetry about OZ, $Q_{+1} = Q_{-1}$. and therefore,

$$Q = Q_0 + 2Q_1$$

Only the Q_0 component results in the excitation of π-radiation therefore, with $K^{\pi} \propto Q_0$ and $K \propto Q$, the polarisation of the above excitation process is given by Eqn. (2.4),

$$P = \frac{3Q_0 - Q_0 - 2Q_1}{Q_0 + Q_0 + 2Q_1} = \frac{Q_0 - Q_1}{Q_0 + Q_1} \qquad (2.5)$$

The threshold excitation is governed by the selection rule $\Delta M_L = 0$ and therefore only the substate with $M_L = 0$ can be excited when excitation from S to P state is considered. The incoming beam of electrons has no component of orbital angular momentum about its own direction and, after an excitation at threshold, the outgoing electron has a very small energy and carries away no angular momentum. Hence the component M_L of the orbital angular momentum of the atom about the incident beam direction is not changed by the collision process at threshold that is, $\Delta M_L = 0$.

Applying the threshold selection rule to the simple case of excitation from a ^1S ground state to a ^1P state with subsequent emission corresponding to a $^1P \rightarrow {}^1S$ transition, one obtains $Q_1 = 0$ and $Q = Q_0$ and hence $P_{thr} = 100\%$ using eqn.(2.5). An excellent example of the 100% threshold polarisation of the above process is provided by the measurement of the polarisation of the $4^1P_1 - 4^1S_0$, $\lambda = 422.7$ nm line of calcium by Ehlers and Gallagher (1973). The threshold polarisations of the $6^3P_1 - 6^1S_0$ ($\lambda = 253.7$ nm) and $6^1P_1 - 6^1S_0$ ($\lambda = 185$ nm) lines of mercury should provide the largest possible difference (±100%) for the line polarisation. For threshold excitation of the 6^1P_1 state, only the substate with $M_J = 0$ is excited because of the selection rule $\Delta M_L = 0$. In the subsequent decay to the ground state, only the transition with

$\Delta M_J = 0$ is possible which gives π-radiation and hence $P_{thr} = +100\%$. For the excitation of the 6^3P_1 state, only $M_J = \pm 1$ substates can be excited at threshold because of the fact that the appropriate Clebsch-Gordon coefficient for the $M_J = 0$ with $M_L = 0$ is zero,

$$C^{S = 1,\ L = 1,\ J = 1}_{M_S = 0,\ M_L = 0,\ M_J = 0} = 0$$

while all the other angular momentum coupling coefficients are non-zero (these coefficients are given in the paper by McConnell and Moiseiwitsch, 1968). Thus when the 6^3P_1 state decays back to the ground state, only the transitions with $\Delta M_J = \pm 1$ can take place which give rise to σ-radiations and therefore $P_{thr} = -100\%$. However the polarisation is considerably reduced due to spin-orbit interactions and precessional effects resulting from fine and hyperfine interactions (Kleinpoppen, 1969). Allowance for departure from LS coupling was made by Penney (1932) for the threshold polarisation of the 253.7 nm line of mercury. He obtained $P_{thr} = -80\%$ for the normal isotope mixture and -92% for zero nuclear spin.

Following the theory of Percival and Seaton (1958), calculations for the polarisations of $6^1P_1 - 6^1S_0$ and $6^3P_1 - 6^1S_0$ lines of mercury were presented by McConnell and Moiseiwitsch (1968). They included the spin-orbit interaction and the effect of different isotopes in their analysis. For the $6^3P_1 - 6^1S_0$ transition, they obtained a threshold polarisation of -68% for the normal isotope mixture and -89% for zero nuclear spin. The effect of resonances on the polarisation has been discussed by Baranger and Gerjouy (1958). They proposed that two negative-ion states are formed just above the excitation threshold of the 253.7 nm line and predicted a

polarisation of 60% and 0% in the centre of resonances with total angular momentum $J = \frac{3}{2}$ and $J = \frac{1}{2}$ respectively. Their calculations ignored the effects of nuclear spin and assumed zero orbital angular momentum of the outgoing electrons. Albert et al (1977) carried out theoretical and experimental investigations of the resonances in mercury and found that the two resonances, also observed by Ottley and Kleinpoppen (1975) and Shpenik et al (1976), are formed in the $^2D_{5/2}$ scattering state with $J = \frac{5}{2}$ and not $J = \frac{3}{2}$ and $\frac{1}{2}$ as first proposed by Baranger and Gerjouy (1958). Comprehensive reviews of the polarisation of atomic line radiation have been presented by Kleinpoppen (1969) and Kleinpoppen and Scharmann (1978).

2.2. Electron-photon Angular Correlations

The theoretical formulation of electron-photon coincidence measurements where photons are detected in delayed coincidence with inelastically scattered electrons has been worked out by various authors. Macek and Jaecks (1971) related the coincidence rates for electron-photon angular correlations to "collision parameters" such as partial substate differential cross sections, excitation amplitudes and their phase difference. Fano and Macek (1973) and Blum and Kleinpoppen (1975,76) have described the electron-photon angular correlation in terms of "target parameters" such as orientation and alignment parameters and to multipole moments of the atom excited during the collisional excitation process. A recent review of electron-photon angular correlation in atomic physics is given by Blum and Kleinpoppen (1979). The theory of electron-photon correlations is most easily demonstrated for the excitation/de-excitation process, $1^1S_0 \rightarrow n^1P_1 \rightarrow 1^1S_0$, in helium where the

compensation of the spins of the atomic electron simplifies the theoretical analysis. Moreover there is no complication from spin-orbit coupling either in the atomic structure or in the scattering process. The helium atom is initially in a ^1S state with only one magnetic substate and after excitation, the atom is in a n^1P state with three magnetic substates. Based upon the assumption of coherent excitation of the degenerate magnetic substates, the excited state of helium can be represented by a linear superposition of magnetic substates:

$$|\psi> = a_{+1}|11> + a_0|10> + a_{-1}|1\,-1>$$

where the amplitudes a_M, $M = 0, \pm 1$, describe the excitation to particular magnetic substates $|JM>$ of the excited state. These excitation amplitudes are functions of the incident electron energy and the electron scattering angles.

The state vector $|\psi> = \Sigma_M\, a_M|JM>$, describing the coherent superposition of magnetic substates, can be normalised by assuming some normalisation constant a so that,

$$<\psi\,|\psi> = a^*a = |\,a\,|^2 = \sigma \qquad (2.6)$$

where σ is the inelastic differential cross section for exciting the ^1P state.

Moreover $<\psi\,|\psi> = (\Sigma_{M'}\, a^*_{M'} <JM'|)\,(\Sigma_M a_M\,|JM>)$

$$= \Sigma_{M'M}\, a^*_{M'}\, a_M <JM'|JM>$$

By using the orthogonality relation $<JM'|JM> = \delta_{M'M}$,

$$<\psi\,|\psi> = \Sigma_{M'M}\, a^*_{M'} a_M\, \delta_{M'M}$$

$$= \Sigma_M\,|\,a_M\,|^2$$

Since from eqn. (2.6), $< \psi \mid \psi > = \sigma$, therefore,

$$\Sigma_M \mid a_M \mid^2 = \sigma, \text{ so that}$$

$$|a_{+1}|^2 + |a_0|^2 + |a_{-1}|^2 = \sigma_{+1} + \sigma_0 + \sigma_{-1}$$

where σ_M , $M = 0, \pm 1$, is the partial differential cross section for exciting the M substate.

Since the scattering process has mirror symmetry in the scattering plane, $a_{+1} = -a_{-1}$

Thus $\sigma_{+1} = \sigma_{-1}$ and hence

$$\sigma = \sigma_0 + 2\sigma_1 = |a_0|^2 + 2|a_1|^2$$

The coherent excitation of the magnetic substates requires a fixed phase relation between the excitation amplitudes. For any given excitation process, determined by the excitation energy and the scattering angle, the amplitudes a_1 and a_0 are expected to have fixed relationship to each other:

$$a_1 = |a_1| \exp(i\alpha_1) \text{ and } a_0 = |a_0| \exp(i\alpha_0)$$

where α_0, α_1 are the phases of the excitation amplitudes.

Since $\mid \psi >$ is defined only up to an overall phase factor, a_0 may be taken to be real and positive. The relative phase χ between a_1 and a_0 is therefore defined by,

$$a_1 = \mid a_1 \mid \exp(i\chi) \text{ where } \chi = (\alpha_1 - \alpha_0)$$

The parameter λ is defined as the ratio of the partial differential cross section for the excitation of the M = 0 substate to the total differential cross section for the n^1P state. It is given by,

$$\lambda = \frac{\sigma_0}{\sigma} = |a_0|^2 / (2|a_1|^2 + |a_0|^2)$$

The angular distribution of the coincident photon radiation is determined by the angular corrlation function N as used by Eminyan et al (1974),

$$N = \lambda \sin^2 \theta_\gamma + \left(\frac{1-\lambda}{2}\right)(\cos^2 \theta_\gamma + 1) - \left(\frac{1-\lambda}{2}\right) \sin^2 \theta_\gamma \cos 2(\phi_\gamma - \phi_e) + \{\lambda(1-\lambda)\}^{\frac{1}{2}} \cos \chi \sin 2\theta_\gamma \cos(\phi_\gamma - \phi_e) \quad (2.7)$$

where θ_γ is the polar angle for the detection of photons and ϕ_e and ϕ_γ are, respectively, azimuthal angles for the electron scattering and the photon emission.

In the experimental study (Eminyan et al, 1974) of electron-photon angular correlations for the excitation process under consideration, the electron beam is incident in the Z direction on the target located at the origin of coordinates (as in fig.1). Scattered electrons are collected in a particular direction θ_e, the polar angle for the detection of electrons, by an analyser whose position defines the scattering plane, which is taken to be the XZ plane. Therefore, $\phi_e = 0$ for all detected scattered electrons. Photons are counted, without regard to polarisation, by a detector placed in any direction in the scattering plane on the opposite side of the electron beam from the analyser, that is, $\phi_\gamma = \pi$. In this case, eqn.(2.7) becomes

$$N = \lambda \sin^2 \theta_\gamma + (1-\lambda) \cos^2 \theta_\gamma - \{\lambda(1-\lambda)\}^{\frac{1}{2}} \cos \chi \sin 2\theta_\gamma \quad (2.8)$$

The collision parameters λ and χ can be determined from the coincidence experiment by fitting the experimental data to the angular correlation function. Since χ appears in a cos χ term in eqn. (2.8), the data yields only the absolute value $|\chi|$ of the phase difference.

The above analysis is based upon the assumption of coherent excitation of the magnetic substates. However the basic assumption of coherent excitation cannot be tested by the coincidence experiment when photons are detected only in the scattering plane. Incoherent excitation of the magnetic substates would also be an interpretation for the electron-photon angular correlation data from observation in the scattering plane, that is, the angular correlation function of eqn.(2.8) can also be fitted to a model of incoherent excitation whereby two oscillators are oscillating randomly parallel to the main axes of the polarisation eclipse. It implies that a more rigorous test of the "degree of coherence" of the substate excitation can only be based upon a complete analysis of the polarisation state of the photons. If completely coherent excitation of the substates occurs then no phase randomness should exist between the excitation amplitudes a_0 and a_1, and consequently the photon radiation should be completely polarised. If there is randomness in the phases of the excitation amplitudes then there should be randomness in the polarisation state of the photons which result from the transitions of the substates. The degree of coherence of the excitation process must then be related to the characteristics of the coherency of the photon radiation.

The polarisation state of the coincident photons can be determined by the elements of the "coherency matrix" or equivalently, the Stokes parameters. The observables in photon polarisation measurements can be directly related to the intensities of any two mutually orthogonal components of the electric vector at right angles to the direction of propagation. For the photon radiation observed along y-axis, perpendicular to the scattering plane, the elements of the "coherency matrix" can be determined (Born and Wolf, 1975) by the linearly polarised light vectors with components along z- and x-axes (see fig.1).

Let $E_z = E_{zo} e^{i(\phi_1 - \omega t)}$ and $E_x = E_{xo} e^{i(\phi_2 - \omega t)}$

represent these components of the electric vector for a light wave, where ω is their common angular frequency and ϕ_1 and ϕ_2 are their phases.

If the x-component is subjected to a retardation δ with respect to z-component by means of a compensator ($\frac{\lambda}{4}$ plate in the present experiment) then the intensity $I(\alpha,\delta)$ of the light in a direction making an angle α with the z-direction can be analysed by passing the light through a polariser with the appropriate orientation. The component of the electric vector in the xz plane making an angle α with the z-direction is given by,

$$E(\alpha,\delta) = E_z \cos\alpha + E_x e^{i\delta} \sin\alpha$$

$$\therefore \quad I(\alpha,\delta) = \langle E(\alpha,\delta)\, E^*(\alpha,\delta) \rangle$$

$$= (E_z \cos\alpha + E_x e^{i\delta} \sin\alpha)(E_z^* \cos\alpha + E_x^* e^{-i\delta} \sin\alpha)$$

$$= \langle E_z E_z^* \rangle \cos^2\alpha + \langle E_x E_x^* \rangle \sin^2\alpha + \langle E_z E_x^* \rangle e^{-i\delta} \cos\alpha \sin\alpha$$

$$+ \langle E_x E_z^* \rangle \sin\alpha \cos\alpha\, e^{i\delta}$$

$$= J_{zz}\cos^2\alpha + J_{xx}\sin^2\alpha + J_{zx}e^{-i\delta}\cos\alpha\sin\alpha + J_{xz}e^{i\delta}\sin\alpha\cos\alpha \qquad (2.9)$$

where the J's are the elements of the "coherency matrix" of the light wave,

$$J = \begin{pmatrix} J_{zz} & J_{zx} \\ J_{xz} & J_{xx} \end{pmatrix} = \begin{pmatrix} \langle E_z E_z^* \rangle & \langle E_z E_x^* \rangle \\ \langle E_x E_z^* \rangle & \langle E_x E_x^* \rangle \end{pmatrix} = \begin{pmatrix} \langle E_{zo}^2 \rangle & \langle E_{zo} E_{xo} e^{i(\phi_1 - \phi_2)} \rangle \\ \langle E_{zo} E_{xo} e^{-i(\phi_1 - \phi_2)} \rangle & \langle E_{xo}^2 \rangle \end{pmatrix}$$

The diagonal elements of the matrix represent the intensities of the components in the z- and x-directions and therefore the trace of the matrix is equal to the total intensity of the light. Following Born and Wolf (1975), a "coherence correlation factor" is defined as follows:

$$\mu_{zx} = |\mu_{zx}| e^{i\beta_{zx}} = \frac{J_{zx}}{(J_{zz} J_{xx})^{\frac{1}{2}}} \qquad (2.10)$$

μ_{zx} is a measure of correlation between the two orthogonal linearly polarised components of the radiation, parallel and perpendicular to the incident electron beam direction. $|\mu_{zx}|$ is the "degree of coherence" between these two orthogonal components and $\beta_{zx} = \phi_1 - \phi_2$ is their "effective phase difference". The radiation will be coherent if the phase difference, β_{zx}, remains constant in time and if β_{zx} changes rapidly in a random manner with time then the radiation will be incoherent.

The coherence correlation factor can be determined from the measurements of the Stokes parameters of the photon radiation as first demonstrated by Standage and Kleinpoppen (1976). The Stokes parameters (P_0, P_1, P_2, P_3) and the elements of the coherency matrix

are related by the formulae,

$$P_0 = J_{zz} + J_{xx}$$

$$P_1 = J_{zz} - J_{xx}$$

$$P_2 = J_{zx} + J_{xz}$$

$$P_3 = i(J_{xz} - J_{zx})$$

These parameters can be determined by observing the intensity, $I(\alpha,\delta)$, of the light for different values of α (orientation of the polariser) and δ (delay introduced by the compensator) and solving the corresponding relations obtained from eqn.(2.9). In terms of the intensity measurements pertaining to a particular pair α,δ; these parameters are given by

$$P_0 = I(0^o,0) + I(90^o,0)$$

$$P_1 = I(0^o,0) - I(90^o,0)$$

$$P_2 = I(45^o,0) - I(135^o,0)$$

$$P_3 = I(45^o,\frac{\pi}{2}) - I(135^o,\frac{\pi}{2})$$

The four Stokes parameters can thus be expressed in terms of the polarised intensities of the photon radiation:

$$P_0 = I(0^o) + I(90^o)$$

$$P_1 = I(0^o) - I(90^o)$$

$$P_2 = I(45^o) - I(135^o)$$

$$P_3 = I(RHC) - I(LHC)$$

$I(\alpha)$ is the intensity of light, linearly polarised at an angle α with respect to the electron beam direction. I(RHC) and I(LHC) are, respectively, the right- and left-handed circularly polarised

intensities of the photon radiation. When the Stokes parameters (P_0, P_1, P_2, P_3) are normalised to P_0, the total intensity, then P_1 and P_2 are equal to the linear polarisations measured with reference to the incident electron beam direction and at 45° to this direction, respectively, and P_3 is equal to the circular polarisation. These normalised Stokes parameters, are thus given by,

$$P_0 = 1$$

$$P_1 = \frac{I(0^o) - I(90^o)}{I(0^o) + I(90^o)}$$

$$P_2 = \frac{I(45^o) - I(135^o)}{I(45^o) + I(135^o)} \qquad (2.11)$$

$$P_3 = \frac{I(RHC) - I(LHC)}{I(RHC) + I(LHC)}$$

The coherence correlation factor ((eqn. (2.10)) is then related to the normalised Stokes parameters ((eqn. (2.11)) as follows:-

$$\mu_{zx} = \frac{P_2 + i\,P_3}{(1 - P_1^2)^{\frac{1}{2}}}$$

$$\text{With} \quad |\mu_{zx}| = \left(\frac{P_2^2 + P_3^2}{1 - P_1^2}\right)^{\frac{1}{2}} \qquad (2.12)$$

$$\text{and} \quad \beta_{zx} = \tan^{-1}\left(\frac{P_3}{P_2}\right) \qquad (2.13)$$

A useful quantity which characterises the coherence of the emitted light is the "vector polarisation" $\underline{P}$. The three normalised Stokes parameters P_1, P_2, P_3 form the components of this three-dimensional vector whose magnitude is the "degree of polarisation" given by,

$$| \underline{P} | = (P_1^2 + P_2^2 + P_3^2)^{\frac{1}{2}} \qquad (2.14)$$

A photon beam is completely coherent that is, every detected photon is in the same polarisation state if and only if the "degree of coherence" and the "degree of polarisation" are equal to unity.

3. APPARATUS

3.1. Apparatus for the Polarisation Measurements

The general description of the main parts of the apparatus, shown schematically in figure 2, is given in the following sections.

3.1.1. The Vacuum System

The vacuum system consisted of two cylindrical stainless steel chambers, bolted together, forming a single chamber of length 830 mm with an internal diameter of 350 mm. There were two NW 350 end flanges and various smaller flanges to take feedthroughs and other components as required. All flanges were flat and the vacuum seals were achieved using viton O rings. The system was evacuated by two mercury diffusion pumps, an Edwards 6M3 A and a Leyhold-Heraeus Quick 505. Both diffusion pumps were fitted with water-cooled baffles and liquid nitrogen cold traps. The vacuum chambers could be isolated from the diffusion pumps by means of electro-pneumatically operated butterfly valves, Edwards QSB6P. The diffusion pumps were connected in parallel to an oil-sealed rotary vane pump, Leybold-Heraeus D12A, which was used as the backing pump. There was an electromagnetic isolating valve in the common part of the backing line. The base pressure achievable in the vacuum chamber was $\sim 1.5 \times 10^{-6}$ Torr.

The effective pumping speed of the system was determined using the intrinsic speeds of the pumps for air. The numbers used in this connection, in sections 3.1.3 and 3.2.2., are therefore only rough estimates since the intrinsic speeds of the pumps for mercury are not known. The effective speed S_e of a pump depends on the compound conductance C, $\frac{1}{C} = \frac{1}{C_1} + \frac{1}{C_2} + \frac{1}{C_3}$, due to conductances

C_1, C_2 and C_3 of cold trap, baffle and butterfly valve. The effective pumping speed S_e is related to the intrinsic pumping speed S_p through the compound conductance C by the formula (Dennis and Heppell, 1968),

$$\frac{1}{S_e} = \frac{1}{S_p} + \frac{1}{C}$$

However due to the Cryo-pumping action of the liquid nitrogen cold traps for mercury vapour, the overall pumping speed was assumed to be twice the speed for air.

In this way the overall pumping speed S_o of the system was found to be $\sim$750 ℓsec^{-1}.

3.1.2 The Mercury Beam Source

The mercury beam source consisted of an oven made of stainless steel with a capacity of 50 mℓ connected to an aperture made from 1 mm bore stainless steel tube, 200 mm long, with a wall thickness of 1 mm. The mercury beam was produced by heating the oven, and the tube along its length. The heating to the oven was achieved by heating rods, made by winding a 0.5 mm thick kanthal wire around grooved ceramic rods. These rods, coated with cataphoretic suspension of aluminium oxide to prevent shorting, were inserted in holes in the oven. The tube was heated by means of the kanthal wire, which was wound around the tube after insulating with glass fibre sleeving. The winding of the wire in each case was carried out in a bifilar manner. The temperatures of the oven and the tube were obtained from chromel-alumel thermocouples and both the oven and the tube were held at 120^oC to within $\pm\frac{1}{2}C^o$ by the use of temperature controllers (Pye, 17-90B). The tube was bent such that the mercury beam effused vertically downwards and was collected in the liquid nitrogen cold trap of the diffusion pump. The pressure

in the chamber with the beam on was $\sim 2.5 \times 10^{-6}$ Torr, allowing for the calibration factor of 0.3 for mercury, compared to 1.5×10^{-6} Torr with the beam off.

3.1.3. The Mercury Beam Density

When the system is running in an equilibrium state then the effusion rate N is related to the pressure P through the overall pumping speed S_o by,

$$N = 3.54 \times 10^{19} \; S_o \times P \qquad (3.1)$$

where the numerical factor converts the flow rate in Torr ℓ sec^{-1} into atoms sec^{-1}.

For the mercury background pressure of $\sim 1 \times 10^{-6}$ Torr and the overall pumping speed of 750 ℓ sec^{-1}, the flow rate according to eqn. (3.1) is,

$$N = 2.7 \times 10^{16} \text{ atom } sec^{-1} \qquad (3.2)$$

The source configuration plays an important role in achieving a high beam intensity. The beam emerging from the source should be strongly peaked in the forward direction. A simple aperture source has the disadvantage of a broad cosine distribution of intensities and therefore a long canal source was used in the present experiment.

The beam formation by long tubes has been studied by Giordmaine and Wang (1960) who derived expressions for intensities and verified them experimentally. They showed that the peak intensity and the collimation of the beam are essentially determined by intermolecular collisions in the tube. Depending on the ratio of the mean free path λ in the tube to the radius r and length ℓ of the tube, different results for the beam intensities are obtained. At very low pressures

with $\lambda >> \ell$ and $\lambda >> r$, simple molecular flow takes place. As the pressure is increased to the point where the mean free path is no longer large compared to the length of the tube but is still greater than the radius throughout the tube ($\lambda >> r \quad \lambda \lesssim \ell$) then the peak intensity on the axis ($\theta = 0$) at the exit from the aperture is given by (Giordmaine and Wang, 1960),

$$I(0) = \frac{1}{2^{\frac{1}{4}}\, 8\delta} \left(\frac{3\, \bar{v}\, r\, N}{\pi} \right)^{\frac{1}{2}} \text{ atoms sterad}^{-1} \text{ sec}^{-1} \qquad (3.3)$$

where δ is the atomic diameter, $\bar{v}$ is the average velocity of atoms in the beam, r is the radius of the tube and N is the flow rate.

As the pressure drops towards the discharge end of the tube, a point is reached at which the mean free path is equal to the remaining length of the tube, called the 'effective length'. Hanes (1960) verified experimentally that the properties of flow through a tube are essentially determined by this final section, effective length, of the tube. Thus the portion of the tube upstream from the effective length contributes little to the collimation of the beam.

The mean free path λ in cm is related to the pressure P in Torr through the relation (Ramsey, 1956),

$$\lambda = 7.321 \times 10^{-20} \frac{T}{P\sigma}$$

where $\sigma = \pi\, \delta^2$ is the collision cross section.

In the present experiment, mercury pressure in the oven was $\sim$ 1 Torr and in the chamber was $\sim 10^{-6}$ Torr. The pressure in the tube was assumed to be $\sim 10^{-3}$ Torr in order to calculate the mean free path λ in the tube. Thus the mean free path was about 5 cm

and, with $r = 0.05$ cm and $\ell = 20$ cm, the condition, $\lambda >> r$ and $\lambda \ll \ell$, for the application of equation (3.3.) was fulfilled.

The average velocity of atoms in the beam is given by (Ramsey, 1956),

$$\bar{v} = \left(\frac{9 \pi k T}{8m}\right)^{\frac{1}{2}} = \left(\frac{9 \pi k T N_a}{8A}\right)^{\frac{1}{2}} \qquad (3.4)$$

where k is the Boltzmann constant, T is the absolute temperature, m is the mass of the atom, N_a is the Avogadro's number and A is the atomic weight.

The forward peak intensity at a distance d cm from the aperture is given by eqn. (3.3) to be,

$$I = I(o)/d^2 = \frac{1}{2^{\frac{1}{2}} 8 \delta d^2} \left(\frac{3 \bar{v} r N}{\pi}\right)^{\frac{1}{2}} \text{ atoms cm}^{-2} \text{ sec}^{-1} \qquad (3.5.)$$

In the present experiment, the values of the different parameters in eqn. (3.5) are as follows:

$\delta = 4.25 \times 10^{-8}$ cm (Lew, 1967)

$d = 1$ cm

$\bar{v} = 2.4 \times 10^4$ cm sec^{-1} (Calculated from eqn. (3.4))

$r = 0.05$ cm

$N = 2.7 \times 10^{16}$ atoms sec^{-1} (given by eqn. (3.2))

Substituting these values in eqn. (3.5), the intensity in the interaction region comes out to be,

$$I = 1.4 \times 10^{16} \text{ atoms cm}^{-2} \text{ sec}^{-1}$$

Hence the beam density is given by,

$$p = \frac{I}{\bar{v}} = 6 \times 10^{17} \text{ atoms m}^{-3}$$

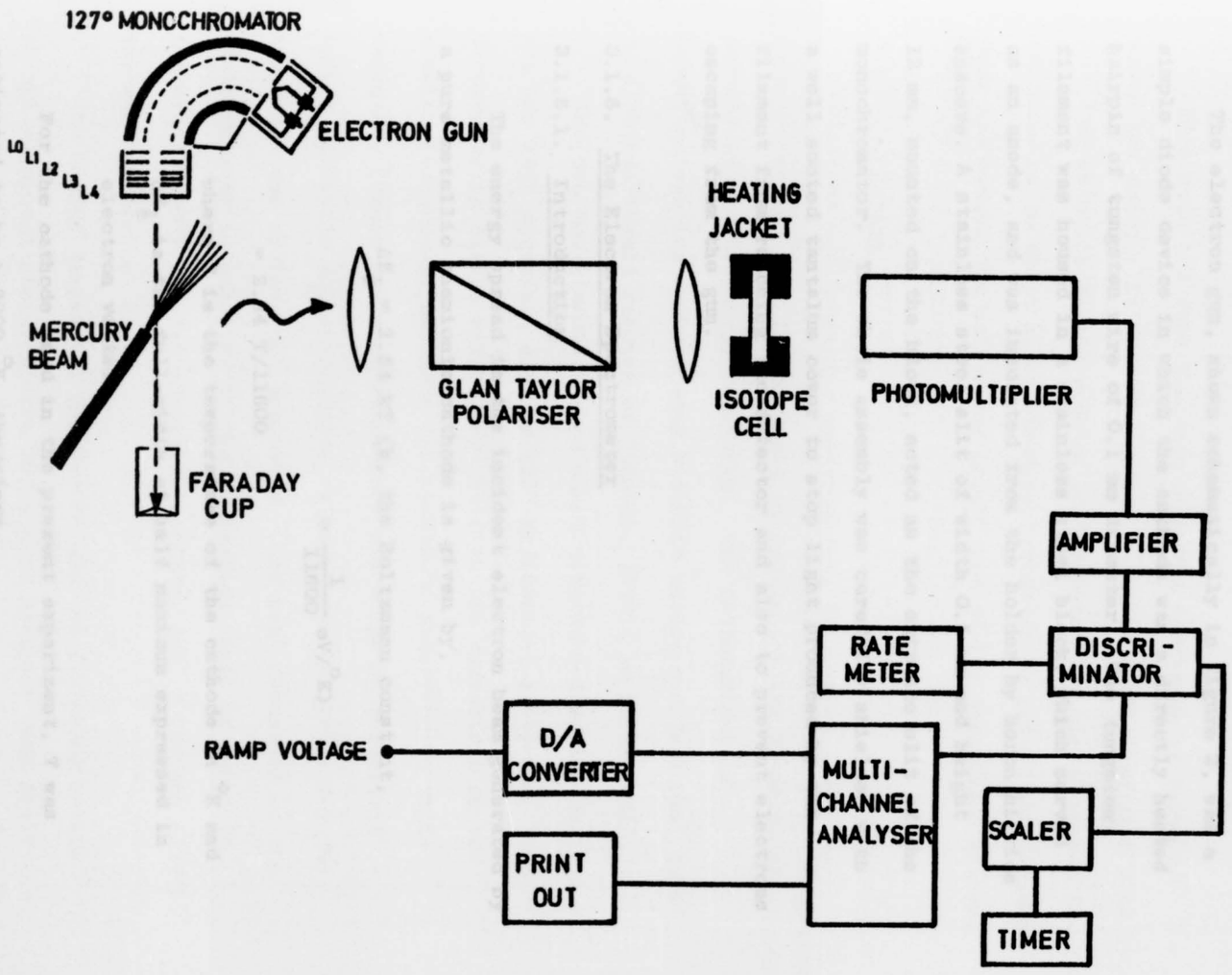

FIG. 2. Schematic diagram of the apparatus for polarisation measurements

3.1.4. The Electron Gun

The electron gun, shown schematically in figure 2, was a simple diode device in which the cathode was a directly heated hairpin of tungsten wire of 0.1 mm diameter. The tungsten filament was housed in a stainless steel block, which served as an anode, and was insulated from the holder by boron nitride spacers. A stainless steel slit of width 0.5 mm and height 12 mm, mounted on the block, acted as the entrance slit of the monochromator. The whole assembly was carefully shielded with a well sooted tantalum cover to stop light produced by the filament from reaching the detector and also to prevent electrons escaping from the gun.

3.1.5. The Electron Spectrometer

3.1.5.1. Introduction

The energy spread in the incident electron beam generated by a pure metallic themionic cathode is given by,

$$\Delta E_{\frac{1}{2}} = 2.54\ kT \quad (k, \text{ the Boltzmann constant,}$$

$$= \frac{1}{11600}\ eV/^{o}K)$$

$$= 2.54\ T/11600$$

where T is the temperature of the cathode in ^{o}K and $\Delta E_{\frac{1}{2}}$ is the full-width at half maximum expressed in electron volts.

For the cathode used in the present experiment, T was estimated to be $\sim$ 2000 ^{o}K, therefore,

$$\Delta E_{\frac{1}{2}} \simeq 0.44 \text{ eV}$$

Even with low work function cathodes operating at temperatures low enough, it is not possible to achieve $\Delta E_{\frac{1}{2}}$ less than 0.25 eV.

The solution to the problem of improving the energy spread in the beam is to adopt an electron spectrometer to filter the incident beam and reduce the half-width below that of its thermionic source.

3.1.5.2. Review

Electron electrostatic spectrometers of various types are nowadays widely used in the field of atomic physics to serve as monochromators or energy analysers. The introduction of spectrometers has enabled many hitherto unobserved features, such as electron impact resonances (Schulz, 1973), to be detected.

The two most commonly used electrostatic deflection analysers are the 180° spherical and the 127° cylindrical analysers. The electrostatic field, established between two concentric or two coaxial electrodes, deflects the electrons according to their energies. These two electrodes have the shape of concentric spherical shells and cylindrical sectors, respectively, for the spherical and cylindrical analysers. The best focussing of the electron beam is achieved if the deflection angle is equal to π radians (180°) for the spherical analyser and $\frac{\pi}{\sqrt{2}}$ radians (127°) for the cylindrical one.

The energy dispersing properties and the focussing action of the spherical electrostatic deflection analyser were first described by Purcell (1938). A detailed survey of the design, construction and operation of this analyser is given by Brunt et al (1977).

The theory of the cylindrical analyser was developed by Hughes and Rajonsky (1929). They investigated the path of electrons in a radial, inverse first power electrostatic field produced by a difference of potentials between two coaxial cylindrical surfaces and showed that re-focussing of electrons took place at a deflection angle of $\frac{\pi}{\sqrt{2}}$ ($127^{o}\ 17'$). Hughes and McMillen (1929) built such a cylindrical analyser and established experimentally that it could be used as an energy selector. Rudberg (1930) utilised a similar analyser for his measurements on energy loss of electrons in nitrogen. It has since found wide acceptance in a variety of applications.

Both the 180^{o} spherical and 127^{o} cylindrical analysers have their advantages and disadvantages. The 180^{o} analyser is inherently a double focussing device and provides focussing in two directions thereby giving a good efficiency for the transmission of electrons. Also this analyser has a resolving power about twice that of a 127^{o} cylindrical analyser of the same radius of curvature (Purcell, 1938). In the 127^{o} analyser, on the other hand, the problem of space charge is less serious than in the 180^{o} analyser (Froitzheim et al 1975). In this experiment, the 127^{o} cylindrical type was used because its design was mechanically simpler than the spherical one.

3.1.5.3. The 127^{o} Cylindrical Analyser

A schematic diagram of such an analyser showing electron trajectories is given in figure 3. It consists of two electrodes which are coaxial cylindrical sectors having radii of curvature R_1 and R_2, $(R_2 > R_1)$, maintained at potentials V_1 and V_2 respectively. The mean, $R_o = \frac{R_1 + R_2}{2}$ is the radius of the central path of electrons through the analyser. α and β are the angular divergences of the beam in the radial and axial planes respectively.

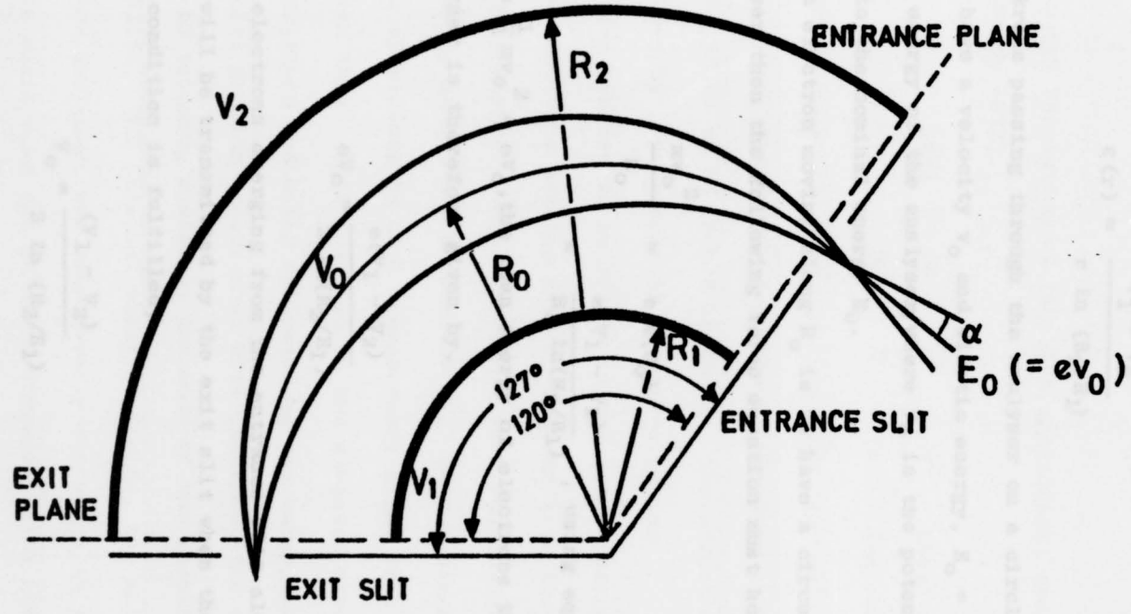

Fig.3. Electron trajectories in a 127° cylindrical analyser

The electric field inside the analyser at a radial distance r from the inner electrode is given by,

$$\varepsilon(r) = \frac{V_1 - V_2}{r \ \ell n \ (R_2/R_1)} \qquad (3.6)$$

Electrons passing through the analyser on a circle with mean radius R_o have a velocity v_o and kinetic energy, $E_o = eV_o$, the mean pass energy of the anslyser, where V_o is the potential corresponding to the nominal energy E_o.

If an electron moving along R_o is to have a circular path in the anslyser then the following force equation must hold,

$$\frac{mv_o^2}{R_o} = e \ \varepsilon(R_o)$$

$$= \frac{e(V_1 - V_2)}{R_o \ \ell n(R_2/R_1)} \ , \text{ using eqn. (3.6)}$$

Since $\frac{1}{2} mv_o^2 = eV_o$, the mean energy of electrons through the analyser is therefore given by,

$$eV_o = \frac{e(V_1 - V_2)}{2 \ \ell n(R_2/R_1)}$$

Thus electrons emerging from the entrance slit along R_o with energy E_o will be transmitted by the exit slit when the following focussing condition is fulfilled,

$$V_o = \frac{(V_1 - V_2)}{2 \ \ell n \ (R_2/R_1)}$$

It can be shown that the potential of the inner electrode is,

$$V_1 = V_o \ \{1 + 2 \ \ell n \ (R_o/R_1)\}$$

and that of the outer one is,

$$V_2 = V_o \ \{1 + 2 \ \ell n \ (R_o/R_2)\}.$$

In general these potentials are nearly symmetric with respect to V_o and are chosen in such a way that the entrance slit, the exit slit and the middle trajectory of the analyser are at the potential V_o.

The energy resolution of the 127° cylindrical analyser is given by (Rudd, 1972),

$$\frac{\Delta E_{\frac{1}{2}}}{E_o} = \frac{\Delta R}{R_o} + \frac{\alpha^2}{3} + \frac{\beta^2}{4},$$

where ΔR is the width of identical entrance and exit slits.

It implies from the above relation that, in order to obtain narrow resolution, the analyser should be operated at low energies and also the value of ΔR should be small. The effect of α and β can be reduced by a pre-selector injection system.

A serious problem in analysers is the space charge build up by unwanted electrons arising from collisions with the slits and walls of the analyser. This effect has been controlled with the use of grids by Marmet and Kerwin (1960). They replaced the solid cylindrical electrodes by high transparency grids with collector plates behind them. This resulted in the unwanted electrons leaving the selector field and being collected by the outer collector plates.

A special problem encountered with electrostatic deflection is the effect of fringing fields at the ends of the electrodes in the region of slits. The internal electric fields, for which these analysers are designed, are considerably distorted at the ends. The electric field does not go discontinuously from its maximum value to zero as the boundary of the region between the electrodes is passed but falls off gradually. This field has the effect of lengthening the electrodes so that the analyser will function as though the angle were somewhat greater than 127°. In order to

reduce end effects, it is possible to put the object and image points at some distance from the actual entrance and exit planes of the analyser. The result is that the entire 127° is not needed and a smaller sector angle can be used. Pavlovic et al (1972) used a sector angle of 112° and Roy et al (1975) employed an angle of 121° 6′. As mentioned in the next section, the sector angle for the monochromator used in this experiment was 120°.

3.1.5.4. Mechanical Design of the 127° Monochromator

The 127° cylindrical monochromator, shown schematically in figure 2, was built to a design by Raible (1974) following the principles outlined by Marmet and Kerwin (1960). The dimensions of the monochromator were as follows:

radius of inner grid	=	12 mm
radius of outer grid	=	18 mm
mean radius	=	15 mm
radius of inner collector plate	=	8 mm
radius of outer collector plate	=	22 mm

The two grids formed a channel 6 mm across and 23 mm high. Slits of different widths and heights could be used (typically ΔR = 0.5 mm and height = 12 mm).

Copper was used for machining these electrodes except for the slits which were made from molybdenum. The deflecting grids were made from 86.5% transparent tungsten gauze and were bonded to cylindrical copper frames with silver epoxy paint. Behind these transparent electrodes were the solid collector plates, held more positive than the grids, to collect electrons which passed through

the grids. All electrodes were sooted in order to reduce the possibility of electrons being reflected off the walls. These sooted electrodes were assembled on two 120° copper sectors, each of radius 26 mm. Ceramic rods and washers were used for holding electrodes in position and also provided the insulation and the correct spacing between them. The field section (sector angle of focussing electrodes) was 120°, and not 127°, to minimise the effect of fringing field at the input and output planes of the monochromator. The complete assembly was held together by an outer stainless steel cylindrical block which could be used as a heating jacket to bake the monochromator.

3.1.6. The Electrostatic Lens System

The electron beam emerging from the monochromator was focussed at the desired energy on to the atomic target by a five element (L_0, L_1, L_2, L_3, L_4) electrostatic lens system (fig.2). The element (L_1) after the exit slit (L_0) was a stainless steel electrode with an aperture of rectangular cross section 5 mm x 20 mm. A piece of tungsten gauze, 86.5% transparent, was spot-welded on to the aperture in order to restrict the divergence of the electron beam resulting from the aperture. The three elements (L_2, L_3, L_4) lens were designed according to calculations by Read (1970) with aperture to aperture spacings of 0.5 D where D, the diameter of the apertures, was 5 mm. The elements L_2 and L_3 were split in halves and were mounted with spacings between respective halves perpendicular to each other in order to deflect the electron beam up/down and left/right to achieve proper alignment. The deflection of the beam was controlled by varying the potential difference between the two halves of the same element whereas the focussing was affected by the potential difference

between the mean potentials of the two elements. L_1 and L_4 were held at ground potential while the potentials on L_2 and L_3 were varied. In this way the electrons were accelerated between L_0 to L_1 to the interaction energy and were focussed at the interaction region by L_1, L_2, L_3, L_4. The elements (L_2, L_3, L_4), rectangular in shape with circular apertures, were made of stainless steel and were insulated from the mounting rods by boron nitride washers. The lens system was covered with a well sooted box of tantalum to restrict stray electrons.

3.1.7. Power Supplies to the Electron Beam System

Power supplies to the electron beam system are shown schematically in figure 4. All power supplies used for the system were highly stabilised constant d.c. voltage sources. Variations in the output voltage of these supplies due to temperature effects over a period of 24 hours were less than 0.2 mV. A potential distribution box was built in which 12 ten-turns Helipot (Beckman Instruments Ltd) high precision potentiometers (100 k Ω, 5W) were connected in parallel. The input to this potential box was a 0-100 V power supply (Kepco, PCX 100). Most elements of the system derived voltages from this potential box other than cathode and anode, which had individual 0-40 V supplies (Kepco, PCX 40). All the voltages were relative to one reference potential which was biased with a 0-40 V supply to off-set these voltages. The ramp voltage was obtained using a digital to analogue converter (Advance Electronics DA 120 B) in conjunction with a multichannel analyser and was used together with off-set voltage to scan the energy of electrons in the interaction region over the desired range between 4.5 to 8.0 eV.

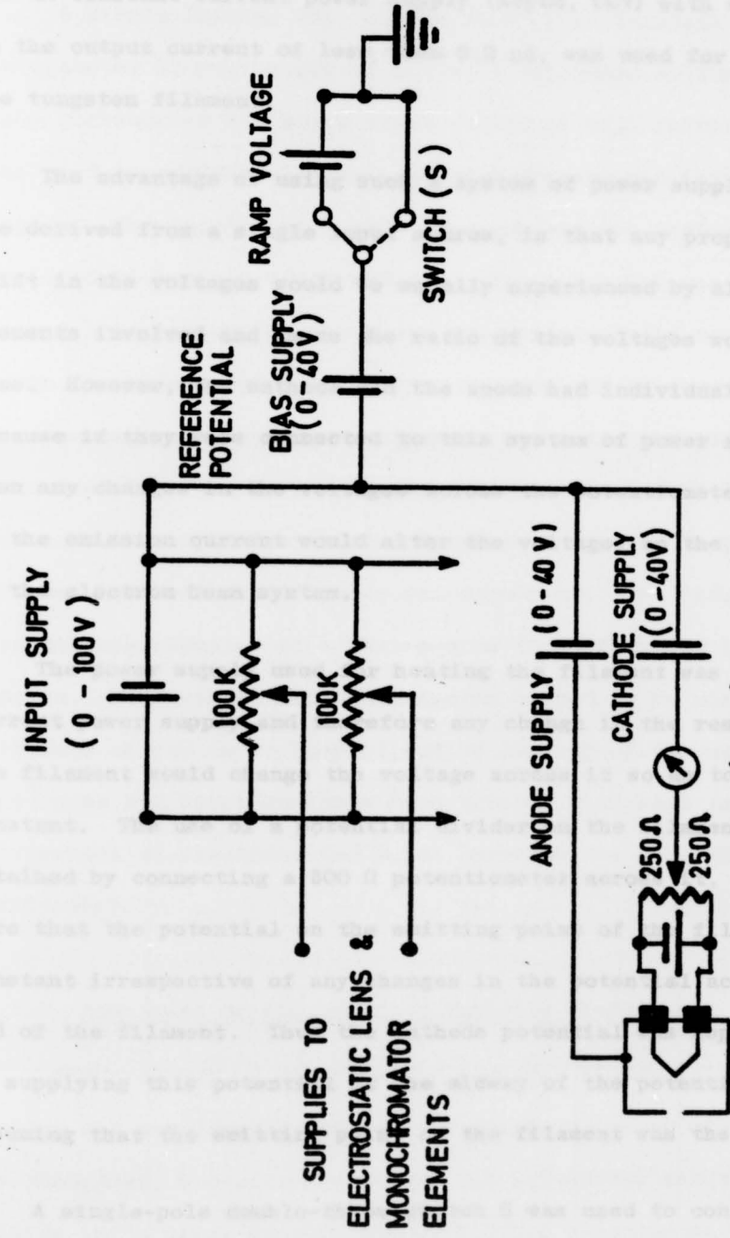

FIG.4. Power supplies to the electron beam system.

A 0-2A constant current power supply (Kepco, CC7) with variations on the output current of less than 0.2 μA, was used for heating the tungsten filament.

The advantage of using such a system of power supplies, which are derived from a single imput source, is that any proportionate drift in the voltages would be equally experienced by all the elements involved and hence the ratio of the voltages would be the same. However, the cathode and the anode had individual supplies because if they were connected to this system of power supplies then any changes in the voltages across the potentiometers due to the emission current would alter the voltages on the elements of the electron beam system.

The power supply used for heating the filament was a constant current power supply and therefore any change in the resistance of the filament would change the voltage across it so as to keep the current constant. The use of a potential divider on the filament, which was obtained by connecting a 500 Ω potentiometer across it, was to make sure that the potential on the emitting point of the filament was constant irrespective of any changes in the potential across each end of the filament. Thus the cathode potential was kept constant by supplying this potential at the midway of the potential divider assuming that the emitting point of the filament was the mid point.

A single-pole double-throw switch S was used to connect the reference potential to earth when the incident energy of electrons was not ramped and had to be fixed by manually adjusting the off-set voltage for the individual polarisation measurements (section 4.1.5).

3.1.8 The Faraday Cup

A simple Faraday Cup, in the form of a stainless steel cylinder of diameter 10 mm, length 25 mm, wall thickness of 2mm and enclosed in a rectangular stainless steel cuboid of wall thickness 2.5 mm, was used to collect electrons passing through the interaction region. The insulation between the cup and the enclosure was achieved by boron nitride washers. The outer box was held at ground potential while the inner cup was connected to an electrometer (Keithley, Model 610 CR) to measure the electron current. The function of the outer box was to eliminate the collection of unwanted electrons as well as to ensure a field free interaction region. The significance of a long inner cup was to provide a greater collection efficiency for electrons. The Faraday Cup (fig.2) assembly was mounted at a distance of 15 mm from the interaction region. For coincidence measurements it had to be moved to a distance of 110 mm to keep it out of the way of the analyser. The inner and outer surfaces were covered with soot to reduce reflection of electrons and hence increase the collection efficiency.

3.1.9 Annulment of Electric and Magnetic Fields

The presence of electric and magnetic fields in the interaction region can considerably affect the trajectories of electrons. It is, therefore, necessary to reduce all extraneous electric and magnetic fields which might disturb the prescribed electron paths.

In this experiment the electric fields were cancelled by keeping all parts of the components viewed by the interaction region at earth potential, and thereby providing a field free region. Shields on

electron gun and lenses restricted stray electrons and eliminated the penetration of potentials into the collision region. The effect of electric fields produced by the potentials on the connecting wires was minimised by keeping these wires away from the interaction region. All surfaces around the interaction region, visible to the electron beam, were coated with soot. In addition to reducing the reflection coeficients, the sooted surfaces limited the production of secondary electrons. McGowan (1961) demonstrated the advantages of using soot for the purpose of obtaining a stable, low reflectivity surface, particularly in low energy electron beams where reflection dominates over secondary emission.

The effect of a magnetic field is particularly serious when performing a deflection type of energy analysis with low energy electrons. The magnetic field deflects the electrons before, during and after analysis so that fewer than expected reach the detector. It is extensively mentioned in the literature (Lindau and Hagstrom 1971, Preston et al 1973) that the successful operation of a low energy electron spectrometer requires the reduction of stray magnetic fields to an acceptable level. The maximum magnetic field B_{max} (in Gauss), which may be tolerated, can be evaluated by means of the following relation (Powell, 1968),

$$B_{max} = 6.74 \frac{E^{\frac{1}{2}} d}{s^2} \qquad (3.7)$$

where E is the electron energy expressed in eV, d is the maximum tolerable beam deflection in cm and s is the electron path length in cm.

The magnetic field was mainly due to the earth's magnetic field but was influenced by the mild steel girders erected for the suspension of the vacuum system and by the liquid nitrogen dewer used. The

field was reduced to less than 10 mG over the region traversed by the electron beam and to less than 5 mG in the centre of interaction region by the use of three mutually perpendicular pairs of rectangular Helmholtz coils. For an operational energy of 2 to 4 eV and a distance of $\sim$ 3.3 cm, given by $\frac{\pi}{\sqrt{2}} R_o$, through the monochromator, the above values of the magnetic field were consistent with the limit set by eqn. (3.7).

In order to eliminate any magnetic field from the apparatus itself; the vacuum chambers, components inside the system and the framework for the Helmholtz coils were made from non-magnetic materials. The magnetic field from the currents for the heating of the filament and the mercury beam source was cancelled due to the opposite flow of the currents in adjacent wires.

3.1.10. The Interlock System

An interlock control unit was incorporated in the system which used, for its operation, the pressure trip level on the ionisation gauge control unit and a thermal switch monitoring the temperature of the water circulating in the baffles for the diffusion pumps. This interlock unit would completely shut down the system in the event of the following faults,

(i) electric power failure

(ii) rise in pressure inside the vacuum chamber.

The rise in pressure would be caused due to a leak developing in the system, the failure of the liquid nitrogen supply to the cold trap or the closure of the butterfly valve as the result of a fault in the compressed air.

(iii) failure of the cooling water supply.

Should any of the above faults occur then the butterfly valves would close and the diffusion pumps together with all power supplies would switch off. The system would not switch on again unless the control unit was reset.

3.1.11. The Isotope Cell

3.1.11.1. Introduction

The radiation emitted from the excited mercury atoms in the interaction region originated from the naturally occurring isotopic mixture (table 1.). The even isotopes with nuclear spin I = 0 have abundance of 70% while the two odd isotopes ^{199}Hg and ^{201}Hg with nuclear spins I = $\frac{1}{2}$ and $\frac{3}{2}$ have abundance of 17% and 13% respectively.

ISOTOPE	196	198	199	200	201	202	204
NATURAL ABUNDANCE %	0.14	10.02	16.84	23.13	13.22	29.80	6.85

Table 1: Isotope contents in natural mercury (Weast, 1975)

The function of the isotope cell was to filter out that part of the observed radiation which had hyperfine effect due to non-zero nuclear spins of the odd isotopes of mercury. The radiation could only be absorbed in the isotope cell if it interacted with a mercury atom in the cell having the same nuclear spin as the emitting atom. The isotope cell contained mercury isotopes ^{199}Hg and ^{201}Hg in the proportion of 48.7% and 48.1% respectively, with the remaining 3.2% being even isotopes arising as impurities in the odd isotopes (table 2). By raising the temperature of the isotope cell and thus increasing the saturated vapour density of mercury atoms in the

light path, the cell could be made increasingly opaque to the radiation from the odd isotopes ($I \neq 0$) which would be absorbed by the odd isotopes in the cell. The radiation intensity from the even isotopes ($I = 0$) should only slightly change due to the small fraction of even isotopes in the cell.

ISOTOPE SAMPLE	ABUNDANCE %						
	196	198	199	200	201	202	204
199	0.00	0.54	97.09	1.84	0.22	0.26	0.05
201	0.00	0.11	0.26	1.13	95.94	2.48	0.08

Table 2: Purity of the odd isotopes used in the cell.

The isotope cell had sufficient mercury to maintain saturated mercury vapour at each stage of the experiment as can be verified by the following consideration.

For n moles at low pressure, the ideal gas equation reads :

$$pv = n R T \qquad (3.8)$$

where p is the pressure, v is the volume, T is the absolute temperature and R is the gas constant.

Since $n = \frac{m}{M}$,where m is the mass and M is the molecular weight of the gas,

therefore eqn. (3.8) becomes,

$$pv = \frac{m}{M} R T$$

Hence $$m = \frac{M v p}{R T} \qquad (3.9)$$

Now supposing that at a certain temperature, say 100°C, the

mercury vapour is no more saturated and can be treated as an ideal gas then the mass of the vapour is calculated by using eqn. (3.9) to compare with the mass of the mercury in the isotope cell. If the calculated mass is less than the mass in the cell then the vapour is still saturated at this temperature.

The parameters of eqn. (3.9) in the present case are,

$$M = A = 200$$

$$v = \pi r^2 \ell, \quad r = \text{radius of the cell} = 1 \text{ cm}$$

$$\ell = \text{length of the cell} = 0.5 \text{ cm}$$

$$\therefore \quad v = 1.57 \text{ cm}^3$$

$$R = 8.3 \times 10^7 \text{ erg mole}^{-1} \text{ K}^{-1}$$

Taking $T = 100^{\circ}C$

$= 373^{\circ}K$

with $p = 0.2729$ mm of Hg (corresponding mercury vapour pressure as taken from the table compiled by Weast, 1975)

Equation (3.9) yields,

$m = 0.0037$ mg

Since 0.6 mg of mercury (0.3 mg each of the two odd isotopes, see the following section 3.1.11.2) was introduced in the cell, it implies that 0.5963 mg of mercury is still in the liquid form and therefore the mercury vapour is saturated even at $100^{\circ}C$. It shows that with this mass of mercury in the isotope cell, we could go to quite high temperatures and would still have saturated mercury vapour.

3.1.11.2. Construction

Mercury isotopes (^{199}Hg and ^{201}Hg) in the form of deposits on gold leaves were supplied by ANVAR, 13 Rue Madeleine Michelis, 92200 Neuilly-Sur-Seine, France. A quartz cell of 20 mm inside diameter and 5 mm inside length with a wall thickness of 1 mm was used to hold the isotopes. The procedure adopted to do this is shown schematically in figure 5. A side arm, made of pyrex, was attached to the pyrex tube leading to the quartz cell. Small pieces of mercury impregnated gold leaves, containing equal amounts $\sim$ 0.3 mg each of the ^{199}Hg and the ^{201}Hg isotopes, were placed in the side arm. The whole assembly was then attached to a mercury free vacuum system via a glass-to-metal seal. After the evacuation, the cell was flamed to outgas it. A tesla coil was run over it a few times to help the outgassing. The mercury was then distilled from the gold foils by heating to about 200°C. A length of cloth, dampened in water, was wrapped round the point where the side arm was connected to the cell. Liquid nitrogen was poured on to the cloth, the purpose being to trap the mercury vapour being emitted from the gold foil by freezing it out. The whole glass assembly was then pulled off by the glass blower and the mercury was collected in the cell by dipping it in liquid nitrogen and allowing the side arm to warm up. The quartz isotope cell was sealed and then pulled off from the rest of the pyrex assembly.

3.1.11.3. Assembly

The isotope cell was enclosed in a brass housing which served as the heating jacket. The isotope cell assembly is shown schematically in figure 6. The diagram shows the lower portion of the brass casing that holds the isotope cell. Both this lower portion and the upper

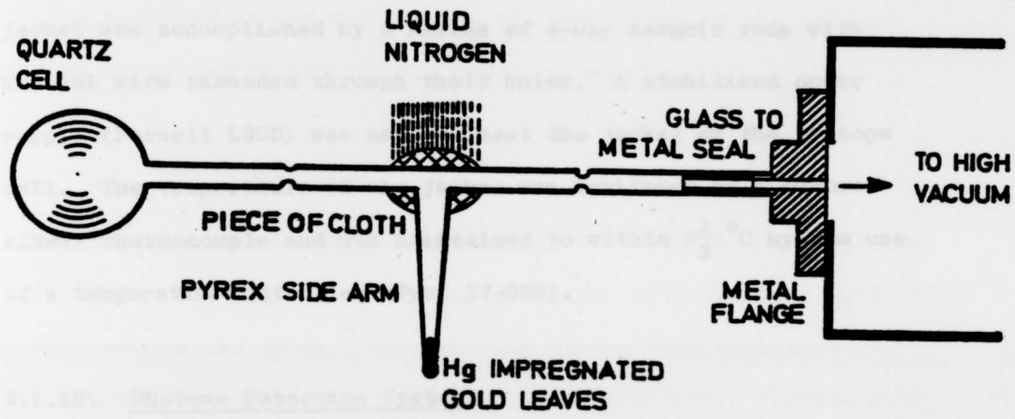

FIG 5. Set-up for the construction of the isotope cell.

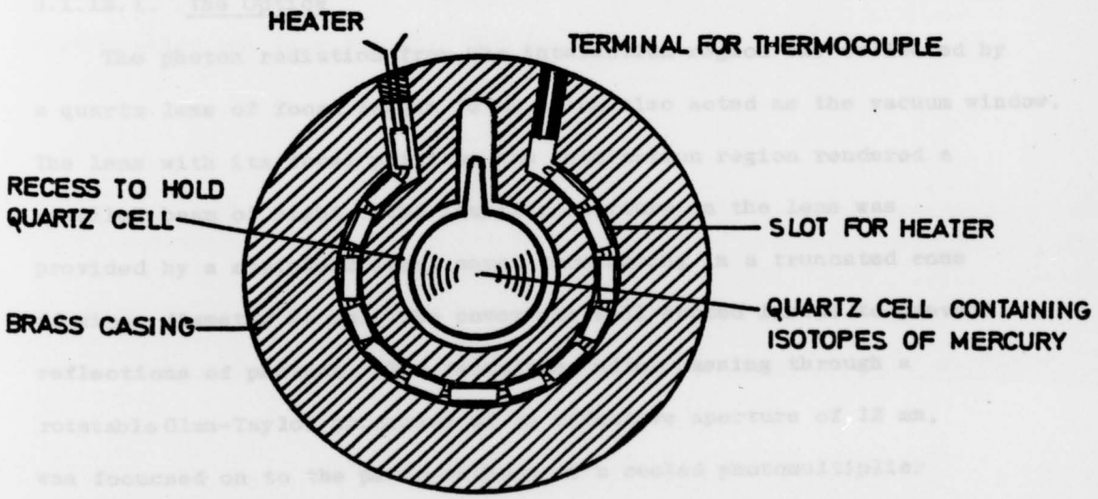

FIG.6. Assembly of the isotope cell.

half of the casing, which was fitted on to the lower half, had knife edged apertures of 12 mm diameter. The brass housing was well sooted before assembling the isotope cell in it. The heating of the brass jacket was accomplished by a series of 4-way ceramic rods with kanthal wire threaded through their holes. A stabilised power supply (Farnell L30D) was used to heat the jacket of the isotope cell. The temperature of the jacket was monitored by a chromel-alumel thermocouple and was maintained to within $\pm\frac{1}{2}$ °C by the use of a temperature controller (Pye, 17-90B).

3.1.12. Photons Detection System

The optics and the electronics for the detection of photons are shown schematically in figure 2.

3.1.12.1. The Optics

The photon radiation from the interaction region was collected by a quartz lens of focal length 70 mm which also acted as the vacuum window. The lens with its focal point on the interaction region rendered a parallel beam of light. The limiting aperture on the lens was provided by a stainless steel cover terminating in a truncated cone of minor diameter 25 mm. The cover was well sooted inside to prevent reflections of photons. The radiation, after passing through a rotatable Glan-Taylor polariser of an effective aperture of 12 mm, was focussed on to the photo-cathode of a cooled photomultiplier tube (EMI 6256 S) by a second quartz lens of focal length 200 mm. The photomultiplier tube was cooled using Peltier cooling modules (Mectron Frigistor Ltd) in order to reduce the dark current counts of the photomultiplier. When cooled down to -2°C, the dark current of the

photon multiplier was $\sim$ 1 count/sec. The isotope cell of effective aperture 12 mm was introduced between the second lens and the photomultiplier in order to eliminate the effect of hyperfine structure in the observed photon radiation. All components of the optical system were mounted outside the vacuum chamber.

3.1.12.2. The Electronics

The pulses from the photomultiplier were fed into an amplifier (NE 4603). The pulses, after amplification, were analysed in a discriminator (NE 4602). The settings of the time constants on the amplifier and the discriminator level were chosen for the best signal to noise ratio. The output pulses from the discriminator were monitored on a ratemeter (NE 4607) and were fed to a Intertechnique Didac 800, multichannel analyser (MCA) for the collection of the data. The MCA was operated in its multiscaling mode and its contents were printed out on a teletype for analysis.

3.2. Apparatus for the Coincidence Measurements

A schematic diagram of the essential parts of the apparatus is given in figure 7. Apart from the vacuum chambers, almost all other parts were modified in order to overcome the shortcomings experienced with the previous apparatus and to add essential components such as a turntable and an electron analyser.

3.2.1. The Vacuum System

Unlike the previous arrangement, where the electron beam source and the mercury oven were mounted from different flanges, the entire collision system was mounted from the same end flange on the chamber. The main advantage of this system was that all components were accessible at the same time for a proper alignment of the mercury and electron beams. The optical system for the detection of photons was mounted from the other end flange on the chamber.

The problem with the previous vacuum system was twofold, firstly the base pressure attainable in the chamber was rather high ($\sim$ 1.5 x 10^{-6} Torr) and secondly the Edwards 6M3A diffusion pump would cease to function after nearly two weeks running. The likely cause of the failure of the pump was the migration of the mercury pump vapour past the water cooled baffle into the liquid nitrogen cold trap where the vapour would freeze and did not trickle down to the mercury reservoir. The result was that the quantity of mercury in the pump would run short developing an artificial leak to the backing line with a consequent increase of the pressure in the chamber. The way this problem was handled in the previous stage was to isolate the vacuum chamber from this pump by closing the butterfly valve on this pump, thus allowing the system to run on one diffusion pump. The defective pump would then be switched off and the liquid nitrogen cold trap

allowed to warm up (generally overnight). The trapped mercury would melt and be collected again in the reservoir. Next day the pump would be switched on again and the system would run satisfactorily for another couple of weeks when the same procedure would be repeated. This solution was only temporary and during the time this pump was off, no data could be collected because the mercury beam had to be cut off since the mercury beam was fired into the cold trap for this pump.

Before starting with the coincidence measurements, it was decided to remedy these problems namely, the high base pressure and the defective diffusion pump. In order to find the cause of the high pressure the whole system was thoroughly checked for leaks. It was found that there was a leak with the first quartz lens which was used as the vacuum seal between the chamber and the outside. The lens assembly was modified and a new viton O ring was placed between the lens and its assembly. This alteration proved useful and the base pressure reduced to a valve $\leq 1 \times 10^{-6}$ Torr.

The faulty diffusion pump was replaced with a new Edwards Diffstak (Model 160 - 700) diffusion pump which used santovac 5 oil as the working fluid. There were two obvious reasons for the choice of this pump, (i) it did not have a liquid nitrogen cold trap and thus the consumption of liquid nitrogen was reduced by more than half, (ii) for the size of the chamber, this pump had sufficient pumping speed (700 ℓ sec^{-1}) to give the desired pressure. However, a mercury diffusion pump had still to be used to collect the mercury beam in the cold trap. The two pumps were exchanged and the Leybold-Heraeus Quick 505 was now used for this purpose.

There could be problems in using an oil diffusion pump in conjunction with a mercury beam. The new pump was used after

enquiring from the manufacturers that Santovac 5 oil did not react with mercury. This information proved to be true since with this system no problem in this direction was noticeable and it worked satisfactorily.

The overall pumping speed of the new system was $\sim$ 1350 ℓ sec^{-1}. With the system running on the Diffstak alone, the base pressure attainable was $\sim 6 \times 10^{-8}$ torr. On opening the butterfly valve on the mercury diffusion pump, the base pressure rose to 1.5×10^{-7} Torr, allowing for a calibration factor of 0.3 for mercury. Thus more than half of this base pressure was due to the mercury vapour from the cold trap of the mercury diffusion pump.

3.2.2. The Mercury Beam Density

In order to improve the collimation of the atomic beam, a honeycombed assembly of stainless steel capillaries was fixed to the end of the tube on the mercury oven. The length and diameter of each capillary were, respectively, 1 mm and 0.1 mm. Also the tube was brought to within 5 mm of the interaction region to increase the beam density. The capillary source reduced the effective area of the aperture by $\sim$ 50%. The working pressure in the chamber with the mercury beam on was $\sim 1 \times 10^{-6}$ Torr compared to 1.5×10^{-7} Torr with the beam off. The oven and the tube were operated at 150°C and 220°C, respectively, to maintain this pressure. The mercury beam density under these conditions was calculated, using eqn. (3.5), to be 7×10^{18} atoms m^{-3}.

3.2.3. The Turntable

3.2.3.1. Description

A stainless steel turntable assembly was built on which the

electron gun, analyser and the Faraday Cup were mounted. The stainless steel support plate on which the turntable rotates had a diameter of 200 mm and was mounted from the end flange using six stainless steel rods. The diameter of the turntable was 110 mm and was held in the support plate by two rings made of teflon. The upper ring was fixed on to the support plate while the lower one was sandwiched between the turntable and the support plate. The electron gun and the Faraday Cup, facing each other, were fixed in positions on the support plate while the analyser was mounted on to the turntable so that it could rotate with the turntable.

The turntable was rotated by means of a system of gears (Reliance Gear Co. Ltd) consisting of a phosphor bronze gear with a stainless steel worm to prevent seizing whilst under vacuum. The gear was fixed to the turntable and the worm, attached to a stainless steel shaft, was held in two stainless steel ball races anchored on the support plate. The gears were turned using a rotary vacuum feed through (Vacuum Generators) coupled to the shaft by a stainless steel flexible drive. The gears had a reduction ratio of 90:1 that is, for 90 turns of the worm the gear would move through 1 turn. Santovac 5, a very low vapour pressure oil, was used to reduce friction in the gears between the stainless steel worm and the phosphor bronze gear.

3.2.3.2. Angular Calibration

The angular calibration of the turntable was performed by using a piece of the resistance wire from a ten-turn Helipot (Beckman Ltd). The total resistance of the portion of the wire used was 22.74 ± 0.02 K Ω. This wire was set into the groove cut in a teflon ring located around the turntable beneath the phosphor bronze gear. A spring

action copper slider from the potentiometer, fixed on to the support plate, shorted the potentiometer wire to earth at this point. The resistance between either end of the wire and earth was a measure of the angular setting of the turntable. In order to measure this resistance, connections from both ends of the wire were taken outside by means of an electrical feed through.

A basic equation relating angular variation to the resistance of the wire was derived which allowed the angle of the turntable to be determined to within $\pm 0.15^{o}$. In order to obtain this equation, six lines at intervals of 60^{o} and four lines at 90^{o} apart were inscribed, respectively, on the turntable and the support plate. Choosing one of the four lines on the support plate arbitrarily as the reference line, the turntable was rotated in steps of 60^{o} with respect to this line. The resistance R_1 between one end of the wire and earth was measured for every 60^{o} rotation of the turntable. Calling the starting position of the turntable (again chosen arbitrarily) as 0^{o} and the subsequent positions as 60^{o}, 120^{o} and so on, the resistance R_1 corresponding to these positions was measured. A graph between angles θ and resistance R_1 was plotted from where the slope ($m = \frac{R_1}{\theta}$) of the line ($R_1 = m\theta + c$) was determined to be 0.066 KΩ/degree.

The equation $R_1 = m\theta + c$ can be written as

$$\theta = m' R_1 + c'$$

where $$m' = \frac{1}{m} = \frac{1}{0.066} = 15.15 \text{ deg./K}\Omega$$

$$\therefore \quad \theta = 15.15 R_1 + c' \qquad (3.10)$$

The angle 0^{o} for the analyser was the straight through position that is, the position where the analyser was in line with the electron gun. For this position, the value of the resistance was found to be

13.60 KΩ. For these values, $\theta = 0^{o}$ and $R_1 = 13.60$ KΩ, eqn. (3.10) yields the value of $c' = 206$, and therefore,

$$\theta = 15.15\ R_1 - 206 \qquad (3.11)$$

which is the basic equation relating θ to R_1.

Using eqn. (3.11), a ready reckoner chart was constructed which was followed to set the turntable (hence the analyser) to the required angle. To do this, the rotary feedthrough was rotated until the resistance R_1 corresponding to the desired angle was reached. In this way the analyser could be set to any angle, in the range -40^{o} to 70^{o}, by measuring the resistance R_1 and using eqn. (3.11)

3.2.4. Cancellation of Magnetic Field

With the arrangement used for the previous measurements, even after the cancellation of the magnetic field in the interaction region, there was an appreciable magnetic field gradient in the vacuum chamber in the vicinity of the analyser. The cause was the incorrect sizes and separations between individual pairs of the Helmholtz coils. The Helmholtz coils were arranged for convenience around the vacuum system since the field cancellation in the previous measurements was only required over a limited interaction region. In the present measurement, however, field cancellation is necessary in the interaction as well as the scattering region. Apart from the deficiency in the Helmholtz coils, the following components were found to be magnetic,

(i) one of the four steel wires with which the chambers were hanging from the girder,

(ii) the flexible drive used for adjusting the position of the mercury oven,

(iii) the kanthal wire used for heating the tube from the mercury oven,

(iv) the chromel/alumel thermocouple used for monitoring the temperature of the tube,

(v) different liquid nitrogen dewers resulted in different magnetic fields.

The first two of these items were highly magnetic. These sources of magnetic field were eradicated as follows:

(i) nylon webbing was used for hanging the chambers,

(ii) the flexible drive was removed from the system,

(iii) molybdenum wire (0.2 mm thick) was used for heating the tube,

(iv) a copper/constantan (purely non-magnetic) thermocouple was used,

(v) the same liquid nitrogen dewer was used all the time in the same position. With this dewer in position, the magnetic field was cancelled by means of the Helmholtz coils.

3.2.4.1. The Helmholtz coils

Two new pairs of Helmholtz coils were constructed and one of the previous pairs was used as the third one. These three mutually perpendicular pairs were based on the system of square coils described by Firester (1966). According to him, the field (in Gauss) at the centre of the pair of square Helmholtz coils is given by,

$$B = 1.629 \frac{NI}{S} \qquad (3.12)$$

where N is the number of turns on each coil, I is the current in amps. and s is the length in cm.

The lengths of the coils were 96.5 cm, 64.5 cm and 107.5 cm, respectively, for the cancellation of the vertical, along the laboratory and across the laboratory components of the earth's magnetic field. The separation between each pair was fixed, according to Firester (1966), to be 0.5445 times the length of one side of the pair. The number of turns on each coil were calculated by using eqn. (3.12) and each pair was connected in series for delivering currents through the coils. With all these modifications, the residual magnetic field was $\sim$ 1 mG in the centre of the interaction region and within 5 mG over a distance of 15 cm from the interaction region.

3.2.5. The Electron Gun

For these measurements, the electron beam was obtained directly from an electron gun system. A monochromator was not used with the electron gun in order to obtain the maximum possible electron current in the interaction region which otherwise would have been considerably reduced due to the transmission loss through the monochromator. The energy resolution of $\sim$ 400 meV was adequate for these measurements (see section 4.2.3.).

A three stage electron gun (figure 7) was designed in the light of the principles described by Simpson and Kuyatt (1963). A tungsten hairpin filament of 0.1 mm diameter was used as the directly heated cathode. The electrode K_0 was held at the same potential as the cathode and had a shaped surface to favour the forward emission. The element L_1 is the anode with a piece of tungsten gauze spot welded on the aperture to limit the divergence of the beam. K_0, L_1 is the extraction stage and the two element lens L_1, L_2 formed the acceleration stage. The three element lens L_2, L_3, L_4 acted as the focussing lens system while the two element lens L_4, L_5 provided the deceleration stage. All these

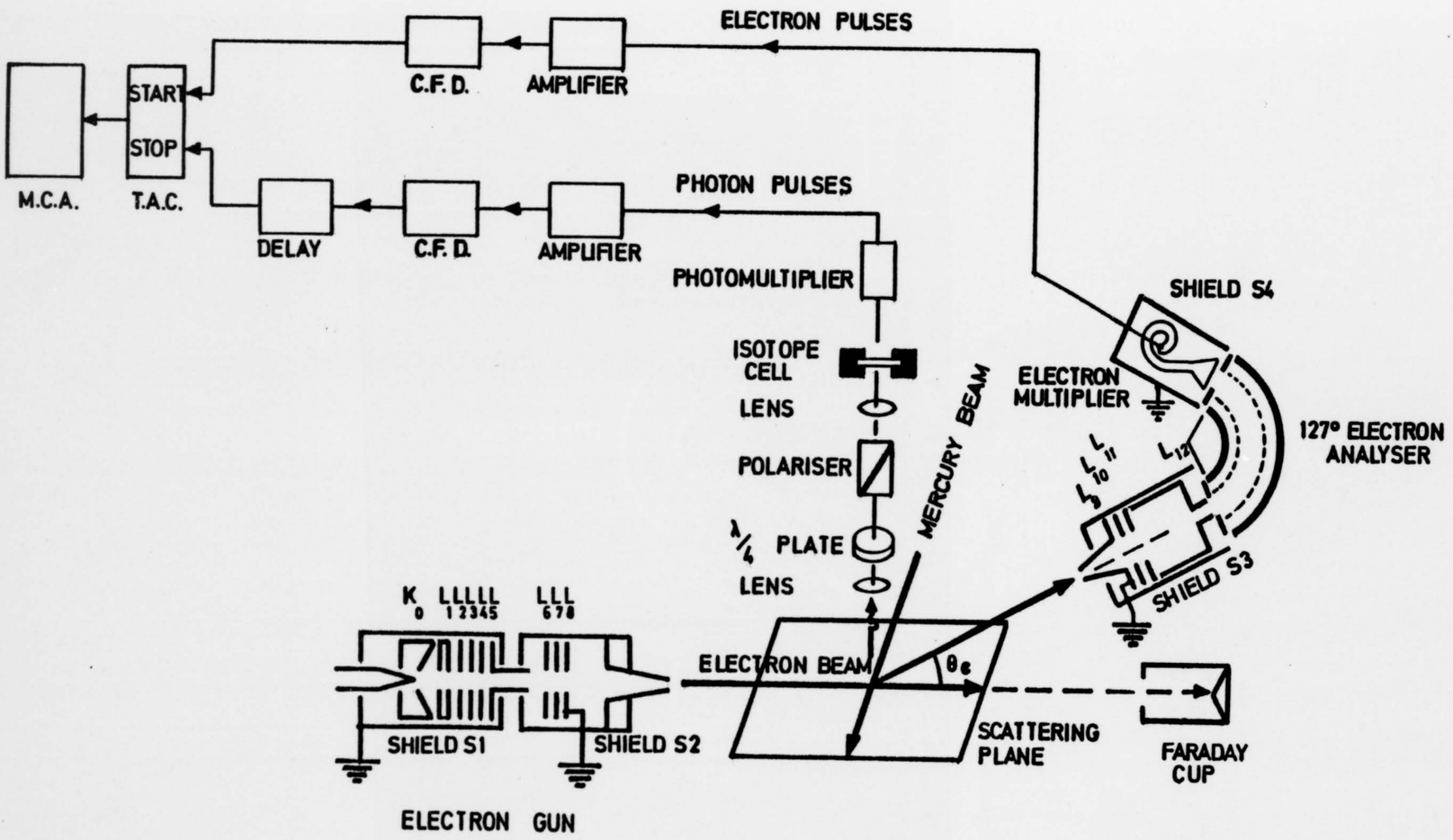

FIG. 7. Schematic diagram of the apparatus for coincidence measurements.

elements were made from molybdenum and used boron nitride washers to insulate them from the mounting rods with baron nitride spacers in between them providing the correct spacings.

The output from the electron gun was matched to the three element lens system L_6, L_7, L_8 in order to focus the electron beam in the interaction region. This three element lens system was the same one which was used before on the output of the monochromator. Before assembling the gun, all elements were cleaned using the electrolytic process described by Rosebury (1965). Also the elements of the matching lens system were taken apart and reassembled after having been chemically cleaned. Shields S1 and S2, made of tantalum and covered with soot, were used to restrict stray electrons. A stainless steel truncated cone of diameter 2.5 mm was fixed on the mounting rods, at ground potential, to restrict the electron beam in the interaction region.

3.2.6. Electrical Connections

Connections to the elements of the electron gun and analyser were made by oxygen free copper wire (0.25 mm thick) inserted in fibre glass sleeving for insulation. Connections to the injection optics for the analyser and the electrostatic lens system on the electron gun were made by teflon insulated single strand (0.4 mm thick) silvered copper wire. The reason for not using the teflon wire on the electron gun was the heat generated by the filament which would damage the teflon insulation on the wire. Also for the analyser elements, copper wire was preferred since it was more flexible than the teflon wire. Stiff connections on the analyser could damage the delicate connection pins on the electrodes. New connections using oxygen free copper wire (0.5 mm thick) were made for the mercury oven heaters. The heating wire on the tube was already

replaced (section 3.2.5) with molyhdenum wire. All these connections were taken outside through electrical feed throughs (EFT 19) to be connected to power supplies. The connection from the Faraday Cup was taken outside separately through a single conductor electrical feed through (EFT 20) where it was connected to the electrometer.

3.2.7. Power Supplies

Another potential distribution box similar to the one described in section (3.1.7) was assembled in which 10 ten-turn Helipot potentiometers (10 KΩ) were connected in parallel. The input power supply to the previous potential box (PB1) was changed to a 0-425 V, 50 mA constant d.c. voltage source (Kepco Model 425M). The input to the new potential box (PB2) was the 0-100 V, 0.2A power supply previously used with PB1. The elements of the analyser and the injection optics derived voltages from PB1 whereas the elements of the electron gun and its associated electron optics obtained voltages from PB2. PB1 and PB2 were biased, respectively, with 0-40 V and 0-100 V power supplies in order to off-set the voltages derived from these potential boxes. The cathode had an individual power supply 0-40 V and the constant current power supply 0-2A was used for the heating of the tungsten filament.

3.2.8. Detection of Electrons

The electrons scattered in the interaction region were focussed on the entrance slit of the analyser by means of a four element (L_9, L_{10}, L_{11}, L_{12}) lens system (fig.7). The elements of the lens system were made from stainless steel and used boron nitride washers and spacers for insulation and correct spacing. A well sooted shield S_3, made from tantalum, was used to cover the lens assembly in order

to restrict stray electrons. There was a stainless steel truncated cone of 1 mm diameter on the first element which was kept at ground potential so that there was no field penetration into the interaction region. Electrons scattered at a particular angle and moving in a field free region entered the cone of acceptance solid angle $\sim 3.5 \times 10^{-3}$ sr.

The 127° electron monochromator, previously used to improve the energy resolution of the incident electron beam, was now employed as an energy analyser (fig.7) for the scattered electrons. The widths of the slits were changed from 0.44 mm to 0.54 mm so that more electrons could reach the electron detector. The electrons after energy selection through the analyser were detected by a channel electron multiplier.

3.2.8.1. The Channel Electron Multiplier

A Mullard B 318 L channel electron multiplier (fig.7), mounted in a teflon block, was housed in a stainless steel tube which was fixed at the output of the analyser. The cone of the channeltron was kept as close as possible at $\frac{1}{2}$ mm from the exit slit of the analyser so that the maximum number of electrons could enter the channeltron. Keeping the channeltron close to the exit of the analyser also reduces electrons reaching the channeltron without going through the analyser. The filter circuit (C_1, C_2, R_1, R_2) for the high voltage input to the channeltron and the decoupling network (C_3, R_3) on the output signal (fig.8) were built inside the cover of the high voltage feedthrough (Vacuum Generators) on the outside of the vacuum chamber. The high voltage to the chenneltron was provided by a Fluke power supply (0-6 KV, Model 408 B).

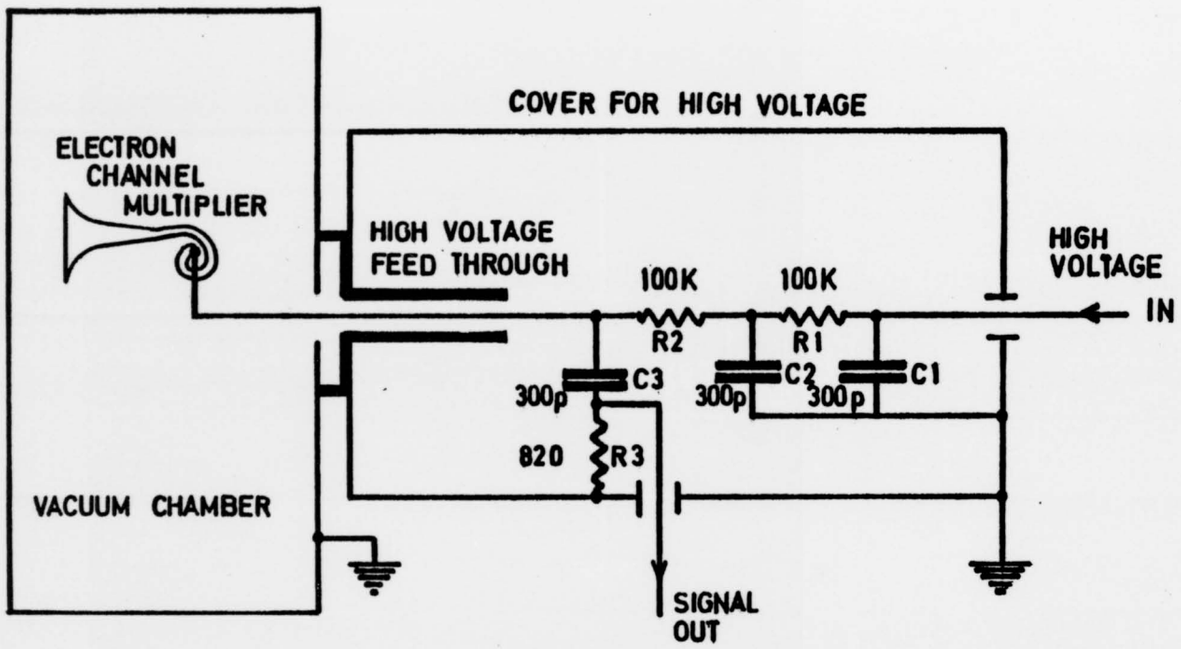

FIG.8. FILTER CIRCUIT AND THE DECOUPLING NETWORK FOR THE ELECTRON MULTIPLIER.

3.2.8.2. Alignment of the Electron Injection Optics

A proper alignment of the axes of the incident electron beam and the atomic beam with the axis of the analyser injection optics is important for the detection of the scattered electrons. This alignment was achieved by fitting alignment rods on the cones of the analyser injection optics and the electron gun optics. Adjustments, if necessary, could be made until the axes of these rods met at the axis of the turntable. The atomic beam tube could be adjusted to align its axis with the point of intersection of the rods.

3.2.8.3. Suppression of Unwanted Electrons

It is important to suppress unwanted electrons in order to reduce the background signal. The shields S1 - S4 (fig.7) were intended to restrict stray electrons but many electrons were still reaching the electron multiplier by-passing the analyser. To stop these stray electrons, thin copper foil was used for covering all possible openings on the analyser and the channeltron mount. Tungsten gauze was wrapped over the fibre glass sleeving on the tube, from the mercury oven, to prevent it from charging up. The gauze was then sooted and connected to earth potential. Likewise a stainless steel cover, properly earthed and well sooted, was fixed on the turntable over the teflon ring. The main function of shielding and earthing these components was to ensure a field free region.

3.2.9. Detection of Photons

The first lens assembly used for the collection of photons in the previous measurements could not be used with the coincidence

measurements because of the modifications to the apparatus. The need to modify the arrangement for the collection of radiation also provided an opportunity to adopt a better way of obtaining the vacuum seal between the chamber and the outside, which so far had been achieved by the lens itself.

A new stainless steel lens holder was designed and mounted from the support plate of the turntable. A quartz lens, with a focal length of 100 mm and effective apperture of 40 mm, was used to collect the radiation from the interaction region. The lens was positioned with its focal point on the interaction region in order to produce a parallel beam of light. The vacuum seal on the chamber was accomplished by means of a quartz window of 10 mm thickness and effective aperture of 25 mm. The refractive index of quartz and hence the focal length of a lens varies with wavelength, therefore, consideration should be given to distances when using focal lengths in the ultra-violet region as against given values in the visible region. According to the data supplied by the manufacturers (Scientific Optics Ltd.), the index of refraction, for the grade of quartz used, showed only slight variations with wavelength. The tabulated values of refractive indices indicated a change of <3% for the focal lengths in going from the visible to the ultraviolet region and, therefore, no correction was made in the distances calculated on the basis of the given focal lengths.

The radiation after being collected by the first lens passed through a rotatable linear polariser (Glan Taylor) and was focussed on to the photomultiplier tube (EMI 6256S) by the second quartz lens of focal length 200 mm. The effective aperture of the polariser was increased from 12 mm to 18 mm so that more photons could reach the photon detector. This arrangement was used for linear polarisation analysis.

A $\frac{\lambda}{4}$ (λ = 253.7 nm) quartz retardation plate (Melles Griot, O2WRQ 005), with an effective aperture of 18 mm, was placed in front of the linear polariser for circular polarisation measurements. The crystalline optic axis direction on the $\frac{\lambda}{4}$ plate, indicated by a pair of diametrically opposite dots, was lined up with the electron beam direction. The isotope cell was introduced, as before, between the second lens and the photomultiplier in order to eliminate the effect of hyperfine structure in the measured photon radiation. The complete optical arrangement is shown schematically in figure 7. Apart from the first lens, which was inside the vacuum chamber, all other optical components were mounted, as before (section 3.1.12.1), outside the chamber. No interference filter was used since, for the results presented here, the energy of the bombarding electrons was not high enough to excite the 6^1P_1 state.

3.2.9.1. Alignment of the Optical System

The optical system of quartz lenses was checked for alignment by shining light from a He-Ne laser (Scientifica & Cook Electronic Ltd) on a point in the centre of interaction region. This point was defined by the intersection of the mercury tube axis with the axes of rods fitted into cones on the electron gun optics and the analyser injection optics. The image of the light spot on the rods was seen on a transparent paper screen placed in the position of the photo-cathode. Double checking of the system, in case of any misalignment of the laser beam, was performed by illuminating the rods with a torch light through the flange on the side of the chamber and looking for the image of the rods on the paper screen. In each case, the position of the image was found to be off centre by the same amount. The position of the image was brought to the centre of the screen

after tilting the optical axis by placing shims in between the flanges.

3.2.9.2. Elimination of Background Photons

The presence of unwanted photons give rise to the background signal and therefore it is necessary to eliminate the light coming from sources other than the interaction region. The two main sources of this light were, the white hot tungsten filament in the electron gun and the ionisation gauge head inside the chamber. The shield on the electron gun was inadequate and a lot of light from the filament was reaching the photon detector. To stop this light, a thin copper foil covered with soot was wrapped around the electron gun and on to every possible opening in the electron beam source. In order to prevent light of the ionisation gauge head from reaching the photon system, a stainless steel baffle after covering with soot was placed on the ionisation gauge head inside the chamber.

3.2.10. The Timing Electronics

A schematic diagram of the timing electronics used for the coincidence measurements is shown in figure 7. Pulses from photon and electron detectors were fed into fast amplifiers (LRS, Model VV100B). These gain-of-10 pulse amplifiers were mounted on the chamber, as near as possible to the output signals, to eliminate pick up of electrical noise. The pulses from these amplifiers were further amplified by another X10 fast amplifier (LRS, Model 133). The amplified pulses were then fed into ORTEC, Model 473 constant fraction discriminators (CFD). A delay of $\sim$ 500 n sec. was introduced in the photon channel by means of 200 meters of coaxial cable (Uniradio 43). The electron timing pulses from the CFD provided

start pulses for an ORTEC, Model 467 time-to-amplitude converter (TAC) while the delayed photon timing pulses were used as stop pulses. The output signal from the TAC, whose amplitude is proportional to the time difference between the start and stop pulses, was connected to the multichannel analyser (MCA). The MCA stored the pulse height distribution spectrum from the TAC and its contents were printed out on a teletype for analysis.

3.2.11. Elimination of the Electrical Noise

Any electrical noise in the detection system for the coincidence measurements would give rise to unwanted counts and therefore had to be eliminated. The mains earth was isolated and all power supplies as well as the vacuum chamber were earthed by using thick copper braid. The earth leads were terminated at one common point to prevent spurious signals due to earth loops. The common point of the earth line was connected to a solid copper rod buried in the ground outside the laboratory. The temperature controllers previously used in conjunction with power supplies for the heating of the mercury oven, tube and the isotope cell were removed because their contacts on making and breaking were generating electrical noise. These components were now directly heated by stabilised power supplies and even without controllers, the temperatures were maintained constant to within $\pm 1\ ^{o}C$.

The most serious source of the electrical noise was the liquid nitrogen filling system. The two time clocks (T.C.1 and T.C.2) used in the liquid nitrogen filling system were mains operated. T.C.1 was a 24 hour clock which operated T.C.2 every 6 hours. T.C.2 operated a solenoid valve for the duration of liquid nitrogen filling which was normally 5 minutes. The filling system, during 5 minutes of its operation, contributed 30% of the 6 hours data due to electrical

noise from the time clocks and the solenoid valve. In order to overcome this problem, a switching circuit was designed and built which would stop the accumulation of data by inhibiting the output from the TAC and stopping the scaler from counting whenever the liquid nitrogen system operated. The system would start accumulating data after the liquid nitrogen filling was over. The wiring on T.C.1. was changed so that one end of the contact on the clock was now connected to ground (0V). Similarly one of the contacts on T.C.2. was connected to ground. The other ends of these contacts were utilised to trigger the switching circuit.

3.2.11.1. The Switching Circuit

The circuit diagram of the switching device is shown in figure 9. It utilised two integrated circuits (74LS 221) as timers, two silicon transistors (BFY51) as drivers, one integrated circuit (74LS 00) as a flip-flop and a 12V relay. All these components were mounted and wired on a printed wire board which was later fitted inside a panel box. The front panel of this box contained the two time clocks, switches and sockets for connections to the TAC and the scaler. The supply of +10V was obtained from the interlock control unit (section 3.1.10). The supply voltage (+5V) for the integrated circuits was derived from a fixed voltage regulator (type 7805) which with its associate components was also wired on the board.

The two timers which are used to start and stop the switching circuit are triggered by the two clocks in the liquid nitrogen filling system. Each of the two timers when triggered produces a pulse of width 350 μsec. after a delay of 0.7 sec. The pulse width and the delay were determined by the components in the timing circuits. The delay of 0.7 sec. was used in timer 2 so that any electrical noise from

the mains voltage associated with the mechanical bouncing of the contact on T.C.2. vanished before the scaler and the TAC would start to accumulate data. In the case of timer 1, the delay eliminated any repetitive triggering. The output pulses from these timers preset or clear the flip-flop and stop or start the scaler.

When the flip-flop is preset then the output 2Y is high and 1Y is low. In this situation the transistor TR1 is OFF and TR2 is ON. TR1 does not conduct and therefore the relay contacts are open, which means the liquid nitrogen filling system is off. Since TR2 is ON and is conducting, there is a voltage drop of ∿1v across it, therefore the inhibit output to the TAC is low and it operates normally.

When the liquid nitrogen system starts then the timer 1 is triggered by T.C.1. The pulse from the timer clears the flip-flop and stops the scaler. In this case, TR1 is switched ON and with a voltage of ∿1v across it, there is a voltage of ∿9v across the relay. The relay operates and starts the time clock T.C.2. This clock in turn operates the solenoid valve and the liquid nitrogen starts to flow into the cold trap. TR2 is now OFF and remains so during the time the liquid nitrogen is filling the cold trap. Consequently there is a voltage drop of ∿6v ($\frac{2}{3}$ of 10v, $\frac{1}{3}$ across 1kΩ and $\frac{2}{3}$ across 2kΩ) to the inhibit input of the TAC, which is therefore inhibited. After the set time for filling is over then the timer 2 is triggered by T.C.2. The pulse from the timer presets the flip-flop and starts the scaler. In this case,TR1 is switched OFF and stops the relay from operating while TR2 is turned ON and resets the TAC which then starts to function.

If the liquid nitrogen filling was required outwith the timings on the clocks then the switching circuit could be operated manually by pressing push-button switches S1 and S2. The single-pole double-throw switch S3, connecting the live line of the mains voltage to the relay, was generally in the on position. L.E.D's 1 and 2 were used to indicate the state of the switching circuit.

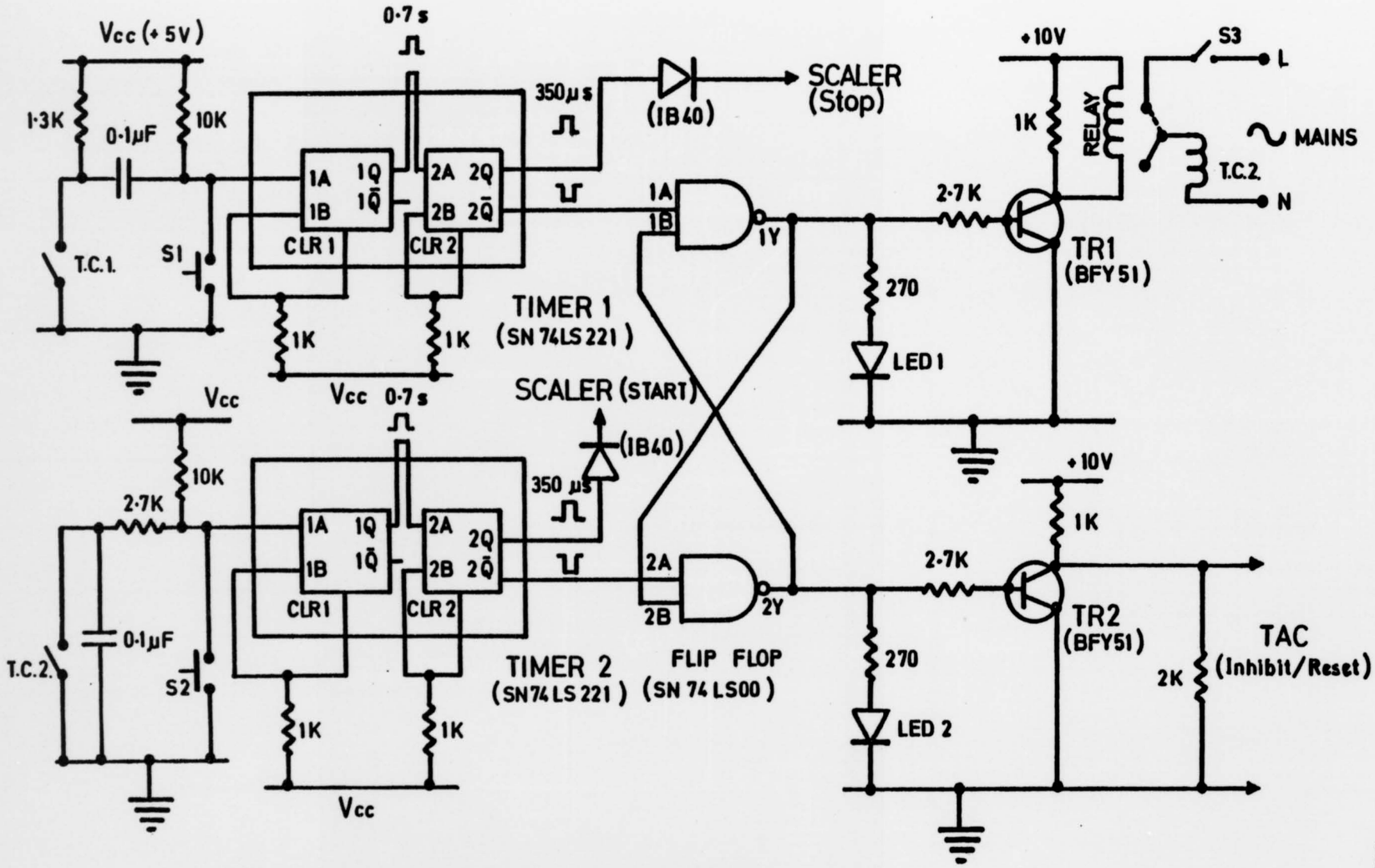

FIG.9. Circuit diagram of the switching device

4. THE EXPERIMENT

4.1. Polarisation Measurements

4.1.1. Introduction

The experiment involved the measurement of the relative intensities $I_{\parallel}$ and $I_{\perp}$ of the emitted light with electric vectors orientated, respectively, parallel and perpendicular to the electron beam direction. The radiation was observed at right angles to the electron beam as a function of the incident energy. The polarisation P was calculated for each electron energy at a given isotope cell temperature from the relationship,

$$P = \frac{I_{\parallel} - I_{\perp}}{I_{\parallel} + I_{\perp}}$$

A multichannel analyser (MCA) was used for the collection of data for these measurements. The MCA used in this experiment had 800 channels and any number of channels could be preselected. The MCA operated in a repetitive mode over the number of channels selected for a preset number of sweeps. The parallel output from the channel address of the MCA was fed into a digital-to-analogue converter which produced a ramp voltage as the channel number advanced. This ramp voltage after being off-set by a bias supply (figure 4) was applied between the elements of the electron beam source and the interaction region (ground potential). In this way the electron energy was scanned synchronously with the channel advance of the MCA. The pulses from the photon detector, after amplification and shaping, were thus stored in individual channels corresponding to the incident electron energy.

Measurements of this type are very sensitive to fluctuations in the operating conditions such as atomic beam pressure and electron

beam current variations. The effect of these drifts in the experimental parameters can be minimised by the continuous scanning of the signal and integrating the individual scans.

4.1.2. Data Collection

In the present experiment the mean height of the ramp voltage was ∿24 mV and with 140 channels scanned in one sweep, a voltage range between 4.5v to 8v was covered. Each run consisted of measuring $I_{\parallel}$ followed by $I_{\perp}$, for a given isotope cell temperature in the range from 4°C to 50°C, for 180,000 sweeps lasting up to eight hours with a preset dwell time of 1 msec per channel. The dwell time per channel was taken to be short so that any drifts in the experimental parameters were equally spread over all the channels. The number of sweeps were selected so that a statistically meaningful spectrum was obtained.

The number of counts accumulated in the MCA were printed out on a teletype and were punched on a paper tape. This paper tape was used as input data for a programme which was run on an ICL 4130 computer for polarisation calculations. The background signal, determined from the first few channels below the threshold for excitation, was subtracted from the data per channel for $I_{\parallel}$ and $I_{\perp}$. The statistical uncertainty in the polarisation was calculated by assuming that Poisson statistics was applicable.

Since the intensities $I_{\parallel}$ and $I_{\perp}$ were observed separately, a method of normalisation was necessary in case there were drifts in the electron current or the atom density between the two measurements. For this purpose individual measurements for $I_{\parallel}$ and $I_{\perp}$ at each isotope cell temperature were made at fixed electron energies of 6.2 eV and 6.7 eV (fig.13) for a duration of 1000 to 6000 seconds. The determination

of the correct incident electron energy was carried out by the procedure described in section 4.2.3. These energies were selected for the spot polarisation measurements since at these energies the polarisation is not susceptible to drifts in the electron energy unlike the changes that are caused in the vicinity of the two resonances due to the negative-ion states being formed in the excitation function at electron energies of 4.9 eV and 5.5 eV (Ottley, 1975). The long counting time ensured that the errors involved in these observations were small. The average value of the measurements at these two energies was used to normalise the data, obtained by multiscaling, for any change in the collision parameters. A run was also taken on the MCA with the isotope cell removed from the optical system so that a comparison of the polarisation data with and without the hyperfine effect could be made. This data too was normalised to the spot polarisation measurements without the isotope cell. All of the above measurements were taken for a fixed electron energy resolution of $\sim$100 meV.

4.1.3. Pressure Dependence of Polarisation

The radiation emitted from excited atoms may be absorbed by atoms in the ground state before it can reach the photon detector (Moiseiwitsch and Smith, 1968). As compared to transitions between excited states, the resonance lines are easily absorbed by the atoms in the ground state. For instance, in mercury at 1 Torr the 253.7 nm line is appreciably absorbed in a distance of 10^{-2} mm (Holstein, 1947). It implies that a high density of mercury atoms along the path length between the interaction region and the vacuum window would result in a significant absorption of the resonance radiation. A photon, re-emitted after absorption by one of these atoms will not have a preferred

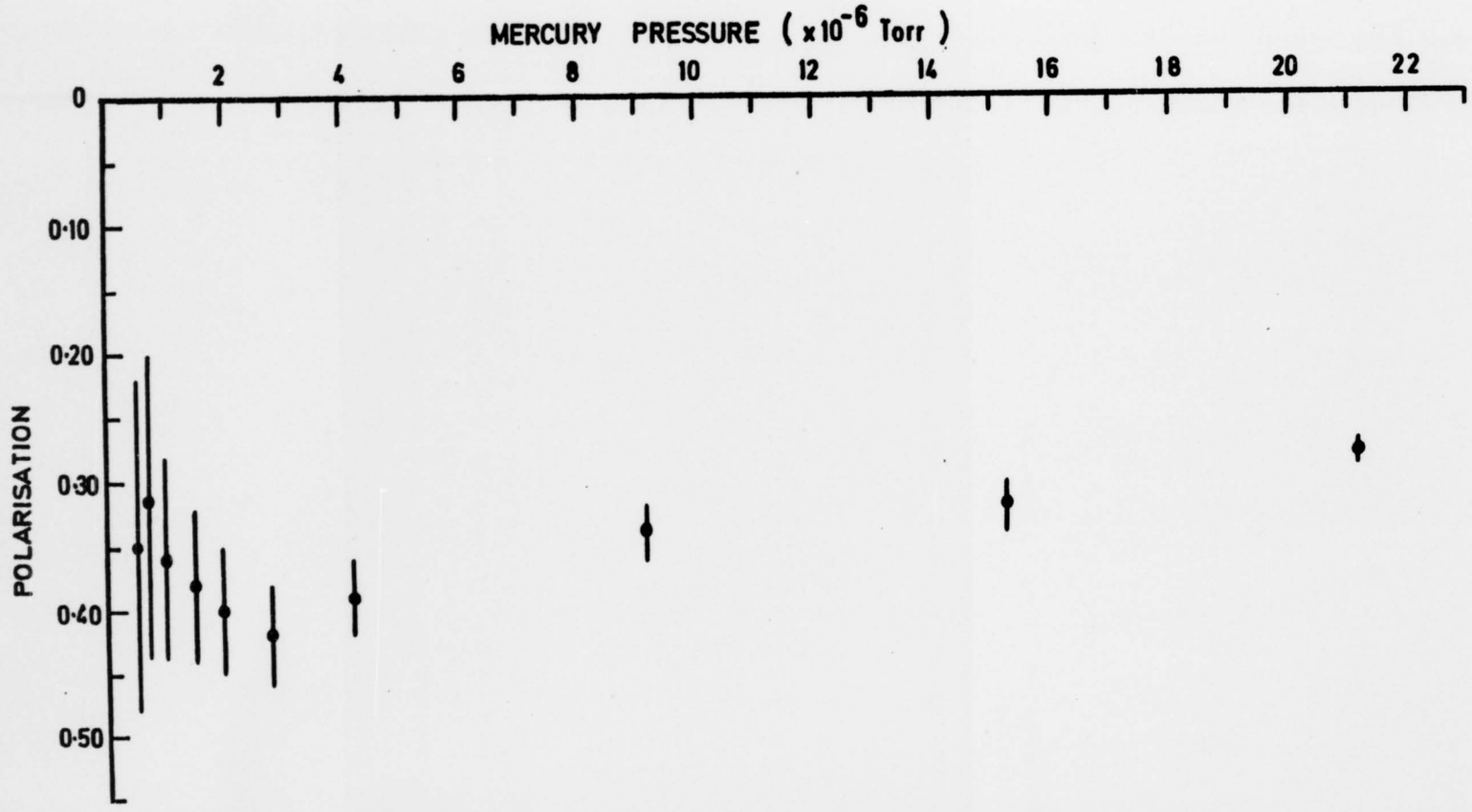

FIG. 10. POLARISATION AS FUNCTION OF PRESSURE AT AN INCIDENT ELECTRON ENERGY OF 6·7 eV WITH THE ISOTOPE CELL IN THE SYSTEM (CELL TEMPERATURE = 12°C).
Error bars indicate ±1 standard deviation.

direction and will thus cause depolarisation of the atomic line radiation. It is, therefore, necessary to ensure that the atom density is low enough so that the absorption is negligible. In order to assess the effect of pressure depolarisation, the polarisation was measured as a function of the mercury vapour pressure at a fixed incident electron energy of 6.7 eV (fig.10). It is clear from this measurement that the onset of depolarisation takes place at a mercury pressure of 3×10^{-6} Torr and therefore all data was taken at a mercury pressure of $\sim 1 \times 10^{-6}$ Torr, well below the region of pressure depolarisation.

4.1.4 Sources of Error and Corrections

The polarisation data from the measurements of $I_{\parallel}$ and $I_{\perp}$ were corrected for errors arising from the following sources:

(i) the divergence angle of the electron beam

(ii) The finite angle of the photon detection system

(iii) any misalignment of the polariser axis

(iv) any instrumental polarisation.

4.1.4.1. The Divergence Angle of the Electron Beam

Ideally all the electron paths should be along the Z-axis (see fig.1) but due to focussing of the electron beam at the interaction region, electrons are inclined to this direction. This divergence of the electron beam would result in the measured $I_{\parallel}$ and $I_{\perp}$ being different from the excitation functions for the ideal case and consequently the measured polarisation would be different from the true polarisation. The relationship between the polarisation P, of the radiation emitted from atoms excited by electrons moving along Z-axis and the measured polarisation P_m, of the radiation from atoms

excited by electrons lying within a cone of semi vertical angle β about the Z-axis is given by (Ottley, 1974),

$$P = \frac{P_m}{1 - \frac{3}{4}\beta^2 + \frac{1}{4}P_m\beta^2}$$

The divergence angle β, of the electron beam was estimated from the geometry of the system to be $\sim 0.10 \pm 0.02$ radians.

4.1.4.2. The Finite Angle of the Photon Detection System

The emitted radiation is observed along the OY direction (see fig.1) but due to the focussing effect of the collecting lens, photons are detected along directions inclined to the Y-axis. The collection of such photons would result in the depolarisation of the measured polarisation. The equation relating the polarisation P, of the radiation along Y-axis to the measured polarisation P_m, of the radiation detected within a cone of semi vertical angle γ about the Y-axis is given by (Ottley, 1974),

$$P = \frac{P_m}{1 - \frac{1}{4}\gamma^2 + \frac{1}{4}P_m\gamma^2}$$

The finite angle γ, of the photon detection was worked out from the geometry of the collecting lens system to be $\sim 0.18 \pm 0.04$ radians.

4.1.4.3. Any Misalignment of the Polariser Axis

A misalignment of the polariser axis with the electron beam direction would alter the polarisation value of the observed radiation. If the misorientation between the polariser axis and the electron beam direction is an angle α', then

$$I_{\parallel} = I_z \cos^2 \alpha' + I_x \sin^2 \alpha'$$

and $$I_{\perp} = I_x \cos^2 \alpha' + I_z \sin^2 \alpha'$$

Here I_z and I_x are the light intensities polarised, respectively, parallel and perpendicular to the electron beam direction and, $I_{||}$ and $I_{\perp}$ are the measured light intensities polarised, respectively, parallel and perpendicular to the polariser axis.

The measured polarisation P_m is given by,

$$P_m = \frac{I_{||} - I_{\perp}}{I_{||} + I_{\perp}}$$

$$= \frac{(I_z - I_x)(\cos^2\alpha' - \sin^2\alpha')}{(I_z + I_x)(\cos^2\alpha' + \sin^2\alpha')}$$

$$= P \cos 2\alpha'$$

This equation shows that the measuredpolarisation would be less than the true polarisation. If the angle α' is known then the polarisation value can be corrected by

$$P = \frac{P_m}{\cos 2\alpha'}$$

The radiation intensity $I(\alpha)$ was measured for different values of the polariser angle α with respect to the electron beam direction and was fitted to the following function, which represents the intensity distribution of partially polarised light,

$$I(\alpha) = I_1 + I_2 \cos 2(\alpha + \alpha') \qquad (4.1)$$

where I_1 and I_2 are, respectively, the unpolarised and polarised fractions of the total intensity.

The angle α' was determined from the least squares fit to this function and the values of α' were found to be

$\alpha' = -4.74 \pm 0.93$ (degrees), without the isotope cell

and $\alpha' = -4.46 \pm 0.40$ (degrees), with the isotope cell.

4.1.4.4 Any Instrumental Polarisation

The instrumental polarisation results from a different sensitivity of the optical system for transmitting and detecting $I_{\parallel}$ compared to $I_{\perp}$. The measured polarisation P_m is related to the true polarisation P through the instrumental polarisation π by the equation (Ottley, 1974),

$$P_m = \frac{\pi + P}{1 + \pi P}$$

Since π is small, therefore the πP term in the denominator can be neglected.

$$\therefore P_m = P + \pi \qquad (4.2)$$

If the polariser axis is rotated through an angle α with respect to the electron beam direction then, following the procedure of the preceding section (4.1.4.3), the polarisation value will vary as $P \cos 2\alpha$.

The measured polarisation P_m, after taking into account the instrumental polarisation π, will be given according to eqn. (4.2),

$$P_m = P \cos 2\alpha + \pi$$

This equation was used to determine the instrumental polarisation by measuring P_m for different values of α and plotting these values as a function of $\cos 2\alpha$ (fig.11). The intercept on the ordinate axis was found by making a least squares fit of the data points to a straight line. In this way the values of π were found to be

$$\pi = 0.022 \pm 0.007, \text{ without the isotope cell}$$

$$\text{and } \pi = -0.013 \pm 0.005, \text{ with the isotope cell.}$$

The instrumental polarisation was checked for different temperatures of the isotope cell and in each case was found to be equal to the above value within the experimental uncertainties.

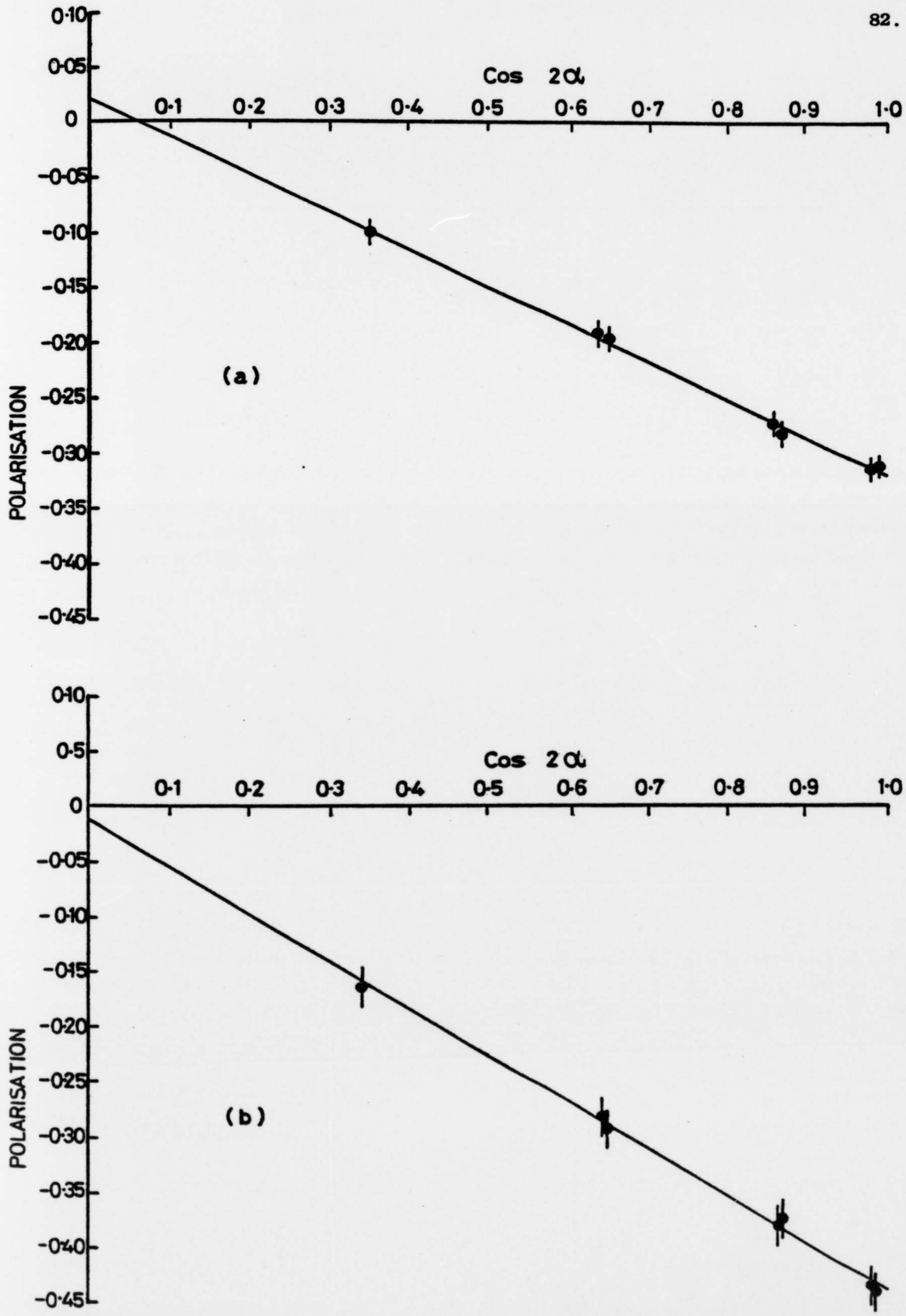

FIG.11. POLARISATION DATA AS A FUNCTION OF COS 2α AT AN INCIDENT ELECTRON ENERGY OF 6·2 eV, (a) WITHOUT ISOTOPE CELL, (b) WITH ISOTOPE CELL (CELL TEMP. = 14°C) THE STRAIGHT LINE IS A LEAST SQUARES FIT.
Error bars represent ± 1 standard deviation.

4.1.5. Results and Discussion

Figure 12 illustrates the variation of the observed photon intensity with the increasing isotope cell temperature. The total observed radiation intensity ($I_{\parallel} + I_{\perp}$) has been plotted as a function of the isotope cell temperature. The background counts, determined after removing the cathode potential and thus cutting off the electron beam, were subtracted from the data for $I_{\parallel}$ and $I_{\perp}$. The resulting total intensity was normalised to the Faraday Cup current and the pressure. The graph, when examined closely, can be divided into three regions describing the absorption of radiation as the temperature of the isotope cell is increased. In the first region up to a temperature of 15°C, the absorption of the radiation is predominently from the odd isotopes. In the second region up to 30°C, the absorption from the even isotopes also starts to show up. In the third region after 30°C, where almost total absorption from the odd isotopes has taken place, the absorption is now mainly from the small amount of the even isotopes in the isotope cell. It may be pointed out that the even isotopes contribute 70% of the observed radiation from the natural isotope mixture of mercury.

Figure 13 shows the results of the individual polarisation measurements at different isotope cell temperatures for two fixed incident electron energies of 6.2 eV (fig.13(a)) and 6.7 eV (fig.13(b)). As mentioned in section 4.1.2., these energies were chosen, beyond the resonance at 5.5 eV, in order to avoid the influence on the polarisation of the resonances at lower energies. It can be seen from these observations that practically total absorption of the radiation from isotopes with non-zero spins ($I \neq 0$) occurred at the isotope cell temperatures in excess of 30°C. As a result, the polarisation levels out beyond this isotope cell temperature, demonstrating the fact that the isotope cell did in fact selectively filter out the radiation. The fractional

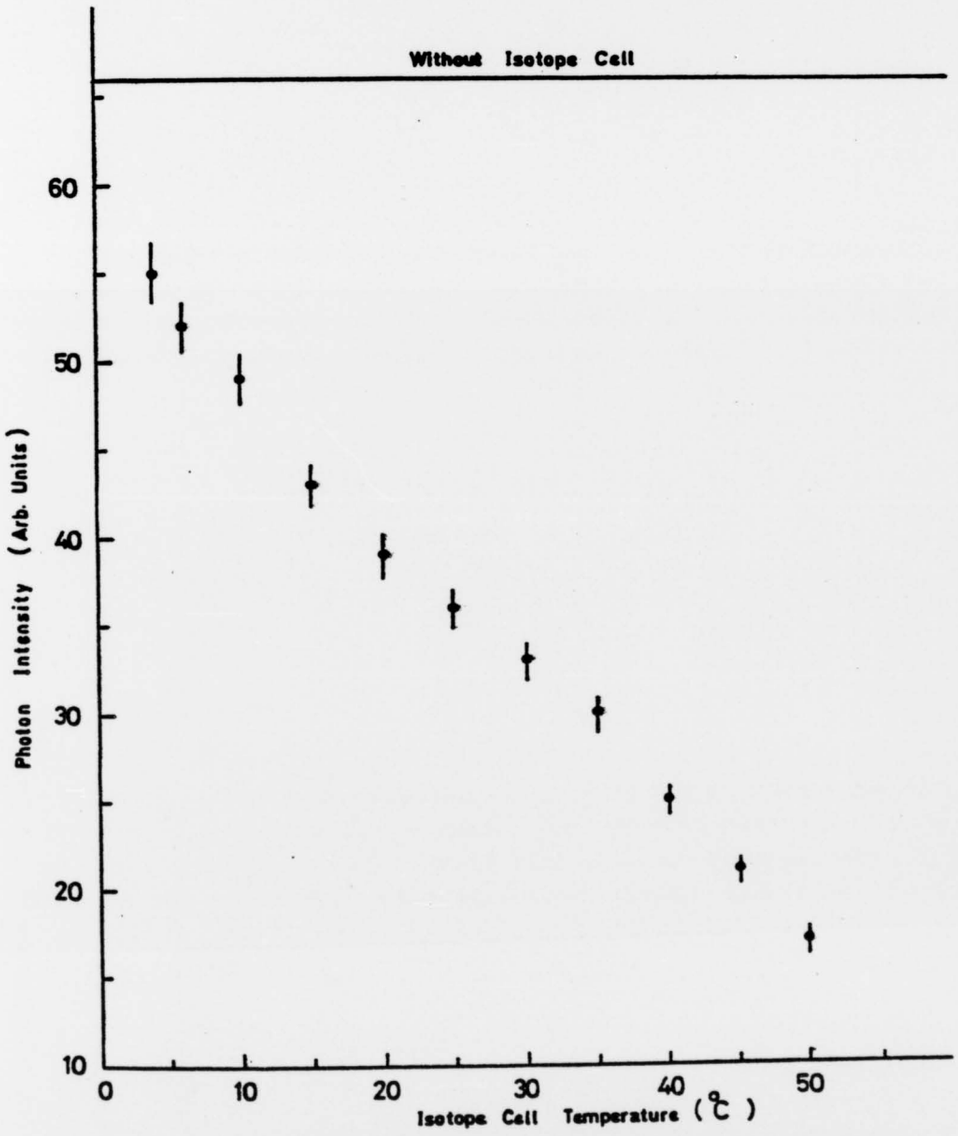

FIG.12. Photon intensity as a function of the isotope cell temperature at an incident electron energy of 6·2 eV. Error bars indicate ±1 standard deviation.

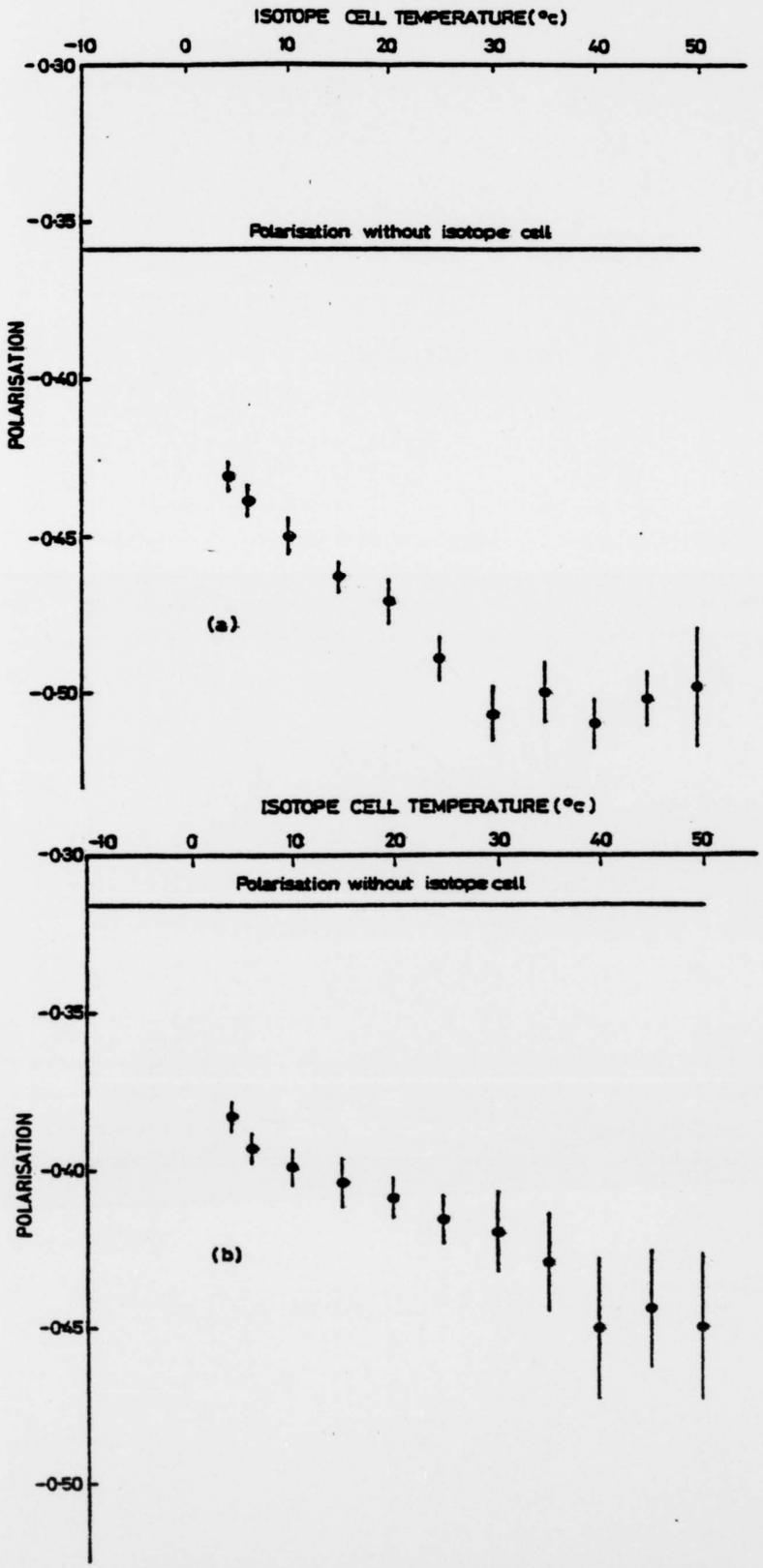

FIG.13. VARIATION OF POLARISATION WITH THE TEMPERATURE OF THE ISOTOPE CELL AT AN INCIDENT ELECTRON ENERGY OF (a) 6·2 eV, (b) 6·7 eV. ERROR BARS REPRESENT ±1 STANDARD DEVIATION.

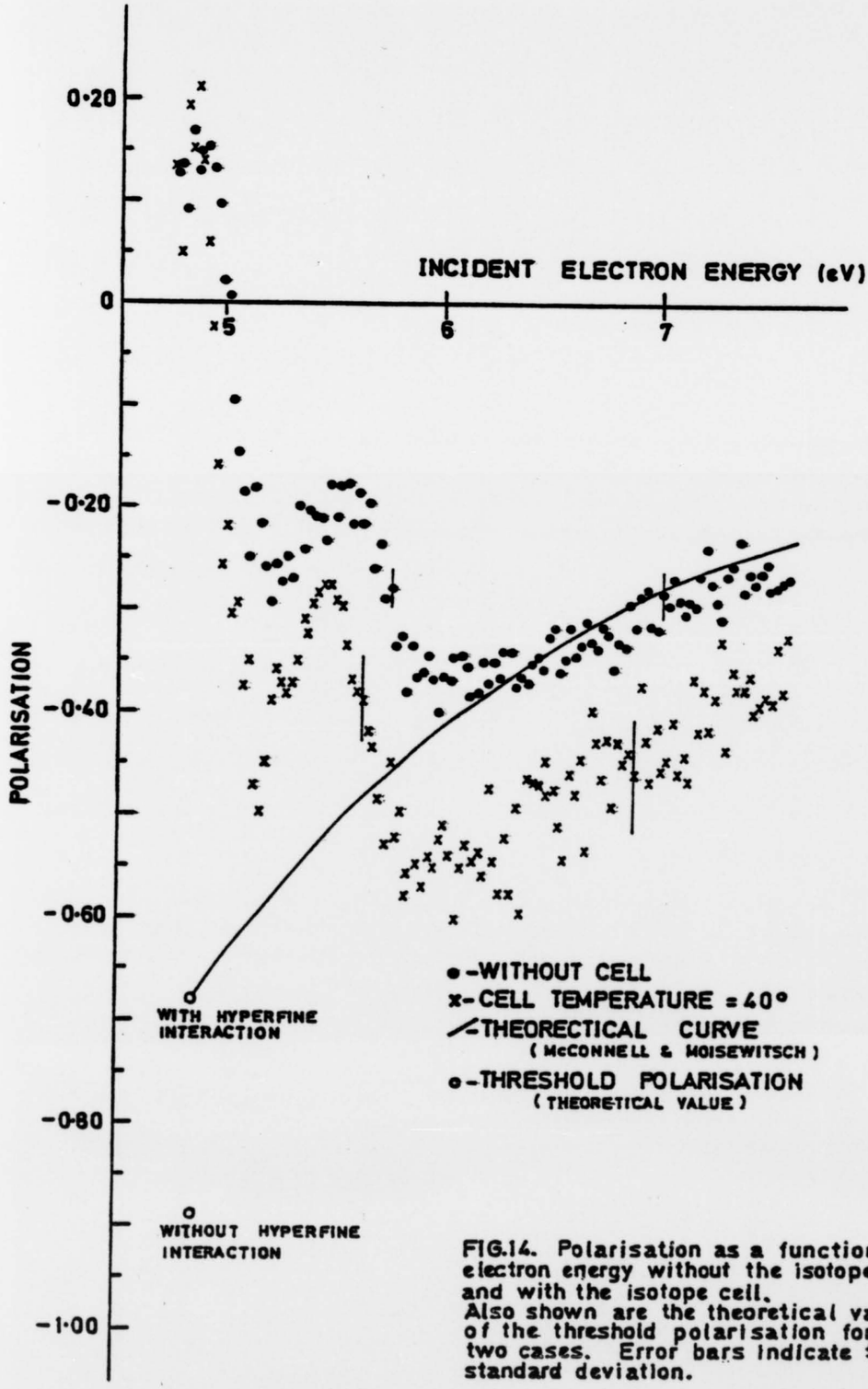

FIG.14. Polarisation as a function of electron energy without the isotope cell and with the isotope cell. Also shown are the theoretical values of the threshold polarisation for the two cases. Error bars indicate ± 1 standard deviation.

polarisations of -0.36 and -0.32, respectively, for electron energies of 6.2 eV and 6.7 eV without the isotope cell (i.e. with hyperfine effect present) increased to -0.51 and -0.45, respectively, by the absorption of radiation from isotopes with $I \neq 0$ (i.e. after the elimination of the hyperfine effect in the observed radiation). This substantial increase in the polarisation clearly indicates the influence which the hyperfine structure has on the polarisation of the $6^3P_1 - 6^1S_0$ intercombination line of mercury.

Figure 14 illustrates the polarisation state of this mercury line as a function of the electron energy. The data provides a comparison of the polarisation without the isotope cell (i.e. hyperfine interaction present) and with the isotope cell at a temperature (40^oC) where total absorption of the radiation for $I \neq 0$ occurred (i.e. hyperfine interaction eliminated). According to the calculations of McConnell and Moiseiwitsch (1968), neglecting the effect of singlet/triplet mixing, the threshold polarisation for the $6^3P_1 - 6^1S_0$ line of mercury is -1.00 for zero nuclear spin and -0.77 for the natural isotope mixture. Including the singlet/triplet mixing in the 6^3P_1 state of mercury, the threshold polarisation is predicted to be -0.89 for $I = 0$ and -0.68 for the natural isotope composition. The experimental result without the isotope cell is in close agreement with the predicted curve of McConnell and Moisewitsch (1968) at energies above the 5.5 eV resonance but the occurrence of the resonances clearly has a large effect on the polarisation at lower energies. In the presence of the isotope cell (hyperfine interaction absent), the polarisation is more negative at energies above the resonances as might be expected from the more negative theoretical polarisation at threshold. In this case the fluctuations caused by the resonances are even larger.

4.2. Coincidence Measurements

4.2.1. Introduction

The scheme of the collision system can be described by referring to figure 7, where in a cartesian coordinate system, the electron beam is considered to be incident in the Z-direction on the atomic target located at the origin and the photons are observed along the Y-direction. The position of the electron detector, which lies in the X-Z plane, defines the scattering plane. At a fixed incident electron energy, the 127^{o} cylindrical analyser was set to a particular scattering angle and was tuned to accept electrons which had lost 4.89 eV energy corresponding to the excitation of the $6^{3}P_{1}$ state of mercury. These inelastically scattered electrons were detected in the scattering plane whilst the photons emitted by the excited mercury atoms were observed perpendicular to the scattering plane.

Pulses from the electron and photon detectors, after processing through amplifiers and constant fraction discriminators (CFD), were fed into the time-to-amplitude converter (TAC). The TAC output signal, whose amplitude was proportional to the time interval between consecutive start and stop pulses, was fed into the multichannel analyser (MCA) operating in the pulse-height analysis mode. In this way electrons and photons from the same scattering event produced a definite time correlation in the resulting time spectrum on the MCA.

The necessary steps leading to the data acquisition of the coincidence measurements are given in the following sections.

4.2.2. Setting of the Discriminator Level for the best Signal to Noise Ratio

The following procedure was adopted to set the discriminator levels for the electron and photon pulses in order to obtain the best signal

to noise ratio.

(i) Pulses from the electron multiplier, after x 10 amplification through a fast amplifier (LRS, VV100B), were connected to the negative input of a slow amplifier (NE 4603). The purpose of this amplifier was to produce pulses which were compatible with the MCA. The output from this amplifier was connected to the MCA in pulse-height analysis mode. A pulse height distribution spectrum was thus obtained for the electron signal (figure 15(a)).

(ii) A pulse generator (Philips PM 5775) was used to give out fast negative pulses at a reasonable repetition rate. These pulses (∿ 5 nsec wide) were comparable in width and amplitude to the pulses from the electron multiplier after x 10 amplification. In other words, pulses similar to the ones from the channeltron were obtained and connected to a x 10 amplifier (LRS, 133). The output from this amplifier was connected to the CFD whose discriminator threshold was set to some value (say 2V). The amplitude of these pulses was varied until the cut-off occurred, i.e. no pulses of amplitude higher than the setting on the discriminator level of 2V were detected.

(iii) These pulses of amplitude set to a given discriminator level were connected to the MCA through the slow amplifier (NE 4603) and a pulse height distribution spectrum was obtained for these pulses of fixed amplitude.

(iv) The two pulse height spectra, obtained in (i) and (iii) and stored in two subgroups of the MCA, were compared by displaying them together on the screen of the MCA. From this, it could be exactly seen where the set discriminator level fell in relation to the electron pulse height

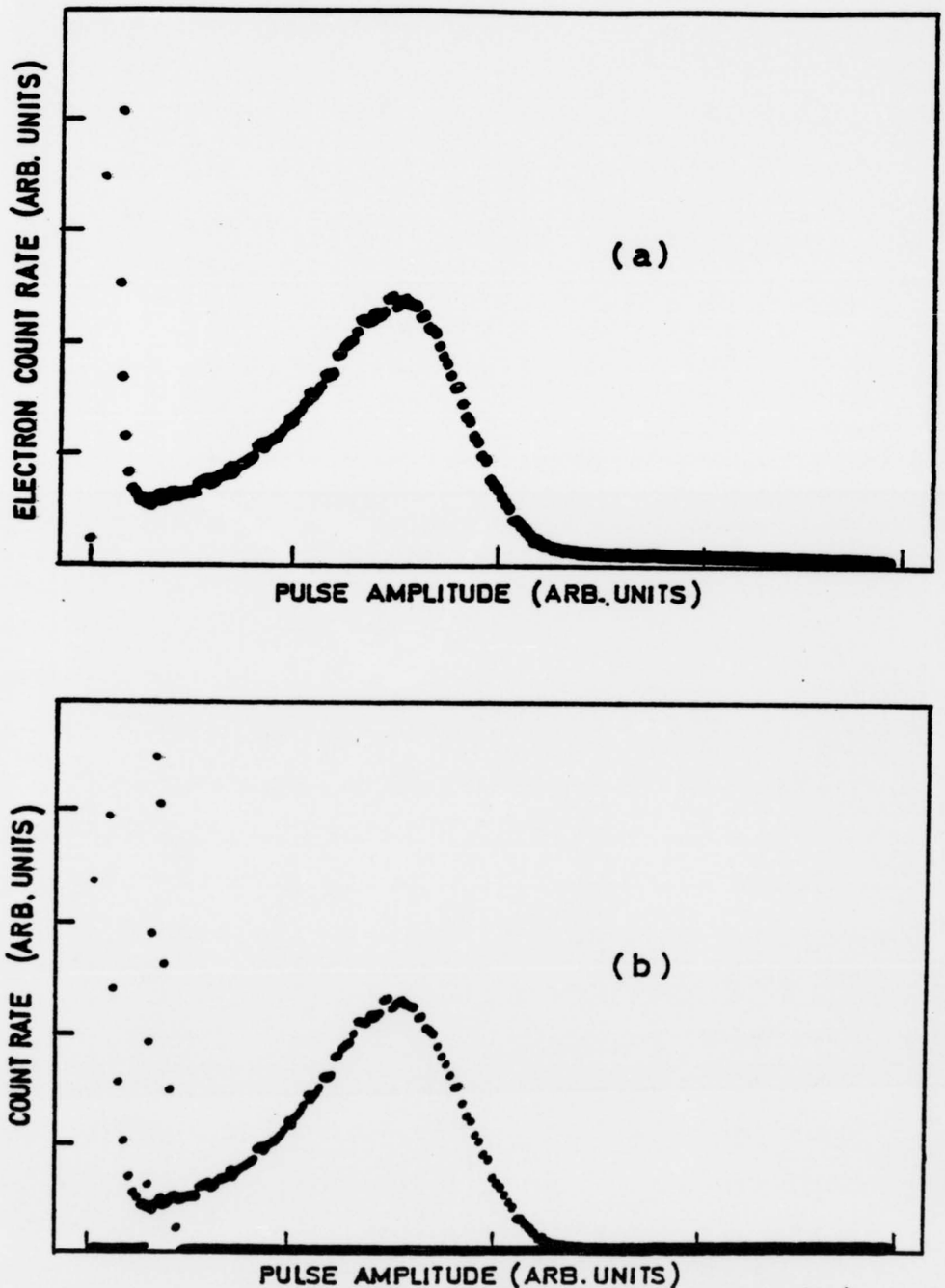

FIG.15. Pulse height spectra for (a) electron pulses, (b) electron pulses and fixed amplitude pulses from pulse generator.

distribution. The procedure in (iii) was repeated for a few settings of the discriminator level and it was found that a discriminator level of 1.0 V was required to eliminate noise without affecting the real signal (figure 15(b)). A similar procedure was used to set the discriminator level for the photon signal from the photomultiplier.

4.2.3. Determination of the Incident Electron Energy

The energy of the electron beam in the target region, at ground potential, should be given by the difference of the cathode and ground potentials. However, in practice, the effective potential difference between the target region and the cathode is different due to the existence of a "Contact potential". The contact potential depends on the material of the cathode and the material surrounding the target region. It is, therefore, necessary to evaluate this contact potential for the correct determination of the electron energy. The contact potential was found by the following two methods,

(1) The cathode potential with respect to ground was changed in steps of 100 mV and photons were observed at each potential. A graph of photon counts versus cathode potential (fig.16) was plotted. The potential corresponding to the intersection of the extrapolations of the onset and background counts determined the threshold of the excitation. The difference between the observed potential and the threshold potential (4.89 V) for the excitation of the 6^3P_1 state is a measure of the contact potential. In the case of the measurement illustrated in fig.16, the measured potential for the threshold comes out to be -4.43 V and therefore the contact potential is -0.46 V. The energy of 5.5 eV, for instance, would be given by the cathode potential of -5.04 V with

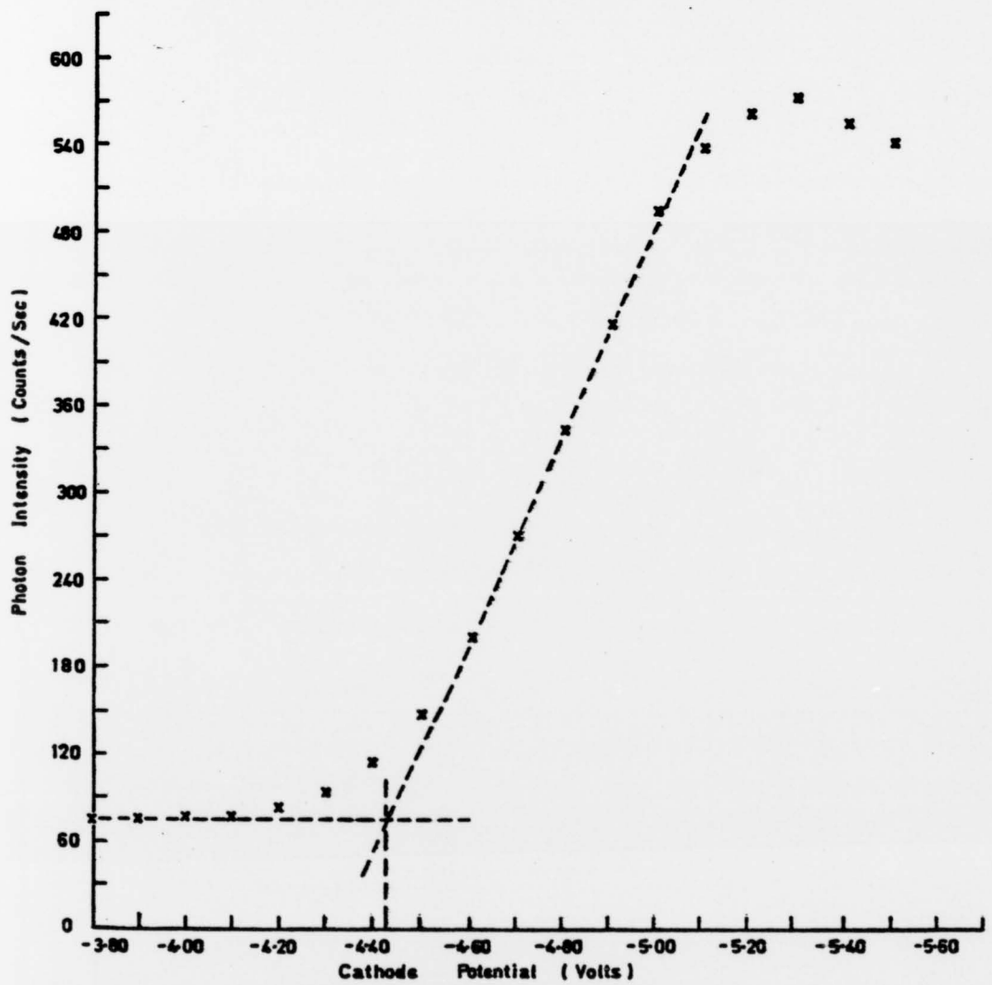

FIG. 16. Determination of Contact Potential

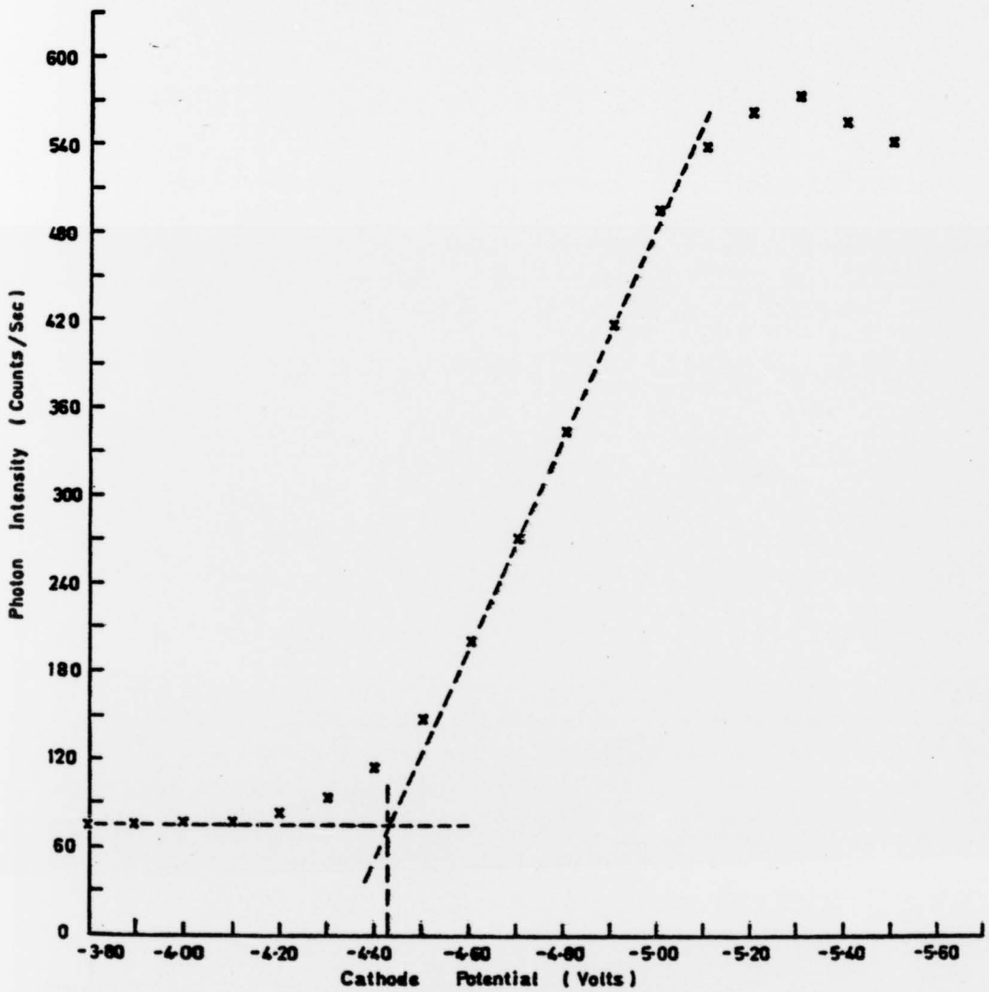

FIG. 16. Determination of Contact Potential

respect to ground, allowing for this contact potential of -0.46 V.

(2) The elements of the electron beam source were ramped over an energy range covering the second resonance occurring at 5.5 eV. The data, with the axis of polariser set to 0^{o} with the electron beam direction, was accumulated in the MCA for a length of time until a reasonable excitation function was obtained. The excitation function so obtained was then scanned slowly so that the cathode potential pertaining to the channel in the peak of the resonance could be measured. The difference between this potential and the potential corresponding to the peak of the resonance at 5.5 eV provides the contact potential.

4.2.4. Energy Loss Spectra

Electrons scattered in the interaction region in a particular direction were energy analysed by the 127^{o} cylindrical analyser when tuned to the energy loss for a given excited state. Those electrons transmitted by the analyser were detected by the channel electron multiplier and the energy loss spectrum was obtained on the MCA, in its multiscaling mode, by scanning the reference voltage of the analyser with the ramp voltage.

An energy loss spectrum, taken at an incident electron energy of 10.5 eV with an energy resolution of 0.40 eV at an electron scattering angle of 70^{o}, is shown in figure 17. The spectrum shows a series of peaks corresponding to different energy levels of the excited states. The energy scale was calibrated with reference to the elastic peak occurring at zero energy loss. Sharp features were observed at energies of 4.88, 5.47, 6.72, 7.91 and 8.83 eV. The energy positions of these

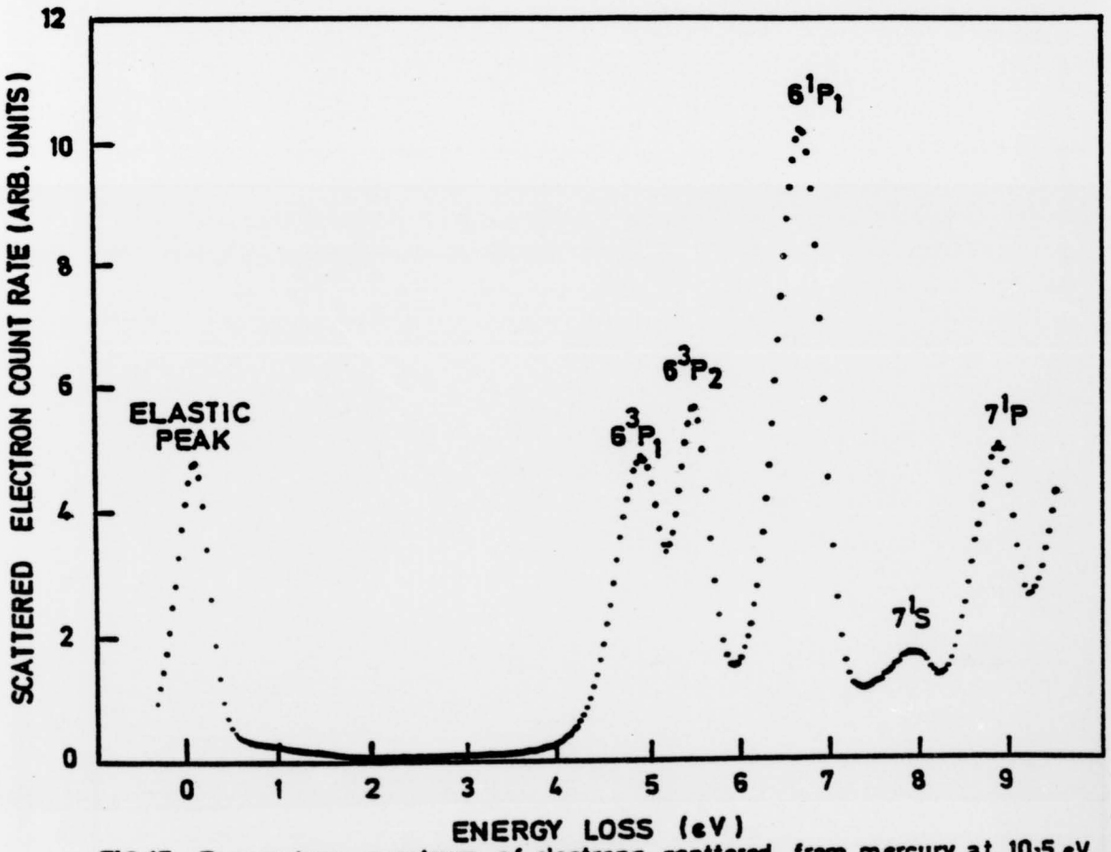

FIG.17. Energy loss spectrum of electrons scattered from mercury at 10·5 eV incident electron energy and 70° scattering angle.

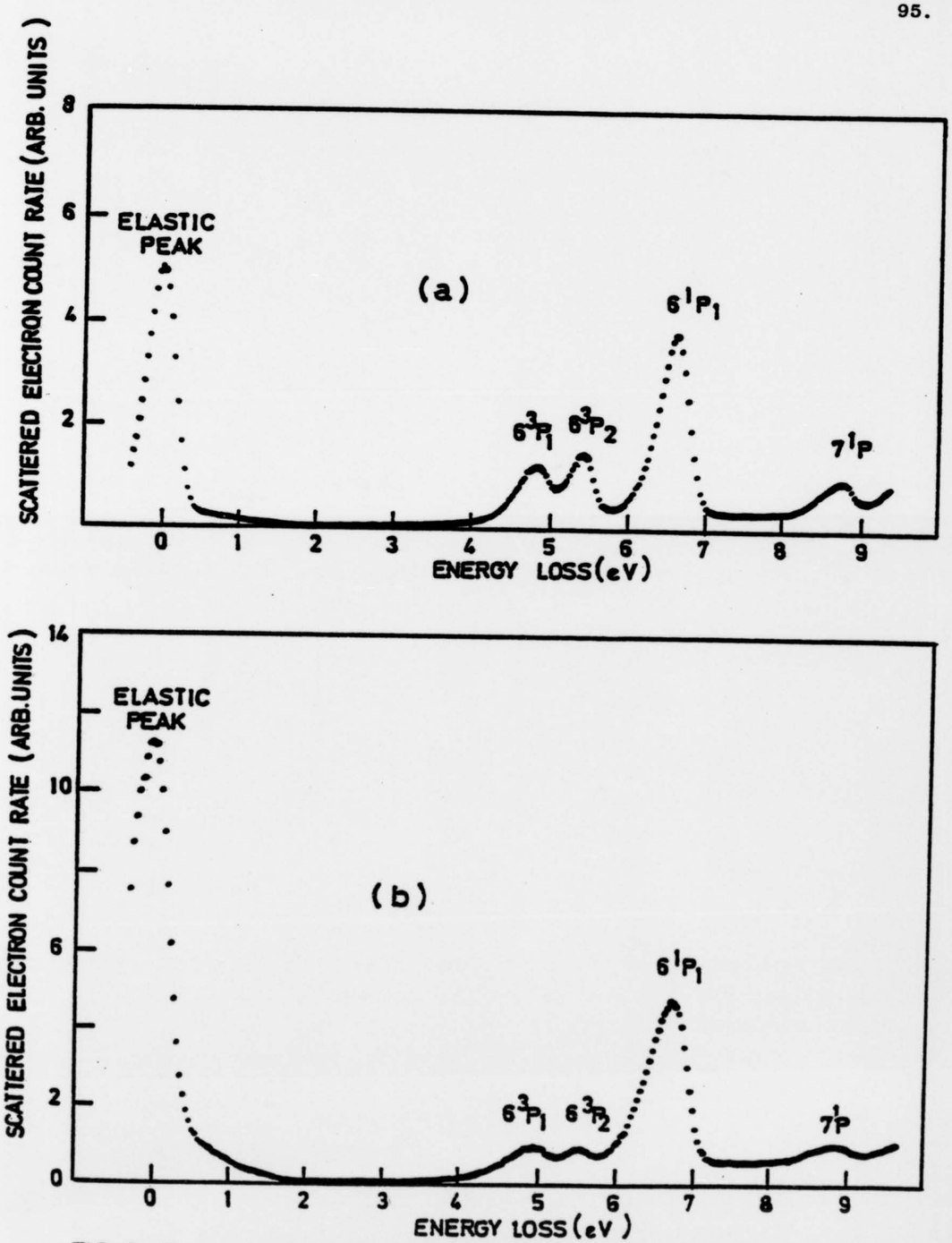

FIG.18. Energy loss spectra of electrons scattered from mercury at 10·5 eV incident electron energy and scattering angle of (a) 50° (b) 35°.

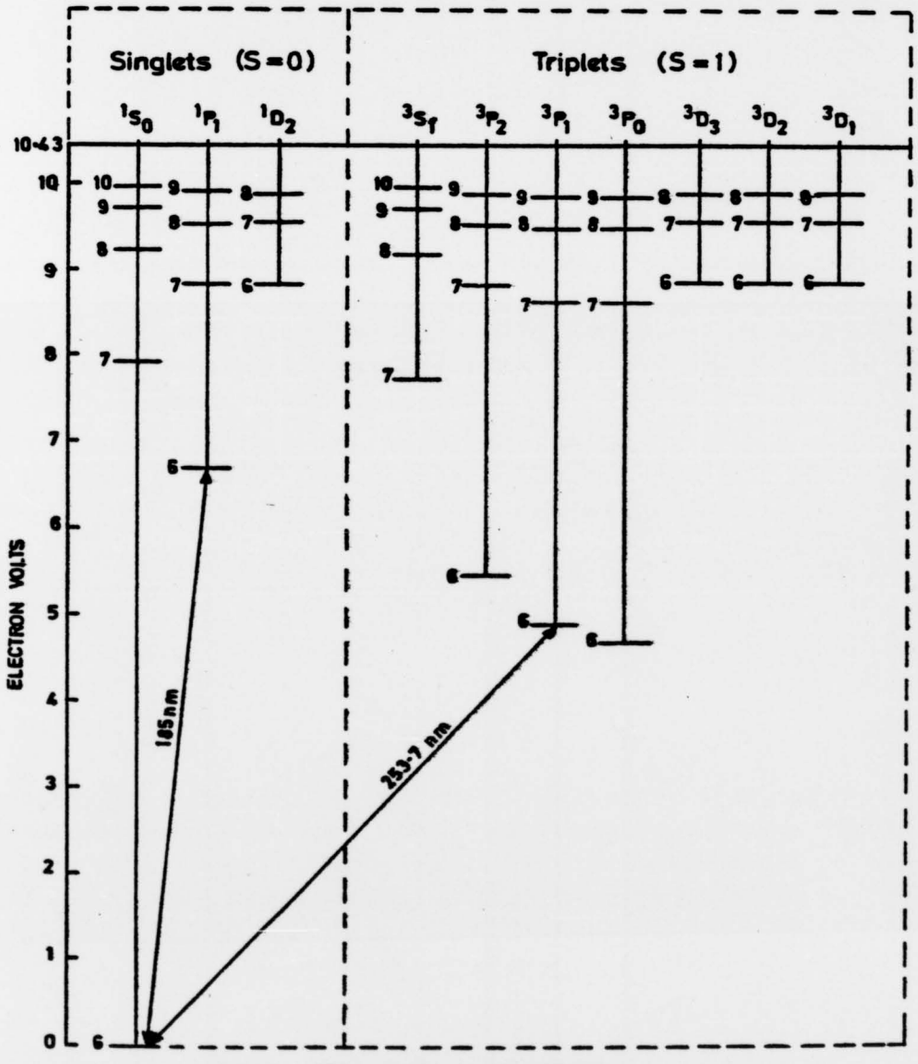

FIG.19. TERM DIAGRAM OF MERCURY.

features are in excellent agreement with the energy levels of Moore (1971) at 4.89, 5.46, 6.70, 7.93 and 8.84 eV respectively.

The energy resolution of the system was sufficient to resolve the 6^3P_1 state (E_{loss} = 4.89 eV) from the 6^3P_2 state (E_{loss} = 5.46 eV) but could not resolve the 6^3P_0 state (E_{loss} = 4.67 eV) which was buried in the shoulder of the 6^3P_1 state. However these metastable states do not pose any problem for coincidence measurements since the time on the TAC window (2 μsec) is very much shorter than the lifetimes of 5.56 sec and 6.67 sec, respectively, for the $6^3P_{0,2}$ states (Krause et al 1977). Electrons scattered into the detector after the excitation of these states do not affect the number of real coincidences but only contribute to the accidental rate.

Energy loss spectra at incident electron energy of 10.5 eV at electron scattering angles of 50^o and 35^o are shown in figure 18. The feature corresponding to the energy loss of 7.93 eV is not observed in these cases.

Figure 19 shows a term diagram of mercury with energy levels corresponding to the data by Moore (1971). The diagram shows the transition under investigation that is, the $6^3P_1 - 6^1S_0$ (253.7 nm) intercombination line. Also shown is the spin allowed non-intercombination line at λ = 185.0 nm, arising from the transition $6^1P_1 \rightarrow 6^1S_0$. The 253.7 nm line of mercury is not typical of intersystem combinations, which are in general weaker than lines due to transitions between levels of the same system. This particular line, though nearly fifty times weaker than the corresponding singlet-singlet line, is very bright because it provides the only route by which an atom can return from the triplet system to the ground state.

The effect of the incident electron energy on the relative intensities of inelastically scattered electrons, resulting from the

excitation of atoms to 6^3P_1, 6^3P_2 and 6^1P_1 states, was observed by taking energy loss spectra for different impact energies at a scattering angle of 70°. The data so obtained on the MCA was printed out and the number of electron counts pertaining to these states were normalised to the Faraday Cup current and pressure. The normalised count rates were then plotted as a function of the incident electron energy (fig.20). It can be seen that the intensity of the inelastic electrons for the 6^3P_1 state (excitation state under investigation) falls with the increasing incident electron energy or in other words the maximum sensitivity is for impact energies close to the threshold of excitation. On the basis of this observation, incident electron energies of 5.5 and 6.5 eV were chosen for coincidence measurements. Moreover scattering angles of 50° and 70° were used for the detection of inelastically scattered electrons because the analyser could not be moved beyond 70° due to the positioning of the tube from the mercury oven. At scattering angles less than 50°, on the other hand, the contribution from the background electrons becomes very large resulting in a deterioration of the signal to noise ratio.

An energy loss spectrum obtained at an incident electron energy of 6.0 eV at a scattering angle of 70° is shown in figure 21. It can be seen from this observation that the sensitivity for the 6^3P_1 peak is greater than those of the elastic and the 6^3P_2 peaks. However, the sensitivity of any peak could be maximised by adjusting the voltages on the injection optics and the analyser elements for an optimum focussing of the scattered electrons relating to that peak. The energy loss spectrum of figure 21 was taken after the best focussing of the inelastic electrons corresponding to the 6^3P_1 peak.

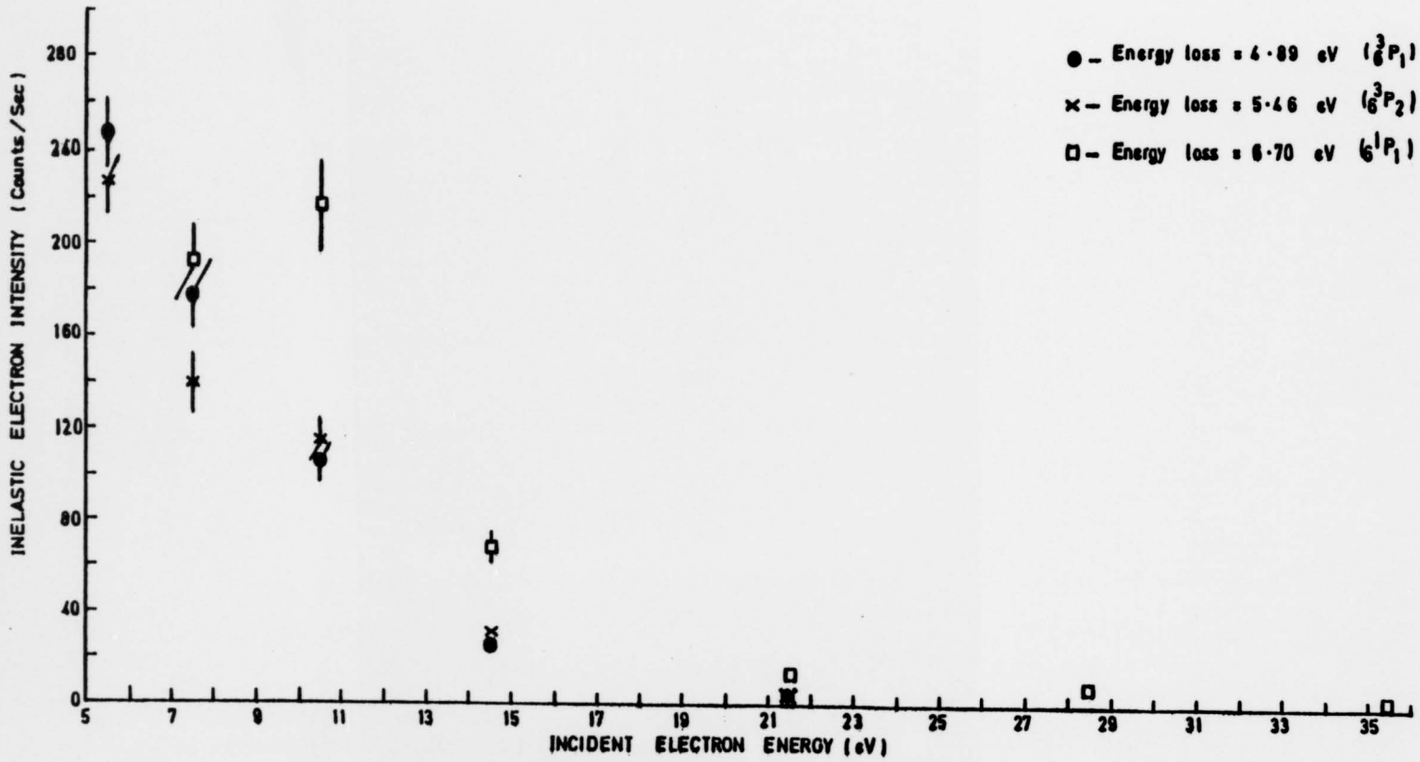

FIG. 20. Inelastic electron intensity as the function of incident electron energy at electron scattering angle of 70°. Error bars indicate ± 1 standard deviation.

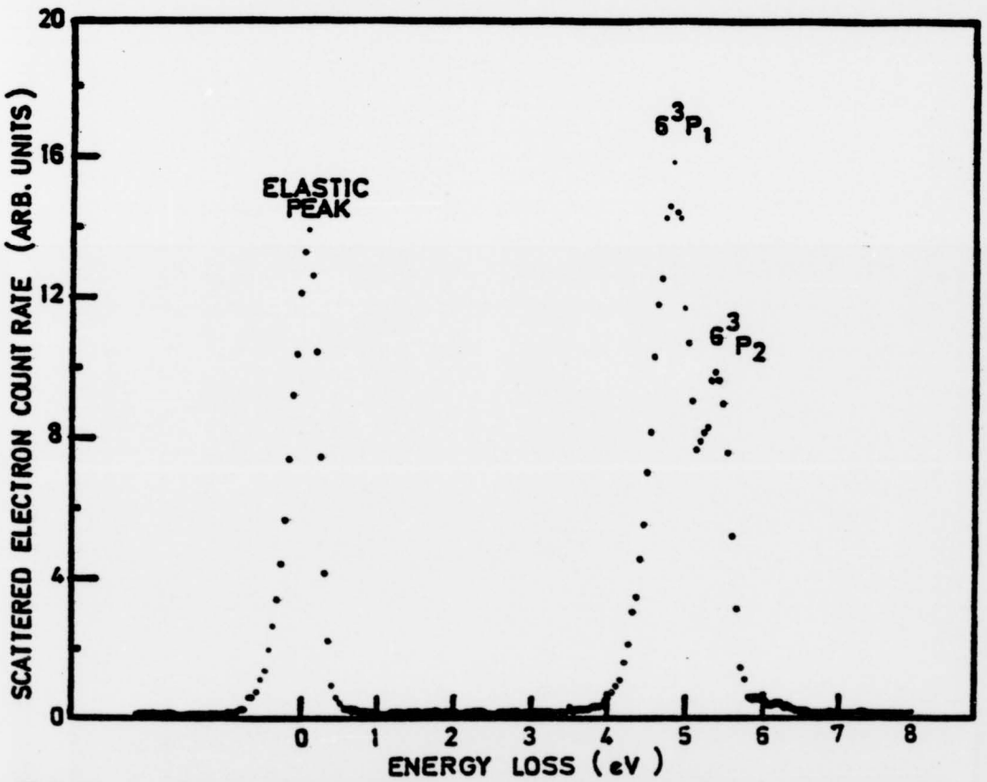

FIG.21. Energy loss spectrum of electrons scattered from mercury at 6·0 eV incident electron energy and 70° scattering angle.

4.2.5. Data Acquisition

The 'true coincidences', due to electrons and photons from the same scattering event, appear in certain channels of the MCA corresponding to a range of times. These times are determined by the resolution time of the apparatus and by the lifetime of the excited state. The lifetime of the 6^3P_1 state is 120 nsec (King and Adams, 1974) and, in comparison, the resolution time of the apparatus was very short.

The resolution time of the apparatus was estimated to be $\sim$ 5 ns. The major contribution to this resolution time results from the spread in the time of flight of electrons from within the atomic beam of finite width. Inelastic electrons of energy 1 eV ($E_{impact} \sim 6$ eV, $E_{loss} \sim 5$ eV) move with a velocity of 5×10^7 cm sec^{-1}. The spread in the time of flight of electrons due to a 0.2 cm width of the atomic beam in the interaction region is $\sim \pm 4$ ns. The spread in timing pulses from the electron and photon dectors with risetimes of 5 ns and 10 ns, respectively, are fractions of these times. Finally the resolution of the timing electronics was measured to be better than 1 ns and was negligible by comparison.

The 'true coincidences' on the MCA must be separated from a background due to 'random coincidences' which are distributed throughout the time spectrum of the MCA. These 'random coincidences' arise when the start and stop pulses of the timing unit originate from different scattering events where the electrons and photons have no common origin. The times of such coincidences are randomly distributed and therefore they contribute a uniform background to the time spectrum of the MCA. In this way a 'true coincidence peak' on top of a background of 'random coincidences' was obtained on the MCA when the time origin of the 'true coincidences' was brought into the range of observed times by means of an additional cable delay inserted into

the stop channel of the TAC (see figure 7). The number of 'true coincidences' was found from the counting rates of the true and random coincidences as follows:

'True Coincidences' appeared in a group of 40 channels corresponding to a time window Δt_1 in the time spectrum of the MCA. 'Random Coincidences' were measured in 155 channels pertaining to a time window Δt_2 in a region which had no or at least a negligible number of true events, i.e. before the origin of true coincidences or long after this origin. The number of 'true coincidences' was found by subtracting the coresponding background, measured in Δt_2, from the total number of coincidences (true and random) appearing in Δt_1. If N_1 and N_2 are the coincidence counts in time windows Δt_1 and Δt_2, respectively, then the total number of 'true coincidences' N_c is given by

$$N_c = N_1 - \frac{\Delta t_1}{\Delta t_2} N_2$$

$$= N_1 - R\, N_2, \text{ where } R = \frac{\Delta t_1}{\Delta t_2}$$

The statistical uncertainty of N_c was calculated by assuming that Poisson statistics was applicable when the standard deviation $\sigma(N)$ is given by $\sqrt{N}$. Thus the standard deviation of N_c is given by

$$\sigma(N_c) = (N_1 + R^2\, N_2)^{\frac{1}{2}}$$

The total number of 'true coincidences' N_c was normalised to the total number of scattered electrons N_e accumulated during this time. The resulting values $\frac{N_c}{N_e}$ and $\frac{\sigma(N_c)}{N_e}$ were thus insensitive to small variations in electron beam current, target density and efficiency of the electron detector. In order to keep a constant check on the stability of the system, count rates of electrons and photons were observed before and after each run.

Electron-photon coincidence counts were measured for various positions of the polariser angle α at fixed incident electron energies and scattering angles. The data so obtained was fitted to a cosine function of period π (eqn. (4.1)). The radiation intensities $I(\alpha = 0^{o}, 45^{o}, 90^{o}, 135^{o})$ were determined from the fitted values of the data. After introducing the $\frac{\lambda}{4}$ plate in front of the linear polariser, similar measurements were performed and I(RHC) and I(LHC) were determined for $\alpha = 45^{o}$ and 135^{o}, respectively. All these intensities were then measured after the elimination of the hyperfine interaction by the same technique as used previously (see Section 3.1.11, also described by Zaidi et al 1978). Accordingly the isotope cell was inserted in the optical system. From the measurements of these intensities, the Stokes parameters (P_0, P_1, P_2, P_3) were calculated by using eqn. (2.11).

4.2.6. Pressure Dependence of Coincidence Signal

As mentioned in section (4.1.3.), the imprisonment of resonance radiation or resonance trapping takes place when the radiation emitted from an excited atom is absorbed by atoms in the ground state. A photon, re-emitted after absorption, will no longer be correlated in time with the scattered electron that caused the initial excitation. The experimental results would thus be affected by resonance trapping and therefore it is necessary to check the effect of pressure on the coincidence signal as well as on the photon and electron intensities.

The coincidence signal was measured as a function of the mercury vapour pressure at an incident electron energy of 5.5 eV and scattering angle of 70^{o} with the polariser set with its polarisation axis at an angle of 135^{o} with the electron beam direction. This angle of the polariser was chosen because at this angle the coincidence signal was maximum and hence it was not susceptible to any variation in

Electron-photon coincidence counts were measured for various positions of the polariser angle α at fixed incident electron energies and scattering angles. The data so obtained was fitted to a cosine function of period π (eqn. (4.1)). The radiation intensities $I(\alpha = 0^{o}, 45^{o}, 90^{o}, 135^{o})$ were determined from the fitted values of the data. After introducing the $\frac{\lambda}{4}$ plate in front of the linear polariser, similar measurements were performed and I(RHC) and I(LHC) were determined for $\alpha = 45^{o}$ and 135^{o}, respectively. All these intensities were then measured after the elimination of the hyperfine interaction by the same technique as used previously (see Section 3.1.11, also described by Zaidi et al 1978). Accordingly the isotope cell was inserted in the optical system. From the measurements of these intensities, the Stokes parameters (P_0, P_1, P_2, P_3) were calculated by using eqn. (2.11).

4.2.6. Pressure Dependence of Coincidence Signal

As mentioned in section (4.1.3.), the imprisonment of resonance radiation or resonance trapping takes place when the radiation emitted from an excited atom is absorbed by atoms in the ground state. A photon, re-emitted after absorption, will no longer be correlated in time with the scattered electron that caused the initial excitation. The experimental results would thus be affected by resonance trapping and therefore it is necessary to check the effect of pressure on the coincidence signal as well as on the photon and electron intensities.

The coincidence signal was measured as a function of the mercury vapour pressure at an incident electron energy of 5.5 eV and scattering angle of 70^{o} with the polariser set with its polarisation axis at an angle of 135^{o} with the electron beam direction. This angle of the polariser was chosen because at this angle the coincidence signal was maximum and hence it was not susceptible to any variation in

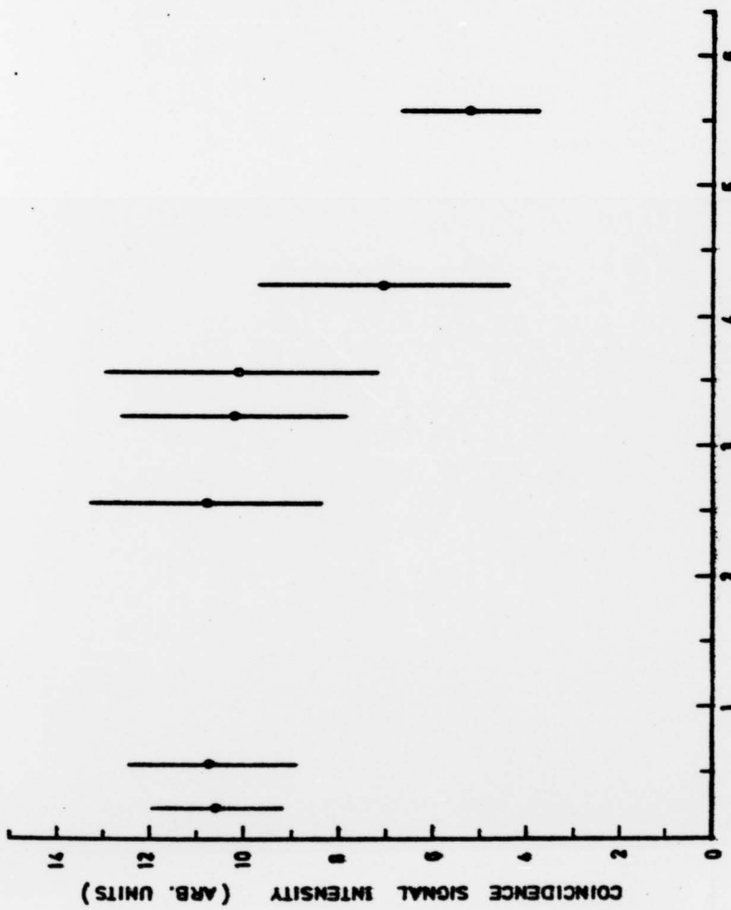

FIG.22. DEPENDENCE OF COINCIDENCE SIGNAL ON PRESSURE AT AN INCIDENT ELECTRON ENERGY OF 5·5 eV. ELECTRON SCATTERING ANGLE OF 70° AND POLARISER ANGLE 135°.
Error bars indicate ± 1 standard deviation.

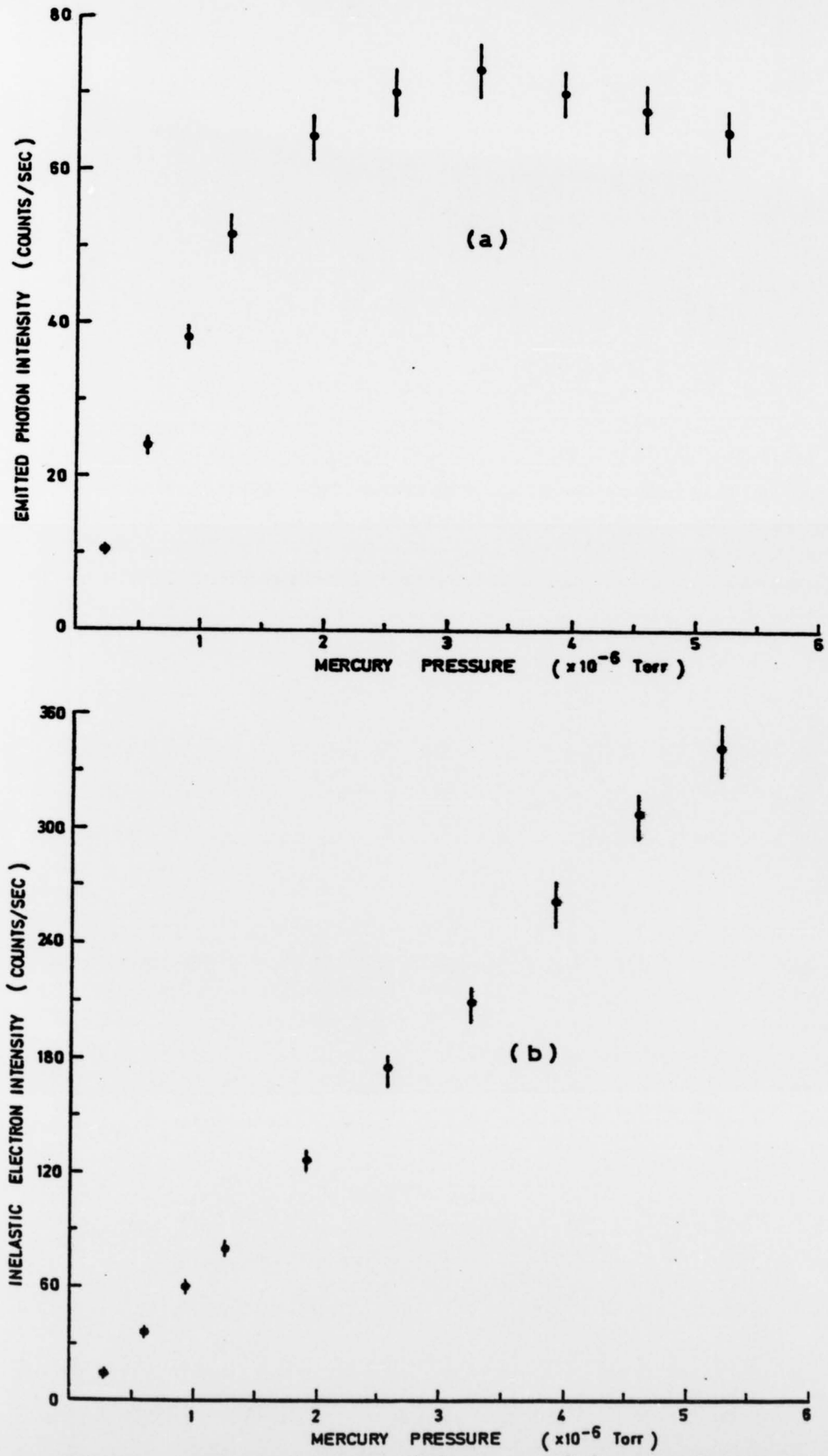

FIG. 23. Dependence on pressure of (a) photon and (b) electron signals, at an incident electron energy of 5·5 eV. Electron scattering angle of 70° and polariser angle of 135°. Error bars represent ± 1 standard deviation.

the angle. It can be seen from this measurement (fig.22) that the coincidence signal reduced significantly at pressures in excess of 4×10^{-6}Torr.

With the same excitation parameters ($E_{impact} = 5.5$ eV, $\theta_e = 70^o$), a study was made of the photon and electron intensities as a function of the mercury pressure. The background counts for photons and electrons were determined by switching off the heating to the tube on the mercury oven and thus blocking the atomic beam. These background counts were subtracted from the photon and electron count rates and the resulting counts were normalised to the Faraday cup current. The normalised count rates were then plotted against the mercury pressure (fig.23). The results show a linear increase in the photon signal up to a pressure of $\sim 1 \times 10^{-6}$Torr followed by a gradual rise and afterwards a decrease in the signal (fig.23(a)). The results exhibit a linear dependence of the electron signal on the pressure (fig.23(b)). To ensure that the effects of resonance trapping were unimportant, the operating pressure was taken in the linear range of the photon signal, i.e. at a pressure less than 1×10^{-6}Torr.

4.2.7. Sources of Systematic Error

Besides the pressure dependent effects described above, the following possible sources of systematic error were taken into account.

(i) A pile-up distortion of the delay time spectrum, caused by stop pulses being unrecorded due to prior arrival of another stop pulse, originating from an uncorrelated event, could result in a loss of coincidence signal at longer times. The possibility of such a pile-up distortion was remote in the present experiment owing to low counting rates $\sim$ 1KHz of the start and stop pulses.

(ii) The detection of photons of correct wavelength reflected from surfaces around the interaction region could give a false contribution to the coincidence signal. In order to reduce reflection coefficients, surfaces from which reflected photons might be detected were blackened.

(iii) Spurious electrical noise would affect the coincidence signal. Every possible effort was made to eliminate any source of such noise (see section 3.2.11). The absence of spurious events is indicated by the uniformity of the background of random coincidences during the runs (see fig.24).

(iv) The results could be affected by changes in the sensitivity of the photon detection system. The absence of any significant drift was demonstrated by the reproducibility of the data from run to run.

4.2.8. Results and Discussion

Figure 24 shows a delayed coincidence spectrum for an incident electron energy of 5.5 eV at a scattering angle of 70^{o} with the polariser making an angle of 135^{o} with the incident electron beam direction.

Figure 25 illustrates an example of the variation of the coincidence radiation intensity as a function of the polariser angle for an incident electron energy of 5.5 eV and scattering angle of 50^{o}.

Initial results were taken with the incident electron energy of 5.5 eV because, as mentioned in section (4.2.4), this state ($6^{3}P_{1}$) exhibited maximum sensitivity at energies close to the excitation threshold. However the existence of a resonance at this energy could have affected the results and therefore results were also taken at an energy of 6.5 eV, away from the resonance.

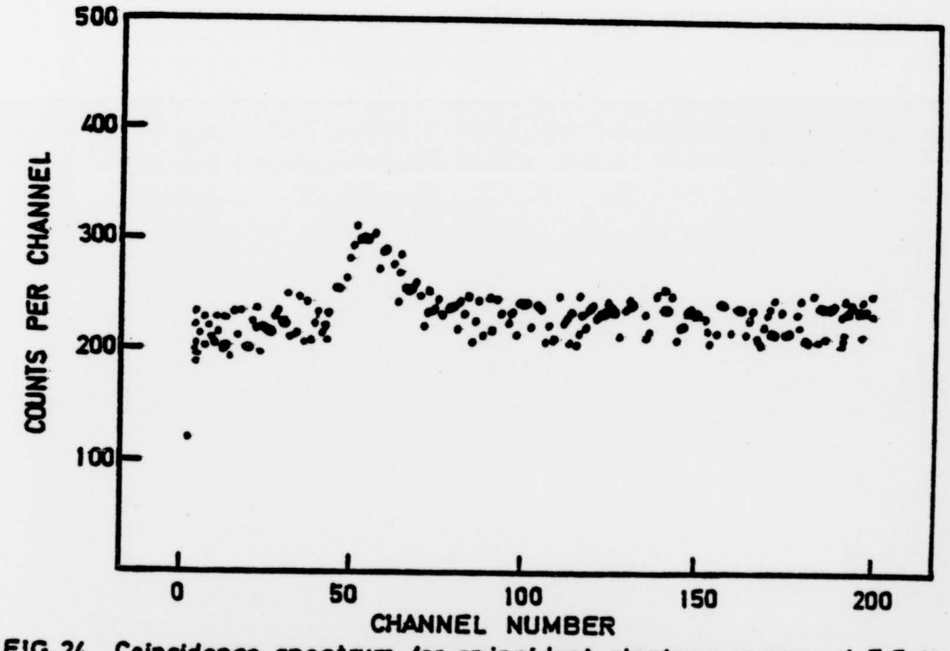

FIG.24. Coincidence spectrum for an incident electron energy of 5·5 eV, electron scattering angle of 70° and polariser angle of 135°. Channel width = 8ns, inelastic electron count rate ~700 Hz, photon rate ~450 Hz and accummulation time~24 hours.

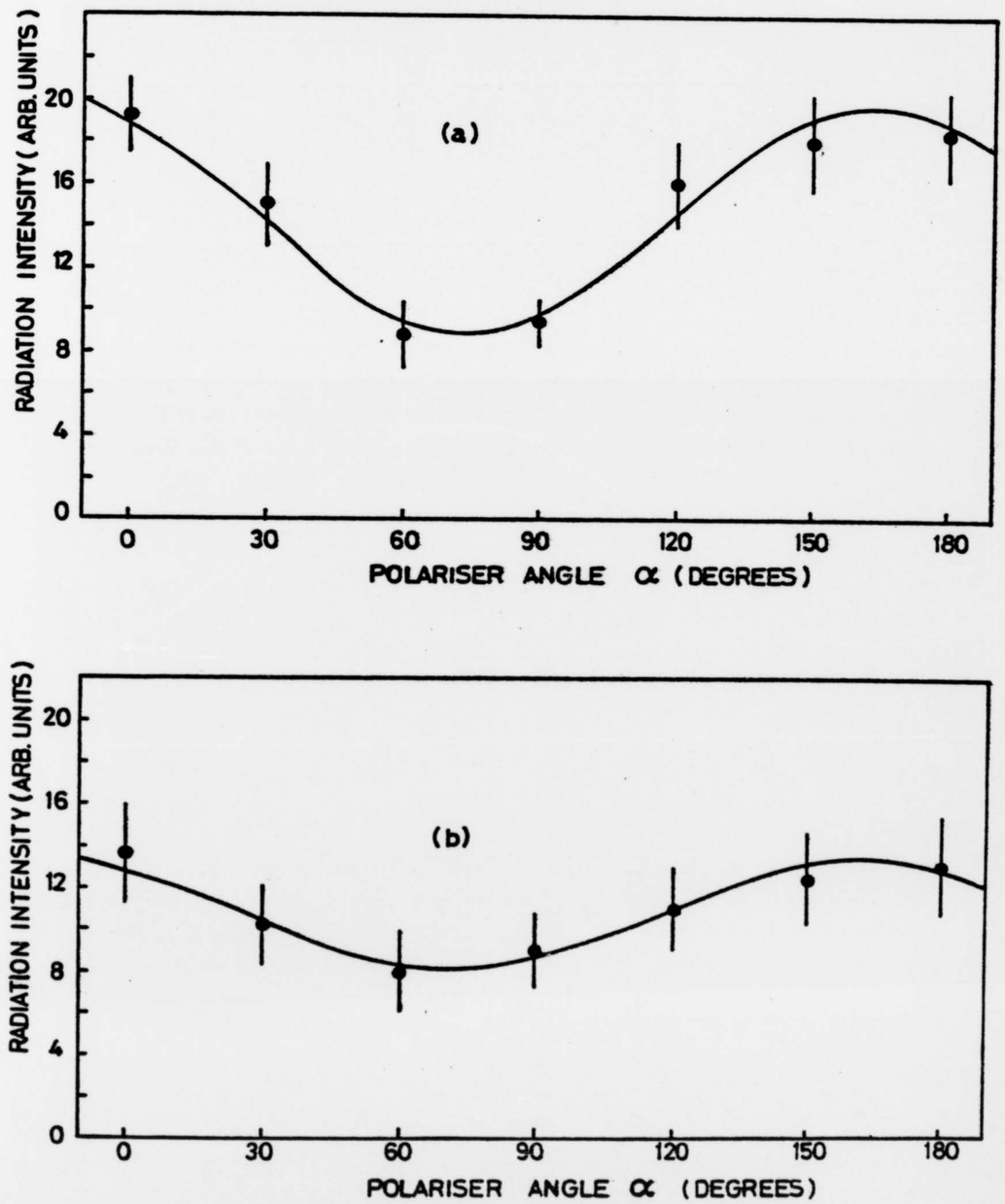

FIG.25. ELECTRON-PHOTON COINCIDENCE RADIATION INTENSITY AS A FUNCTION OF THE POLARISER ANGLE FOR 5.5 eV INCIDENT ELECTRON ENERGY AND 50° SCATTERING ANGLE, (a) WITHOUT $\frac{\lambda}{4}$ PLATE (b) WITH $\frac{\lambda}{4}$ PLATE.
Error bars indicate ± 1 standard deviation.

Standage and Kleinpoppen (1976) performed a similar experiment on helium for linear and circular polarisation measurements of the $3^1P - 2^1S$ (501.6 nm) photons detected in delayed coincidence with electrons inelastically scattered after the excitation of the 3^1P state. Their measurements of the vector polarisation and coherence parameters provided direct experimental evidence of the coherent nature of the excitation process. In their case, for the excitation of the 3^1P state of helium, the connection between the collision parameters and the photon polarisation is simple. The components of the vector polarisation '$\underline{P}$' can be expressed in terms of the parameters λ and χ (discussed in section 2.2) by the following relations (Blum and Kleinpoppen 1979),

$$P_1 = 2\lambda - 1$$

$$P_2 = -2\{\lambda(1 - \lambda)\}^{\frac{1}{2}} \cos \chi$$

$$P_3 = -2\{\lambda(1 - \lambda)\}^{\frac{1}{2}} \sin \chi$$

They were able to extract the values for λ and $|\chi|$ from the linear polarisation data and found an overall agreement with the previous angular correlation measurements of Eminyan et al (1975). However in the present experiment, for the excitation of the 6^3P_1 state of mercury, these simple relations are not valid due to fine structure splitting and spin-orbit interactions. Nevertheless the measurements of the vector polarisation and the coherence correlation factor can still provide useful information regarding the coherent nature of the excitation process.

The advantage of using the coherence correlation factor compared to the vector polarisation is that information about the effective phase difference between two orthogonal light vectors is obtained.

The effective phase difference between light polarised along the z and x directions is given by

$$B_{zx} = \tan^{-1}\left(\frac{P_3}{P_2}\right) \qquad \text{(eqn.(2.13))}$$

where the relative intensities I_z and I_x are calculated from the data for P_1 (eqn.(2.11)).

The magnitudes of vector polarisation and coherence correlation factor are deduced by using the relations,

$$|\underline{P}| = (P_1^2 + P_2^2 + P_3^2)^{\frac{1}{2}} \qquad \text{(eqn.(2.14))}$$

$$|\mu_{zx}| = \left(\frac{P_2^2 + P_3^2}{1 - P_1^2}\right)^{\frac{1}{2}} \qquad \text{(eqn.(2.12))}$$

The experimental results are given in table 3. The components P_1, P_2, P_3 of the vector polarisation, the degree of polarisation $|\underline{P}|$ and the coherence parameters $|\mu_{zx}|$ and B_{zx}, together with I_z and I_x are tabulated here as functions of incident electron energy and scattering angle. These measurements were taken for fixed incident electron energies of 5.5 eV and 6.5 eV at electron scattering angles of 50^o and 70^o. Values of 0.40 and 0.27 (table 3(a)), respectively, for the degree of polarisation and the degree of coherence, determined for an incident electron energy of 5.5 eV at a scattering angle of 50^o without the isotope cell (i.e. when the effect of hyperfine interaction was present), increased to 0.65 and 0.55 (table 3(b)), respectively, when the isotope cell was present and the effect of hyperfine structure had been eliminated. This comparison clearly shows the substantial influence of the hyperfine effect on these parameters.

In comparison with the $1^1S \rightarrow 3^1P \rightarrow 2^1S$ process in helium (Standage and Kleinpoppen, 1976) which is completely coherent, that is $|\underline{P}| = |\mu| = 1$, the values of $|\underline{P}|$ and $|\mu|$ obtained in the present experiment, as given

(a) HYPERFINE EFFECT PRESENT

INCIDENT ELECTRON ENERGY	SCATTERING ANGLE	NORMALISED STOKES PARAMETERS			$\lvert \underline{P} \rvert$	$\lvert \mu_{zx} \rvert$	β_{zx} (rad)	I_z	I_x
		P_1	P_2	P_3					
5.5 eV	50^o	0.31 ± 0.05	-0.21 ± 0.06	-0.14 ± 0.05	0.40 ± 0.05	0.27 ± 0.05	0.59 ± 0.13	0.66 ± 0.03	0.34 ± 0.03

(b) HYPERFINE EFFECT ELIMINATED

INCIDENT ELECTRON ENERGY	SCATTERING ANGLE	NORMALISED STOKES PARAMETERS			$\lvert \underline{P} \rvert$	$\lvert \mu_{zx} \rvert$	β_{zx} (rad)	I_z	I_x
		P_1	P_2	P_3					
5.5 eV	50^o	0.42 ± 0.08	-0.34 ± 0.08	-0.37 ± 0.07	0.65 ± 0.08	0.55 ± 0.08	0.83 ± 0.15	0.71 ± 0.04	0.29 ± 0.04
	70^o	0.13 ± 0.08	-0.52 ± 0.08	-0.27 ± 0.04	0.60 ± 0.07	0.59 ± 0.08	0.48 ± 0.08	0.57 ± 0.04	0.43 ± 0.04
6.5 eV	50^o	0.26 ± 0.09	-0.39 ± 0.09	-0.44 ± 0.04	0.64 ± 0.07	0.61 ± 0.07	0.85 ± 0.12	0.63 ± 0.04	0.37 ± 0.04
	70^o	0.13 ± 0.06	-0.45 ± 0.09	-0.42 ± 0.07	0.63 ± 0.08	0.62 ± 0.09	0.75 ± 0.13	0.56 ± 0.03	0.44 ± 0.03

Table 1: Coincident photon parameters for the $6^1S_0 \rightarrow 6^3P_1 \rightarrow 6^1S_0$ excitation/de-excitation process in mercury. Quoted experimental uncertainties represent one standard deviation.

(a): Results taken without the isotope cell and so the hyperfine effect was present.

(b): Results taken using the isotope cell so as to eliminate the hyperfine effect.

in table 3 and reported before (Zaidi et al 1979), indicate that the $6^1S_0 \rightarrow 6^3P_1 \rightarrow 6^1S_0$ excitation/de-excitation process in mercury is not completely coherent even when the effect of hyperfine structure has been eliminated. This discrepancy may be attributed to fine structure and spin-orbit interactions in this process. It has been shown by da Paixao et al (1979) that as a consequence of spin-orbit coupling, the radiation emitted from an excited state will not be completely polarised. Zehnle et al (1978) observed depolarisation and incoherency due to the influence of electronic amd nuclear spins on the $4^2S \rightarrow 4^2P \rightarrow 4^2S$ process for potassium.

It is interesting to note from the present results (table 3(b)) that for a given scattering angle, the degrees of coherence and also the degrees of polarisation are equal for incident electron energies of 5.5 eV and 6.5 eV. Since 5.5 eV corresponds to the position of one of the resonances caused by a negative-ion state in mercury and 6.5 eV is free of such intermediate excitation states, this might indicate that the degree of coherence of this excitation process is independent of the detailed excitation mechanism, and the incoherency arises during the period of the relaxation of the excited state. This is consistent with the negative-ion state decaying very quickly, with a lifetime $\sim 10^{-14}$s, to the 6^3P_1 state. However, it may be seen that the components of the vector polarisation (normalised Stokes parameters) do show significant changes at these energies.

5. CONCLUSIONS

This work has involved extensive polarisation measurements of the $6^3P_1 - 6^1S_0$ line of mercury, excited by electron impact. An important consequence of the fine structure and hyperfine structure splittings is the reduction of the polarisation of the emitted line radiation. The polarisation is influenced by the periods of the precessional motions associated with the fine structure and hyperfine structure interactions. The effect is negligible if the lifetime τ of the excited state is small compared both to fine structure and hyperfine structure precessional periods, τ_{fs} and τ_{hfs}, since in such a case emission takes place before the precessional motions can be set up. On the other hand if τ is large compared to both τ_{fs} and τ_{hfs} then, while the atom radiates the precessional motions reduce the anisotropy of the angular distribution and hence the polarisation of the line radiation. In the case of mercury, the lifetime of the 6^3P_1 state is $\sim 10^{-7}$s, whereas the fine structure splitting frequency is $\sim 10^{14}$Hz ($\tau_{fs} \sim 10^{-14}$s) and the hyperfine structure splitting frequency is $\sim 10^{10}$ Hz ($\tau_{hfs} \sim 10^{-10}$s). It follows therefore that the fine structure and hyperfine structure interactions will reduce the polarisation of the $6^3P_1 - 6^1S_0$ line of mercury.

In the first stage an isotope cell has been used to eliminate the effect of hyperfine structure on the polarisation of this intercombination line of mercury, excited by electron impact. This effect was observed by comparing the polarisation of the above line radiation from mercury of natural isotope composition with the polarisation of the line radiation from even isotopes having zero nuclear spin (see figure 14). The existence of the resonances at 4.9 eV and 5.5 eV has a large effect on the polarisation at lower energies. However, if one considers the observed results only for energies

greater than 6.0 eV, one may make plausible extrapolations which are in good agreement with the calculated threshold polarisation of McConnell and Moiseiwitsch (1968). The effect of the hyperfine structure on the polarisation can be clearly seen from figure 14 where at an incident electron energy of 6.0 eV, the polarisation of -0.35 without the isotope cell (i.e. when the hyperfine effect is present) increased to -0.55 in the presence of the isotope cell when the effect of the hyperfine structure in the observed radiation had been eliminated by the absorption of radiation from the isotopes having non-zero nuclear spins. This remarkable observation has beautifully demonstrated that the hyperfine structure has a substantial influence on the polarisation of this line of mercury. It may be emphasised that these measurements were made possible by the novel technique of using an isotope cell to selectively filter the radiation. It would have been difficult, if not impossible, on the basis of the cost alone of obtaining isotopically pure mercury to carry out such measurements in the manner Hafner and Kleinpoppen (1967) performed their experiment, using isotopically pure atom beams, to measure the polarisations of the resonance lines of Li^6, Li^7 and Na^{23}.

The effect of the hyperfine interaction on the polarisation has also been found to be prominent in the second stage of the experiment where the electron-photon delayed coincidence technique has been used to measure linear and circular polarisations of the coincident photon radiation for the $6^1S_0 \rightarrow 6^3P_1 \rightarrow 6^1S_0$ transitions of mercury by electron impact. These measurements have been made difficult by the long life-time of the excited state in a system where the background count rates were significant. The problem was further complicated by the appreciable reduction in the observed photon radiation due to absorption in the isotope cell. At the working temperature (40^oC) of the isotope

cell, the radiation intensity had fallen to ∿ 38% of the intensity without the isotope cell (see figure 12). Despite these problems, it has been possible to show from the evaluation of the vector polarisation and coherence parameters that the excitation/de-excitation process, $6^1S_0 \rightarrow 6^3P_1 \rightarrow 6^1S_0$, in mercury is not completely coherent even after the elimination of the hyperfine effect. This incoherency may be associated with the fine structure and spin-orbit interactions in this process. This view is supported by da Paixao et al (1979) who have shown that as a consequence of the spin-orbit coupling the photon radiation will not be completely polarised. It may be noted that the degree of polarisation and the degree of coherence are equal for the two incident electron energies (5.5 eV and 6.5 eV). Since at 5.5 eV, the excitation involved the formation of a temporary negative-ion state unlike the excitation at 6.5 eV, this could be explained if the incoherency of this process arises during the time the atom spends in the excited state, that is in the decay mechanism rather than during the excitation process.

The present work as a whole provides an opportunity to compare the polarisation measurements as performed with a traditional experiment to those carried out using the electron-photon coincidence method. It is interesting to note how the polarisation is dramatically different when the radiation analysis is done averaged over all scattered electrons directions and how significantly the polarisation can change when the analysis takes place with regard to the direction of the inelastically scattered electrons. Values of the linear polarisations, after the elimination of the hyperfine effect, at incident electron energies of 5.5 eV and 6.5 eV obtained in the first experiment (see figure 14) are, respectively, -0.28 and -0.48. Values of the same measurements with the second experiment are 0.42 and 0.26, respectively,

at an electron scattering angle of 50^{o} and both values become equal to 0.13 at a scattering angle of 70^{o} (see table 3(b)).

In order to obtain further information about the vector polarisation and coherence parameters of the coincident photon radiation, improvement of the apparatus is required. The use of a monochromator together with electron optics to control the energy spread and the collimation of the electron beam would certainly be of advantage provided the intensity of the electron current in the interaction region is not reduced significantly. In this way the background counts would be lowered and hence an increase in the signal to noise ratio would allow a longer range of the electron scattering angles to be covered. The range of the incident electron energy should be extended to find out the effect of increase in energy, if any, on the degrees of polarisation and coherence.

In addition the possibility of studying the $6^{1}P_{1} - 6^{1}S_{0}$ (185.0 nm) line in preference to the $6^{3}P_{1} - 6^{1}S_{0}$ (253.7 nm) line can be considered. This line at 185.0 nm has a much shorter lifetime, $\tau = 1.31 \times 10^{-9}$s (Lurio, 1965), than the 253.7 nm line whose lifetime $\tau = 1.20 \times 10^{-7}$s. For this 185.0 nm line the signal to noise ratio is expected to be better due to a larger sensitivity for the excitation of the $6^{1}P_{1}$ state in comparison to the $6^{3}P_{1}$ state (see figures 17 and 20) and, in any case, the theoretical interpretation would be easier in the absence of the fine structure after having eliminated the effect of the hyperfine structure by the use of the isotope cell. However a complete polarisation analysis may not be possible since it is difficult to obtain a quartz $\frac{\lambda}{4}$ plate for the wavelength of 185.0 nm but, on the other hand, the values of λ and $|\chi|$ may still be determined from the linear polarisation data alone.

REFERENCES

Albert K., Christian C., Heindorff T., Reichert E. and Schön S. (1977), J.Phys.B., 10, 3733-9.

Andersen N., Andersen T., Cocke C.L. and Horsdal Pedersen E. (1979), J.Phys.B., 12, 2541-51.

Arriola H., Teubner P.J.O., Ugbabe A. and Weigold E. (1975), J.Phys.B., 8, 1275-9.

Backx C., Wight G.R., Tol R.R. and Van der Wiel M.J. (1975), J.Phys.B., 8, 3007-19.

Baranger E. and Gerjuoy E. (1958), Proc. Phys. Soc., 72, 326-36.

Blum K. and Kleinpoppen H. (1975), J.Phys.B., 8, 922-5

_____ (1976), "Electron and Photon Interactions with Atoms", eds. H. Kleinpoppen and M.R.C. McDowell (Plenum, New York) pp 501-14.

_____ (1979), Phys. Rep., 52, 203-61.

Born M. and Wolf E. (1975), "Principles of Optics" (Pergamon, Oxford) pp.544-55.

Brannen E., Hunt F.R., Adlington R.H. and Nicholls R.W. (1955), Nature, 175, 810-1.

Brunt J.N.H., Read F.H. and King G.C. (1977), J.Phys. E., 10, 134-9.

da Paixao F.J., Padial N.T. and Csanak Gy. (1979), Preprint SEPARATA S-041/79, Universidade Estadual de Campinas, Brasil.

Dennis N.T.M. and Heppell T.A. (1968), "Vacuum System Design" (Chapman, London) p.10.

Dixon A.J., Hood S.T. and Weigold E. (1978), Phys. Rev. Lett., 40, 1262-6.

Ehlers V.J. and Gallagher A. (1973), Phys. Rev. A., 7, 1573-85.

Ehrhardt H., Schulz M., Tekaat T. and Willmann K. (1969), Phys.Rev. Lett., 22, 89-92.

Ehrhardt H., Hesselbacher K.H., Jung K., Schubert E. and Willmann K. (1974), J.Phys.B., 7, 69-78.

Eminyan M., MacAdam K.B., Slevin J. and Kleinpoppen H. (1973), Phys.Rev. Lett., 31, 576-9.

_____ (1974), J.Phys.B., 7, 1519-42.

Eminyan M., MacAdam K.B., Slevin J., Standage M.C. and Kleinpoppen H. (1975), J.Phys. B., 8, 2058-66.

Enemark E.A. and Gallagher A. (1972), Phys.Rev.A., 6, 192-205.

Fano U. and Macek J.H. (1973), Rev.Mod.Phys., 45, 553-73.

Fedorov V.L. and Mezentsev A.P. (1965), Opt. Spectrosc., 19, 5-8.

Firester A.H. (1966), Rev. Sci. Instrum., 37, 1264-5.

Flower D.R. and Seaton M.J. (1967), Proc.Phys.Soc., 91, 59-62.

Fon W.C., Berrington K.A. and Kingston A.E. (1979), J.Phys.B., 12, L171-3.

Froitzheim H., Ibach H. and Lehwald S. (1975), Rev.Sci.Instrum., 46, 1325-8.

Giordmaine J.A. and Wang T.C. (1960), J.Appl.Phys., 31, 463-71.

Hafner H. and Kleinpoppen H. (1967), Z.Phys., 198, 315-20.

Hanes G.R. (1960, J.Appl.Phys., 31, 2171-5.

Heddle D.W.O. and Keesing R.G.W. (1967), Proc.R.Soc.A., 299, 212-20.

Heddle D.W.O., Keesing R.G.W. and Watkins R.D. (1974), Proc. R. Soc. A., 337, 443-50.

Heideman H.G.M., Smit C. and Smit J.A. (1969), Physica, 45, 305-20.

Heideman H.G.M., van de Water W., van Eck J. and van Moergestel L.J.M. (1979), "Book of Abstracts", XIth ICPEAC, Kyoto, pp 178-9.

Hollywood M.T., Crowe A. and Williams J.F. (1979), J.Phys.B., 12, 819-34

Holstein T. (1947), Phys.Rev., 72, 1212-23.

Holt R.A. and Pipkin F.M. (1974), Phys.Rev.A., 9, 581-4.

Hood S.T., Weigold E. and Dixon A.J. (1979), J.Phys.B., 12, 631-48.

Hughes A.L. and McMillen J.H. (1929), Phys. Rev., 34, 291-5.

Hughes A.L. and Rojansky V. (1929), Phys.Rev., 34, 284-90.

Imhof R.E. and Read F.H. (1969), Chem.Phys.Lett., 3, 652-4.

_____ (1971a), J.Phys.B., 4, 450-60.

_____ (1971b), J.Phys.B., 4, 1063-9.

_____ (1971c), Chem.Phys.Lett., 11, 326-8.

_____ (1977), Rep.Prog.Phys., 40, 1-104.

Jung K., Schubert E., Paul D.A.L. and Ehrhardt H. (1975), J.Phys.B., 8, 1330-7.

Kaul R.D. (1966), J. Opt. Soc. Am., 56, 1262-3.

King G.C. and Adams A. (1974), J.Phys.B., 7, 1712-8.

King G.C., Adams A. and Cvejanovic D. (1975a), J.Phys.B., 8, 365-71.

King G.C.M., Adams A. and Read F.H. (1972), J.Phys.B., 5, L254-7.

King G.C., Mohamed K.A., Read F.H. and Imhof R.E. (1976), J.Phys.B., 9, 1274-50.

King G.C., Read F.H. and Imhof R.E. (1975b), J.Phys.B., 8, 665-73.

Kleinpoppen H. (1969), "Physics of the One- and Two-Electron Atoms", eds. F. Bopp and H. Kleinpoppen (North-Holland, Amsterdam), pp 612-31.

Kleinpoppen H. and McGregor I. (1979), "Coherence and Correlation in Atomic Collisions", eds. H. Kleinpoppen and J.F. Williams (Plenum New York) pp 109-19.

Kleinpoppen H. and Scharmann A. (1978), "Progress in Atomic Spectroscopy", part A, eds. W. Hanle and H.Kleinpoppen (Plenum, New York), pp 329-90.

Krause H.F., Johnson S.G. and Datz S. (1977), Phys. Rev. A., 15, 611-8.

Lew H. (1967), "Methods of Experimental Physics", Vol.4, Part A., eds. V.W. Hughes and H.L. Schultz (Academic, New York), p 160.

Lindau I. and Hagstrom S.B.M. (1971), J.Phys. E., 4, 936-40.

Lurio A. (1965), Phys. Rev., 140, A1505-8.

Macek J. and J aecks D.H. (1971), Phys.Rev.A., 4, 2288-300.

Malcolm I.C. and McConkey J.W. (1979), J.Phys.B., 12, 511-9.

Marmet P. and Kerwin L. (1960), Can.J.Phys., 38, 787-96.

McConnell J.C. and Moiseiwitsch B.L. (1968), J.Phys.B., 1, 406-13.

McFarland R.H. (1964), Phys.Rev., 133, A986-90.

McGowan J.W. (1967), Rev.Sci.Instrum., 38, 285-7.

Moiseiwitsch B.L. and Smith S.J. (1968), Rev.Mod.Phys., 40, 238-353.

Moore C.E. (1971), "Atomic Energy Levels", Vol.III, Nat.Bur.Stand. Circular No.467 (U.S. Govt. Printing Office, Washington), pp 191-5.

Oppenheimber J.R. (1927), Proc.Nat.Acad.Sci., 13, 800-5.

_____ (1928), Phys. Rev., 32, 361-76.

Ottley T.W. (1974), Ph.D. thesis, University of Stirling.

Ottley T.W. and Kleinpoppen H. (1975), J.Phys.B., 8, 621-7.

Pavlovic Z., Boness M.J.W., Herzenberg A. and Schulz G.J. (1972), Phys. Rev. A., 6, 676-85.

Penney W.G. (1932), Proc.Nat.Acad.Sci., 18, 231-7.

Percival I.C. and Seaton M.J. (1958), Phil. Trans. R. Soc. A., 251, 113-38.

Popp M., Schäfer G. and Bodenstedt E. (1970), Z.Phys., 240, 71-92.

Powell C.J. (1968), "Methods of Experimental Physics", Vol.7, Part B., eds. B. Bederson and W.L. Fite (Academic, New York), p.282.

Preston J.A., Hender M.A. and McConkey J.W. (1973), J.Phys.E., 6, 661-6.

Purcell E.M. (1938), Phys.Rev., 54, 818-26.

Raible V. (1974), Ph.D. thesis, University of Stirling.

Ramsey N.F. (1963), "Molecular Beams" (Clarendon, Oxford), pp 12-21.

Read F.H. (1970), J.Phys.E., 3, 127-31.

Rosebury F. (1965), "Handbook of Electron Tube and Vacuum Techniques" (Addison-Wesley, Reading, Massachusetts), pp 15-7.

Roy D., Delage A. and Carette J.D. (1975), J.Phys.E., 8, 109-14.

Rudberg E. (1930), Proc.R.Soc.A., 129, 628-51.

Rudd M.E. (1972), "Low Energy Electron Spectroscopy", ed. K.D. Sevier (Wiley-Interscience, New York), pp 3-34.

Schulz G.J. (1973), Rev.Mod.Phys., 45, 378-486.

Shaw D.A., Adams A. and King G.C. (1975), J.Phys.B., 8, 2456-60.

Shpenik O.B., Souter V.V., Zavilopulo A.N., Zapesochnyi I.P. and Kontrosh E.E. (1976), Sov.Phys. JETP, 42, 23-8.

Simpson J.A. and Kuyatt C.E. (1963), Rev.Sci.Instrum., 34, 265-8.

Skinner H.W.B. and Appleyard E.T.S. (1928), Proc.R.Soc.A., 117, 224-44.

Smith A.J., Imhof R.E. and Read F.H. (1973), J.Phys.B., 6, 1333-8.

Smith A.J., Read F.H. and Imhof R.E. (1975), J.Phys.B., 8, 2869-79.

Standage M.C. and Kleinpoppen H. (1976), Phys.Rev.Lett., 36, 577-80.

Sutcliffe V.C., Haddad G.N., Steph N.C. and Golden D.E. (1978), Phys. Rev.A., 17, 100-7.

Tan K.H., Fryar J., Farago P.S. and McConkey J.W. (1977), J.Phys.B., 10, 1073-82.

Ugbabe A., Teubner P.J.O., Weigold E. and Arriola H. (1977), J.Phys.B., 10, 71-9.

Weast R.C. (1975), ed. "Handbook of Chemistry and Physics", 55th edition (Chemical Rubber Co. Cleveland, Ohio), pp B306 and D161.

Weigold E., Hood S.T. and Teubner P.J.O. (1973), Phys.Rev.Lett., 30, 475-8.

Williams J.F. (1975), "The Physics of Electronic and Atomic Collisions", eds. J.S. Riseley and R. Geballe (Univ. of Washington, Seattle, Washington), pp 139-50.

Schulz G.J. (1973), Rev.Mod.Phys., 45, 378-486.

Shaw D.A., Adams A. and King G.C. (1975), J.Phys.B., 8, 2456-60.

Shpenik O.B., Souter V.V., Zavilopulo A.N., Zapesochnyi I.P. and Kontrosh E.E. (1976), Sov.Phys. JETP, 42, 23-8.

Simpson J.A. and Kuyatt C.E. (1963), Rev.Sci.Instrum., 34, 265-8.

Skinner H.W.B. and Appleyard E.T.S. (1928), Proc.R.Soc.A., 117, 224-44.

Smith A.J., Imhof R.E. and Read F.H. (1973), J.Phys.B., 6, 1333-8.

Smith A.J., Read F.H. and Imhof R.E. (1975), J.Phys.B., 8, 2869-79.

Standage M.C. and Kleinpoppen H. (1976), Phys.Rev.Lett., 36, 577-80.

Sutcliffe V.C., Haddad G.N., Steph N.C. and Golden D.E. (1978), Phys. Rev.A., 17, 100-7.

Tan K.H., Fryar J., Farago P.S. and McConkey J.W. (1977), J.Phys.B., 10, 1073-82.

Ugbabe A., Teubner P.J.O., Weigold E. and Arriola H. (1977), J.Phys.B., 10, 71-9.

Weast R.C. (1975), ed. "Handbook of Chemistry and Physics", 55th edition (Chemical Rubber Co. Cleveland, Ohio), pp B306 and D161.

Weigold E., Hood S.T. and Teubner P.J.O. (1973), Phys.Rev.Lett., 30, 475-8.

Williams J.F. (1975), "The Physics of Electronic and Atomic Collisions", eds. J.S. Riseley and R. Geballe (Univ. of Washington, Seattle, Washington), pp 139-50.

Zaidi A.A., McGregor I. and Kleinpoppen H. (1978), J.Phys.B., 11, L151-5.

_____ (1979), "Book of Abstracts", XIth ICPEAC, Kyoto, pp 170-1.

Zehnle L., Clemens E., Martin P.J., Schäuble W. and Kempter V. (1978), J.Phys.B., 11, 2865-74.